159904

Radiometric Correction Procedure Study

(NASA-CR-159904) RADIOMETRIC CORRECTION PROCEDURE STUDY Final Report, Sep. 1977 - Jun. 1978 (IBM Federal Systems Div.) 159 p
HC A08/MF A01 CSCL 14B
N79-15284
Unclas
G3/35 43203

IBM

RADIOMETRIC CORRECTION PROCEDURE STUDY

Final Report for Period September 1977 to June 1978

June 1978

Prepared for

Goddard Space Flight Center
Greenbelt, Maryland 20771

by

C P Colby, Jr.
R. L. Sands
S. W. Murphrey

Federal Systems Division
INTERNATIONAL BUSINESS MACHINES CORPORATION
Gaithersburg, Maryland 20760

TECHNICAL REPORT STANDARD TITLE PAGE

1. Report No.	2 Government Accession No	3 Recipient's Catalog No.
4 Title and Subtitle Radiometric Correction Procedure Study		5 Report Date June, 1978 6. Performing Organization Code
7 Author(s) C. Colby, R. Sands, S. Murphrey		8 Performing Organization Report No FSD 78-0015
9. Performing Organization Name and Address IBM Federal Systems Division Gaithersburg, Maryland 20760		10 Work Unit No 11. Contract or Grant No NAS 5-24276
12 Sponsoring Agency Name and Address Goddard Space Flight Center Greenbelt, Maryland 20771 Benard Peavey, Technical Officer		13 Type of Report and Period Covered Final Report Sept. 1977-June 1978 14. Sponsoring Agency Code
15 Supplementary Notes		

16 Abstract

A comparison of MSS radiometric processing techniques identified as a preferred radiometric processing technique a procedure which equalizes the mean and standard deviation of detector-specific histograms of uncalibrated scene data. Evaluation of MSS calibration data demonstrated that the relationship between detector responses is essentially linear over the range of intensities typically observed in MSS data, and that the calibration wedge data possesses a high degree of temporal stability. An analysis of the preferred radiometric processing technique showed that it could be incorporated into the MDP-MSS system without a major redesign of the system, and with minimal impact on system throughput.

17. Key Words (Selected by Author(s))	18. Distribution Statement
MSS Radiometric Equalization MSS Radiometric Calibration	

19. Security Classif. (of this report)	20. Security Classif (of this page)	21. No. of Pages	22 Price*

*For sale by the Clearinghouse for Federal Scientific and Technical Information, Springfield, Virginia 22151.

APPROVAL

This final report for the Radiometric Correction Procedure Study has been reviewed and approved by the undersigned.

Charles P. Colby, Jr.
Project Engineer
IBM Federal Systems Division
Gaithersburg, Maryland

Ralph Bernstein
Senior Engineer
IBM Federal Systems Division
Gaithersburg, Maryland

ACKNOWLEDGEMENT

The technical group which performed the Radiometric Correction Procedure Study wishes to acknowledge with gratitude the financial and technical support provided by NASA-GSFC for this study. In particular the interest, encouragement and technical assistance provided by the Technical Officer for this contract, Bernard Peavey, is greatly appreciated.

CONTENTS

Section		Page
1	INTRODUCTION	1-1
2	PROCESSING DESCRIPTION	2-1
2.1	Preprocessing	2-2
2.2	Radiometric Processing	2-2
2.2.1	IBM's Destriping Procedures	2-2
2.2.2	Modified MSS Calibration Procedures	2-3
3	EVALUATIONS OF PROCESSED IMAGES	3-1
3.1	Evaluation by Detector-Specific Histograms	3-3
3.2	Evaluation by Visual Inspection	3-12
3.3	Evaluation by Power Spectra Analysis	3-14
3.4	Evaluation by Multispectral Classification	3-30
3.5	Summary of Comparative Evaluation Results	3-33
4	EVALUATION OF MSS CALIBRATION DATA	4-1
4.1	Temporal Variation of Reported Calibration Wedge Values	4-2
4.2	Gain and Bias Coefficient Time Series	4-9
4.3	Interdetector Correlation Plots	4-75
4.4	Summary of Calibration Data Evaluation	4-91
5	INTERDETECTOR RESPONSE EQUALIZATION IN THE MDP	5-1

Appendix

A	IBM DESTRIPPING PROCEDURES	A-1
B	MSS CALIBRATION PROCEDURE	B-1
C	PLATES	C-1

ILLUSTRATIONS

Figure		Page
3-1	Data Flow for Radiometric Processing Evaluations	3-2 3-2
3.1-1	Detector-specific Histograms for Uncalibrated Scene Data from MSS Band 1 After Type a1 Radiometric Processing	3-6
3.1-2	Detector Specific Histograms for Uncalibrated Scene Data from MSS Band 1 After Type a2 Radiometric Processing	3-7
3.1-3	Detector-specific Histograms for Uncalibrated Scene Data from MSS Band 1 After Type a3 Radiometric Processing	3-8
3.1-4	Detector-specific Histograms for Unicalibrated Scene Data from MSS Band 1 after Type 1b Radiometric Processing	3-9
3.1-5	Detector-specific Histograms for Uncalibrated Scene Data from MSS Band 1 after Type b2 Radiometric Processing	3-10
3.1-6	Detector-specific Histograms for Calibrated Scene Data from MSS Band 1 after Type a1 Radiometric Processing	3-11
3.3-1	Power Spectrum for High Frequency Region in Uncalibrated Scene Data	3-17
3.3-2	Power Spectrum for High Frequency Region in Uncalibrated Scene Data after Type a1 Processing	3-18
3.3-3	Power Spectrum for High Frequency Region in Uncalibrated Scene Data after Type a2 Processing	3-19
3.3-4	Power Spectrum for High Frequency Region in Uncalibrated Scene Data after Type a3 Processing	3-20

Figure		Page
3.3-5	Power Spectrum for Low Frequency Region in Uncalibrated Scene Data	3-21
3.3-6	Power Spectrum for Low Frequency Region in Uncalibrated Scene Data after Type a1 Processing	3-22
3.3-7	Power Spectrum for Low Frequency Region in Uncalibrated Scene Data after Type a2 Processing	3-23
3.3-8	Power Spectrum for Low Frequency Region in Uncalibrated Scene Data after Type a3 Processing	3-24
3.3-9	Power Spectrum for Smaller Low Frequency Region in Uncalibrated Scene Data	3-25
3.3-10	Power Spectrum for Smaller Low Frequency Region in Uncalibrated Scene Data after Type a1 Processing	3-26
3.3-11	Power Spectrum for Smaller Low Frequency Region in Uncalibrated Scene Data after Type a2 Processing	3-27
3.3-12	Power Spectrum for Smaller Low Frequency Region in Uncalibrated Scene Data after Type a3 Processing	3-28
3.4-1	Field Structure of the Hand County LACIE Intensive Study Site	3-34
4.1-1	Plot of Decompressed Calibration Wedge Data Values and their Standard Deviations for Detector 1, Band 1	4-3
4.1-2	Plot of Decompressed Calibration Wedge Data Values and their Standard Deviations for Detector 2, Band 1	4-4
4.1-3	Plot of Decompressed Calibration Wedge Data Values and their Standard Deviations for Detector 3, Band 1	4-5
4.1-4	Plot of Decompressed Calibration Wedge Data Values and their Standard Deviations for Detector 4, Band 1	4-6

Figure		Page
4.1-5	Plot of Decompressed Calibration Wedge Data Values and their Standard Deviations for Detector 5, Band 1	4-7
4.1-6	Plot of Decompressed Calibration Wedge Data Values and their Standard Deviations for Detector 6, Band 1	4-8
4.2-1	Time Series of Normalized Gain Values for Band 1, Detector 1	4-15
4.2-2	Time Series of Normalized Bias Values for Band 1, Detector 1	4-20
4.2-3	Time Series of Normalized Gain Values for Band 1, Detector 2	4-25
4.2-4	Time Series of Normalized Bias Values for Band 1, Detector 2	4-30
4.2-5	Time Series of Normalized Gain Values for Band 1, Detector 3	4-35
4.2-6	Time Series of Normalized Bias Values for Band 1, Detector 3	4-40
4.2-7	Time Series of Normalized Gain Values for Band 1, Detector 4	4-45
4.2-8	Time Series of Normalized Bias Values for Band 1, Detector 4	4-50
4.2-9	Time Series of Normalized Gain Values for Band 1, Detector 5	4-55
4.2-10	Time Series of Normalized Bias Values for Band 1, Detector 5	4-60
4.2-11	Time Series of Normalized Gain Values for Band 1, Detector 6	4-65
4.2-12	Time Series of Normalized Bias Values for Band 1, Detector 6	4-70

Figure		Page
4.3-1	Interdetector Correlation Plot for Corresponding Decomposed Calibration Wedge Samples and Their Standard Deviations, Detector 2 versus Detector 1, Band 1	4-80
4.3-2	Interdetector Correlation Plot for Corresponding Decomposed Calibration Wedge Samples and Their Standard Deviations, Detector 3 versus Detector 1, Band 1	4-79
4.3-3	Interdetector Correlation Plot for Corresponding Decomposed Calibration Wedge Samples and Their Standard Deviations, Detector 4 versus Detector 1, Band 1	4-80
4.3-4	Interdetector Correlation Plot for Corresponding Decomposed Calibration Wedge Samples and Their Standard Deviations, Detector 5 versus Detector 1, Band 1	4-81
4.3-5	Interdetector Correlation Plot for Corresponding Decomposed Calibraton Wedge Samples and Their Standard Deviations, Detector 6 versus Detector 1, Band 1	4-82
4.3-6	Interdetector Functional Relationships for Detector 1 and Detector 2, Band 1	4-84
4.3-7	Interdetector Functional Relationships for Detector 1 and Detector 3, Band 1	4-85
4.3-8	Interdetector Functional Relationships for Detector 1 and Detector 4, Band 1	4-86
4.3-9	Interdetector Functional Relationships for Detector 1 and Detector 5, Band 1	4-87
4.3-10	Interdetector Functional Relationships for Detector 1 and Detector 6, Band 1	4-88

TABLES

Tables		Page
3.1-1	Chi-squared Values for Comparison of Detector-Specific Histograms	3-5
3.2-1	Results of Visual Evaluation of Radiometrically Processed Scene Data for Landsat MSS Scene 2183-16433, MSS Band 1	3-13
3.3-1	Relative (to Average Power) Power Spectrum Values for Restricted Low Frequency Image Region at Frequencies Corresponding to Striping	3-29
3.4-1	Results of Evaluation by Multispectral Classification	3-32
3.5-1	Summary of Evaluation Results (1 = Best)	3-35
4.2-1	Summary of Variations in Gain and Bias Coefficients	4-13
4.2-2	Variations of Calibration Function Coefficients	4-14
4.3-1	Positions in Calibraton Wedge Data of Samples Represented in Interdetector Correlation Plots	4-76
4.3-2	Functional Interdetector Relationship for MSS Calibration Wedge Data	4-89

Section 1
INTRODUCTION

The objectives of this study were to provide both qualitative and quantitative comparisons of several radiometric processing procedures applied to MSS data, to assess the adequacy of present MSS calibration procedures, and to assess the impact of a modified MSS radiometric processing procedure on the throughput of the Master Data Processor.

The radiometric calibration currently performed by NASA on image data received from the Landsat Multispectral Scanner (MSS) is based on a linear radiometric transformation derived dynamically from six samples of the calibration wedge data provided by the MSS for each image line. This radiometric calibration procedure leaves a residual periodic variation in image radiometry which is termed striping. This radiometric variation, in addition to its impact on the visual quality of processed imagery, introduces a systematic radiometric error which may compromise the validity of results obtained by machine processing for information extraction.

Over the years, various techniques have been proposed to compensate MSS digital data for striping. These proposals have concentrated on techniques which characterize the response of individual MSS detectors by examining the image data reported by each, and equalize this response across the detectors of a spectral band. These techniques have been shown to provide considerable reduction in visible striping. They fail, however, to address the questions of why the calibration procedures employed are not effective in eliminating striping originally, and whether the calibration procedures can be modified to eliminate striping.

These questions could only be answered by studying the calibration procedures and the data available to perform the calibration. It was anticipated that investigation of the temporal stability of the complete set of calibration wedge data, together with interdetector comparisons of this data, would provide the information necessary to formulate a more effective MSS calibration procedure, thus eliminating these interdetector variations as part of the calibration process.

Section 2
PROCESSING DESCRIPTION

The study was designed to empirically investigate both destriping procedures and the MSS calibration procedure, evaluating their effectiveness by both visual and quantitative procedures. It also considered the characteristics of MSS calibration wedge data in order to elucidate the temporal and interdetector effects which exist in this data.

The study consisted of the following tasks:

a. Preprocessing of scene CCT to produce band separated images with associated calibration data

b. Destriping processing and MSS calibration processing

c. Visual evaluation of processing results

d. Power spectrum analysis of processed image data

e. Detector-specific image histogram generation

f. Multispectral classification of agricultural areas in processed scene data

g. Evaluation of MSS Calibration Data

h. Evaluation of the impact on MDP throughput of the selected destriping procedure.

One Landsat scene, provided in both calibrated and uncalibrated form, was used in this study. This MSS scene, E-2183-16433, contains water, rural crop areas, and areas of high and low radiance. Both the radiometrically calibrated and radiometrically uncalibrated versions of this scene were processed and evaluated as described below.

2.1 PREPROCESSING

Each of the two versions (calibrated and uncalibrated) of the scene were reformatted to produce complete images of each of the four MSS bands, with the calibration data from the CCT provided for each MSS mirror sweep. These images were radiometrically adjusted to match the characteristics of the IBM Drum Scanner/Plotter, and recorded on photographic film, to permit inspection for data quality.

2.2 RADIOMETRIC PROCESSING

The radiometric processing techniques investigated in this study are outlined below.

2.2.1 IBM's Destriping Procedures

Type a1. Mean and standard deviation equalization based on the data from a single MSS mirror sweep (i.e., six contiguous lines of image date), with the resulting detector unique gain and bias radiometric compensations applied to the data from the subsequent mirror sweep.

Type a2. Mean and standard deviation histogram equalization based on the data from the first 60 mirror sweeps of the image (approximately 15% of the image data in an MSS frame), with the resulting detector unique gain and bias radiometric compensations applied to the data for the entire image.

Type a3. Mean and standard deviation histogram equalization based on the data from the first 195 mirror sweeps of the image (50% of the image data), with the resulting detector unique gain and bias radiometric compensations applied to the data for the entire image.

Details of this processing are presented in Appendix A.

2.2.2 Modified MSS Calibration Procedures

Type b1. The smoothed gain and offset values developed for the lines of the initial 98 mirror sweeps of a spectral image (approximately 25% of the image data) were averaged for each of the six detectors in a spectral band, and these six averaged gain and bias sets were used as the radiometric correction for the entire image. This smoothed gain and offset calibration employed the six calibration wedge values present in the CCT data for the scene.

Type b2. The smoothed gain and offset values developed for the lines of the entire spectral image (100%) were averaged for each of the six MSS detectors of that band, and these six averaged gain and bias sets were used as the radiometric correction for the entire image.

The algorithm used to calculate the smoothed gain and offset is presented in Appendix B.

Section 3
EVALUATIONS OF PROCESSED IMAGES

The comparative evaluations which were performed in this study of radiometric processing procedures are shown in Figure 3-1, together with the data processing required to generate products for comparison. These results of evaluations are discussed in the following subsections. All the evaluations except multispectral classification were performed on the scene data from MSS band 1 (0.5 to 0.6 micrometers), which exhibited the greatest visually apparent striping in photographic recordings of the unprocessed, uncalibrated scene data. The multispectral classification evaluation employed data from all four MSS bands.

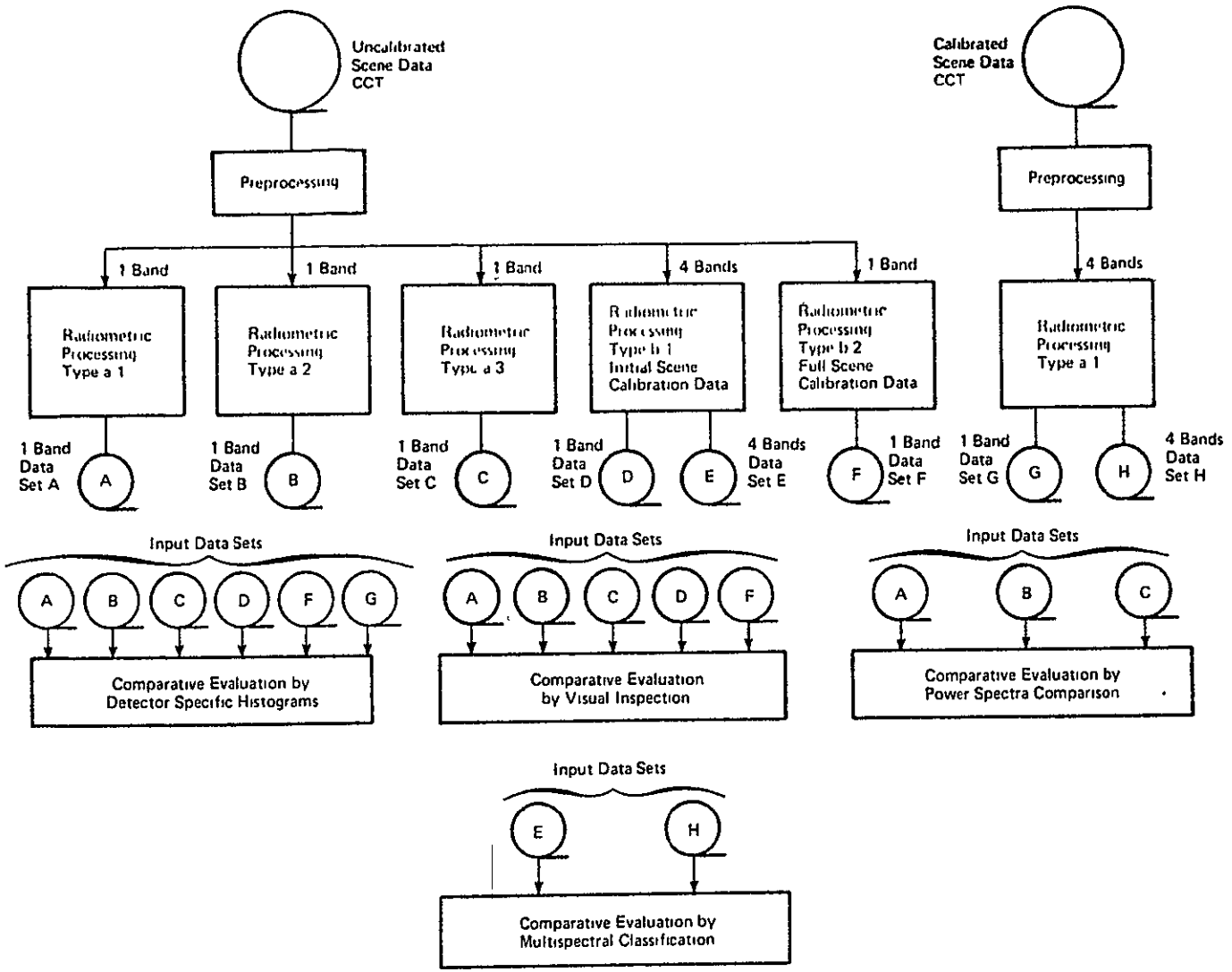

Figure 3-1. Data Flow for Radiometric Processing Evaluations

3.1 EVALUATION BY DETECTOR-SPECIFIC HISTOGRAMS

A comparative evaluation among images of MSS band 1 was made using radiometrically uncalibrated data processed by the type a1, a2, and a3 destriping procedures and the type b1 and b2 MSS calibration procedures, and radiometrically calibrated data processed by the type a1 destriping procedure. The evaluation was made on the basis of histograms of the data reported from each of the six MSS detectors in each of the six radiometrically processed spectral images. Detector-specific and aggregate histograms of this data were generated, and the consistency of each individual detector histogram with the corresponding aggregate histogram was considered. These histograms are presented in Figures 3.1-1 through 3.1-6.

A conventional statistical approach to evaluating the goodness of fit between the aggregate histograms and their associated detector-specific histograms was used to test the hypothesis that the frequency distribution of pixel values for an individual detector is one sixth of the frequency distribution of pixel values over all detectors, using the statistic:

$$X_j^2 = \sum_{i=1}^{k} \frac{N_{ji} - (N_i/6)}{(N_i/6)}$$

Where N_{ji} is the number of occurrences of pixel value i for detector j, and

N_i is the number of occurrences of pixel value i for all detectors.

All of the calculated X_j^2 values for the histogram sets, as given in Table 3.1-1, greatly exceed the critical X^2 value at the 0.005 level of significance (i.e., there is less than a 0.5% probability that a random set of pixel values, taken from a population whose frequency distribution is given by the aggregate histogram, would show such poor agreement with

the aggregate histogram), forcing the conclusion that none of the processing techniques has achieved a completely satisfactory equalization across the detectors.

The calculated X_j^2 values do, however, provide a summary measure of the deviations of the distributions in each of the detector-specific histograms from the distribution in the corresponding aggregate histograms. By summing the X_j^2 values for the six detectors of a spectral image, an overall measure of these deviations is obtained which can be used to rank the performance of the various radiometric processing techniques. On this basis the best equalization of the detector histograms was obtained with the type a2 processing of the uncalibrated scene data.

Table 3.1-1. Chi-squared Values for Comparison of Detector-Specific Histograms

Radiometric Processing	Degrees of Freedom in X^2	X_j^2 Values						Sum of X_j^2	$X^2_{0.005}$
		j = 1	j = 2	j = 3	j = 4	j = 5	j = 6		
Uncalibrated Scene Data after Type a1 Processing	10	254587	1316226	375530	9126	39104	8929	2,003,503	25.2
Uncalibrated Scene Data after Type a2 Processing	10	36392	50097	65716	47192	127396	52941	379,733	25.2
Uncalibrated Scene Data after Type a3 Processing	10	35113	178514	41636	80355	102538	80897	519,054	25.2
Uncalibrated Scene Data after Type b1 Processing	17	487846	69935	174762	67419	92641	63042	955,646	35.7
Uncalibrated Scene Data after Type b2 Processing	17	488333	69918	175037	67403	92638	63020	956,348	35.7
Calibrated Scene Data after Type a1 Processing	19	130507	104505	259655	341799	417700	421118	1,675,284	38.6

PIXEL INTENSITY DISTRIBUTIONS: LANDSAT SCENE 2183-16433 BAND 4 UNCALIBRATED, UNSTRIPED, LINE-LENGTH ADJUSTED

PIXEL VALUE	DETECTOR 1 OF 6	DETECTOR 2 OF 6	DETECTOR 3 OF 6	DETECTOR 4 OF 6	DETECTOR 5 OF 6	DETECTOR 6 OF 6	AGGREGATE HISTOGRAM
4	0	0	0	0	0	1	1
5	0	0	0	0	0	0	0
6	0	0	0	0	0	0	0
7	0	0	0	0	0	0	0
8	0	0	0	0	0	0	0
9	0	0	0	0	0	0	0
10	0	0	0	0	0	0	0
11	0	0	0	0	0	0	0
12	0	9	13	7	1	0	30
13	30	106	222	138	69	78	643
14	424	418	598	465	479	474	2854
15	972	770	1227	833	959	877	5638
16	2992	3163	5333	2401	3681	2405	20075
17	21755	18228	32271	16445	28769	16620	142088
18	960777	811131	1293608	839044	1267308	846895	6020973
19	2008772	1830166	2313608	1906477	2481908	1905896	12446741
20	2771748	2741618	2920828	2859678	3159268	2830658	17283754
21	2681158	2863808	2534258	2866728	2586988	2860998	16393938
22	1885978	2029388	1548788	1899848	1460748	1970918	10795628
23	1031488	1046048	745338	1031718	660588	1000868	5510028
24	478748	523288	350678	455558	287668	467408	2563348
25	206248	210368	150648	206368	117988	198398	1089938
26	99678	98908	76348	100188	54198	95178	524458
27	44868	46908	35968	51528	26278	46138	253648
28	23098	25138	19918	25358	14178	22628	130278
29	13428	14358	11528	15048	7388	13568	75278
30	7168	8678	6938	9898	3708	7528	43898
31	2958	3988	3128	4748	1698	3148	19628
32	1548	2048	1308	2208	478	2038	9588
33	368	618	428	1208	128	888	3798
34	228	158	78	428	38	158	1048
35	58	58	48	28	38	118	308
36	48	88	38	88	08	28	258
37	28	18	18	48	08	18	98
38	28	08	38	08	08	28	78
39	08	18	08	38	18	18	68
40	28	28	08	18	08	18	68
41	18	08	18	28	08	18	58
42	38	28	18	18	08	18	88
43	08	08	08	08	08	18	18
44	18	08	08	08	08	08	18
45	08	08	08	08	08	08	08
46	08	08	08	08	08	08	08
47	08	08	18	08	08	08	18

Figure 3.1-1. Detector-specific Histograms for Uncalibrated Scene Data from MSS Band 1 after Type al Radiometric Processing

PIXEL INTENSITY DISTRIBUTIONS: LANDSAT SCENE 2183-16433 BAND 4 UNCALIBRATED, UNSTRIPED (TYPE B)

PIXEL VALUE	DETECTOR 1 OF 6	DETECTOR 2 OF 6	DETECTOR 3 OF 6	DETECTOR 4 OF 6	DETECTOR 5 OF 6	DETECTOR 6 OF 6	AGGREGATE HISTOGRAM
2	0	0	0	0	0	1	1
3	0	0	0	0	0	0	0
4	0	0	0	0	0	0	0
5	0	0	0	0	0	0	0
6	0	0	0	0	0	0	0
7	0	0	0	0	0	0	0
8	0	0	0	0	0	0	0
9	0	0	0	0	0	0	0
10	0	0	0	0	0	0	0
11	0	0	13	7	1	0	21
12	24	43	222	138	69	73	569
13	401	381	0	467	479	465	2193
14	819	697	594	839	959	877	4765
15	2552	2005	1227	2511	3681	2381	14357
16	21130	11644	5333	16542	0	16334	71183
17	0	70015	39271	84234	29769	84407	307696
18	95904	174287	129360	0	126730	0	526281
19	201116	0	231360	190986	248190	190455	1062107
20	277465	277061	292082	285941	315926	283354	1731829
21	268527	295794	253425	286439	258698	286529	1649412
22	188584	211774	154878	189752	0	197244	942232
23	103406	107200	74533	103000	146074	100132	634345
24	48014	54284	0	45487	66058	46740	260563
25	20682	21744	35067	20611	28766	19852	146722
26	9972	10245	15064	10005	11794	9526	66606
27	4498	4982	7634	5151	5419	0	27664
28	0	2568	3596	0	0	4614	10778
29	2313	0	1991	2529	2627	2264	11724
30	1343	1470	1152	1499	1417	1356	8237
31	719	888	693	988	738	754	4760
32	298	411	312	471	370	315	2177
33	155	212	130	220	169	203	1089
34	36	81	42	120	0	88	367
35	22	15	0	42	47	15	141
36	5	5	7	2	12	0	31
37	4	8	4	8	3	11	38
38	0	0	3	4	3	2	12
39	2	1	1	0	0	1	5
40	2	0	3	0	0	2	7
41	0	1	0	3	0	1	5
42	2	2	0	1	0	1	6
43	1	0	1	2	1	1	6
44	3	2	1	1	0	0	7
45	0	0	0	0	0	1	1
46	1	0	0	0	0	1	2
47	0	0	0	0	0	0	0
48	0	0	0	0	0	0	0
49	0	0	0	0	0	0	0
50	0	0	1	0	0	0	1

Figure 3.1-2. Detector Specific Histograms for Uncalibrated Scene Data from MSS Band 1 after Type a2 Radiometric Processing

PIXEL INTENSITY DISTRIBUTIONS: LANDSAT SCENE 2183-16433 BAND 4 UNCALIBRATED, UNSTRIPED (TYPE C)

PIXEL VALUE	DETECTOR 1 OF 6	DETECTOR 2 OF 6	DETECTOR 3 OF 6	DETECTOR 4 OF 6	DETECTOR 5 OF 6	DETECTOR 6 OF 6	AGGREGATE HISTOGRAM
1	0	0	0	0	0	1	1
2	0	0	0	0	0	0	0
3	0	0	0	0	0	0	0
4	0	0	0	0	0	0	0
5	0	0	0	0	0	0	0
6	0	0	0	0	0	0	0
7	0	0	0	0	0	0	0
8	0	0	0	0	0	0	0
9	0	0	0	0	0	0	0
10	0	0	0	0	0	0	0
11	0	0	13	7	1	0	21
12	24	43	222	138	69	73	569
13	401	381	594	467	479	465	2787
14	819	697	0	839	959	877	4191
15	2552	2005	1227	2611	3681	2381	14357
16	21130	11844	5333	16542	0	16334	71183
17	0	70015	39271	84234	29769	84407	307696
18	95904	174287	129360	0	126730	0	526281
19	201116	277061	231360	190986	248190	190455	1339168
20	277465	0	292082	285941	315926	283354	1454768
21	268527	295794	253425	286439	258698	286529	1649412
22	188584	211774	154878	189752	0	197244	942232
23	103406	107200	74533	103000	146074	100132	634345
24	48014	54284	0	45487	66058	46740	260583
25	20582	21744	35067	20611	28766	19852	146722
26	9972	10245	15064	10005	11794	9526	66606
27	0	4962	7634	0	5419	0	18015
28	4498	0	3596	5151	0	4614	17859
29	2313	2568	1991	2529	2627	2264	14292
30	1343	1470	1152	1499	1417	1356	8237
31	719	888	693	988	738	754	4780
32	298	411	312	471	370	315	2177
33	155	212	130	220	169	203	1089
34	36	81	0	120	0	88	325
35	22	15	42	42	47	0	168
36	5	0	7	2	12	15	41
37	0	5	4	0	3	11	23
38	4	8	3	8	3	2	28
39	2	1	1	4	0	1	9
40	2	0	3	0	0	2	7
41	0	1	0	3	0	1	5
42	2	2	0	1	0	1	6
43	1	0	1	2	1	0	5
44	3	0	0	1	0	1	5
45	0	2	1	0	0	1	4
46	1	0	0	0	0	1	2
47	0	0	0	0	0	0	0
48	0	0	0	0	0	0	0
49	0	0	0	0	0	0	0
50	0	0	1	0	0	0	1

Figure 3.1-3. Detector-specific Histograms for Uncalibrated Scene Data from MSS Band 1 after Type a3 Radiometric Processing

PIXEL INTENSITY DISTRIBUTIONS: LANDSAT SCENE 2183-16433 BAND 4 UNCALIBRATED, UNSTRIPED (TYPE B)

PIXEL VALUE	DETECTOR 1 OF 6	DETECTOR 2 OF 6	DETECTOR 3 OF 6	DETECTOR 4 OF 6	DETECTOR 5 OF 6	DETECTOR 6 OF 6	AGGREGATE HISTOGRAM
2	0	0	0	0	0	1	1
3	0	0	0	0	0	0	0
4	0	0	0	0	0	0	0
5	0	0	0	0	0	0	0
6	0	0	0	0	0	0	0
7	0	0	0	0	0	0	0
8	0	0	0	0	0	0	0
9	0	0	0	0	0	0	0
10	0	0	0	0	0	0	0
11	0	0	13	7	1	0	21
12	24	43	0	138	69	73	347
13	401	381	222	0	479	465	1948
14	819	0	598	467	0	0	1880
15	0	697	0	839	0	0	1536
16	2552	0	1227	0	959	877	5615
17	0	2005	5333	2511	3681	2381	15911
18	21130	17844	0	16542	0	16334	65850
19	0	70015	39271	0	29769	84407	223462
20	95904	0	129360	84234	126730	0	436228
21	201116	174267	0	0	0	0	375403
22	277465	0	231360	190586	248190	190455	1138456
23	0	0	0	285941	0	0	285941
24	0	277061	0	0	0	283354	560415
25	268527	295794	292082	286439	315926	286529	1745297
26	0	0	253425	0	258698	0	512123
27	188584	211774	0	189752	0	197244	787354
28	0	0	154878	0	0	0	154878
29	103406	107200	74533	103000	146074	100132	634345
30	0	0	0	0	66058	0	66058
31	48014	54284	0	45487	0	46740	194525
32	0	0	35067	0	0	0	35067
33	20682	21744	0	20611	28766	19852	111655
34	0	0	15064	0	0	0	15064
35	9972	0	0	10005	11794	0	31771
36	0	10245	0	5151	0	9526	24922
37	0	0	7634	0	0	0	7634
38	4498	4962	0	0	5419	4614	19493
39	0	2568	3596	2529	0	2264	10957
40	0	0	1991	0	0	0	1991
41	2313	0	0	1499	2627	0	6439
42	0	1470	0	0	1417	1356	4243
43	1343	0	1152	988	0	0	3483
44	0	888	0	0	738	754	2380
45	719	0	693	471	0	0	1883
46	0	411	0	0	0	315	726
47	298	0	312	0	370	0	980
48	0	0	0	220	0	0	220
49	0	212	0	0	0	203	415
50	155	0	130	120	169	0	574
51	0	81	0	0	0	88	169
52	36	0	42	42	47	0	167
53	0	15	0	0	0	15	30
54	0	0	0	2	0	0	2
55	22	0	7	0	12	0	41
56	0	5	0	8	0	11	24
57	0	0	4	0	3	0	7
58	5	8	0	0	0	2	15
59	0	0	3	4	0	0	7
60	4	0	0	0	3	1	8
61	0	1	0	0	0	0	1
62	0	0	1	0	0	0	1
63	2	0	0	0	0	2	4
64	0	0	3	3	0	0	6
65	0	0	0	0	0	0	0
66	2	1	0	0	0	1	4
67	0	0	0	1	0	0	1
68	0	0	0	0	0	0	0
69	0	2	0	0	0	1	3
70	0	0	0	0	0	0	0
71	2	0	0	2	0	0	4
72	0	0	0	0	1	1	2
73	0	0	0	1	0	0	1
74	0	0	1	0	0	0	1
75	1	0	0	0	0	0	1
76	0	2	0	0	0	1	3
77	3	0	0	0	0	0	3
78	0	0	1	0	0	1	2
79	0	0	0	0	0	0	0

Figure 3.1-4. Detector-specific Histograms for Uncalibrated Scene Data from MSS Band 1 after Type b1 Radiometric Processing

PIXEL INTENSITY DISTRIBUTIONS: LANDSAT SCENE 2183-16433 BAND 4 UNCALIBRATED, UNSTRIPED (TYPE F)

PIXEL VALUE	DETECTOR 1 OF 6	DETECTOR 2 OF 6	DETECTOR 3 OF 6	DETECTOR 4 OF 6	DETECTOR 5 OF 6	DETECTOR 6 OF 6	AGGREGATE HISTOGRAM
2	0	0	0	0	0	1	1
3	0	0	0	0	0	0	0
4	0	0	0	0	0	0	0
5	0	0	0	0	0	0	0
6	0	0	0	0	0	0	0
7	0	0	0	0	0	0	0
8	0	0	0	0	0	0	0
9	0	0	0	0	0	0	0
10	0	0	0	0	0	0	0
11	0	0	13	7	1	0	21
12	24	43	0	138	69	73	347
13	401	381	222	0	479	465	1948
14	819	0	594	467	0	0	1880
15	0	697	0	839	0	0	1536
16	2552	0	1227	0	959	877	5615
17	0	2005	5333	2511	3681	2381	15911
18	21130	11844	0	16542	0	16334	65850
19	0	70015	39271	0	29769	84407	223462
20	95904	0	129360	84234	126730	0	436228
21	201116	174267	0	0	0	0	375403
22	277465	0	231360	190986	248190	190455	1138456
23	0	0	0	285941	0	0	285941
24	0	277061	0	0	0	283354	560415
25	268927	295794	292082	286439	315926	286529	1745297
26	0	0	253425	0	258698	0	512123
27	188584	211774	0	189752	0	197244	787354
28	0	107200	154878	0	0	0	262078
29	103406	0	74533	103000	146074	100132	527145
30	0	0	0	0	66058	0	66058
31	48014	54264	0	45487	0	46740	194525
32	0	0	35067	0	0	0	35067
33	20682	21744	0	20611	28766	19852	111655
34	0	0	15064	0	0	0	15064
35	9972	0	0	10005	11794	0	31771
36	0	10245	0	5151	0	9526	24922
37	0	0	7634	0	0	0	7634
38	4498	4962	0	0	5419	4614	19493
39	0	2568	3596	2529	0	2264	10957
40	0	0	1991	0	0	0	1991
41	2313	0	0	1499	2627	1356	7795
42	0	1470	0	0	1417	0	2887
43	1343	0	1152	988	0	0	3483
44	719	888	0	0	738	754	3099
45	0	0	693	471	0	0	1164
46	0	411	0	0	0	315	726
47	298	0	312	0	370	0	980
48	0	0	0	220	0	0	220
49	0	212	0	0	0	203	415
50	155	0	130	120	169	0	574
51	0	81	0	0	0	88	169
52	36	0	42	42	47	0	167
53	0	15	0	0	0	15	30
54	0	0	0	2	0	0	2
55	22	0	7	0	12	0	41
56	0	5	0	8	0	11	24
57	0	0	4	0	3	0	7
58	5	8	0	0	0	2	15
59	0	0	3	0	0	4	7
60	4	0	0	0	3	1	8
61	0	1	0	0	0	0	1
62	0	0	1	0	0	0	1
63	2	0	0	0	0	2	4
64	0	0	3	0	0	0	6
65	2	0	0	0	0	0	2
66	0	0	0	0	0	1	1
67	0	1	0	1	0	0	2
68	0	0	0	0	0	1	1
69	0	2	0	0	0	0	2
70	0	0	0	0	0	0	0
71	2	0	0	2	0	0	4
72	0	0	0	0	1	1	2
73	0	0	0	1	0	0	1
74	0	0	1	0	0	0	1
75	1	0	0	0	0	1	2
76	0	2	0	0	0	0	2
77	3	0	1	0	0	0	4
78	0	0	0	0	0	1	1
79	0	0	0	0	0	0	0

Figure 3.1-5. Detector-specific Histograms for Uncalibrated Scene Data from MSS Band 1 after Type b2 Radiometric Processing

PIXEL INTENSITY DISTRIBUTIONS: LANDSAT SCENE 2163-16433 BAND4 CALIBRATED COMPLETE IMAGE

PIXEL VALUE	DETECTOR 1 OF 6	DETECTOR 2 OF 6	DETECTOR 3 OF 6	DETECTOR 4 OF 6	DETECTOR 5 OF 6	DETECTOR 6 OF 6	AGGREGATE HISTOGRAM
1	0	0	0	0	0	1	1
2	0	0	0	0	0	0	0
3	0	0	0	0	0	0	0
4	0	0	0	0	0	0	0
5	0	0	0	0	0	0	0
6	0	0	0	0	0	0	0
7	0	0	0	0	0	0	0
8	0	0	0	0	0	0	0
9	0	0	0	0	0	0	0
10	0	0	0	4	1	0	5
11	0	10	13	85	21	9	138
12	9	52	218	86	55	106	496
13	139	362	574	194	462	423	2154
14	538	0	22	448	10	60	1078
15	1535	697	2	340	946	910	4430
16	1575	2005	1197	647	1674	2144	9242
17	0	11844	5250	4166	2392	2252	25904
18	10098	42887	38747	14564	29128	21549	156973
19	56427	27128	128405	5965	124994	77084	420003
20	71828	0	1592	78269	2005	15199	168893
21	133156	174287	3958	7132	56339	174510	549382
22	196618	0	225836	191792	191851	4364	810461
23	127488	277061	1566	278003	0	186436	870554
24	162777	295794	289890	5223	312650	112853	1179187
25	195750	0	254188	282480	260413	266976	1169807
26	0	4505	1429	188488	1561	10891	206874
27	141442	207269	144434	0	383	189812	683340
28	129452	107200	10998	2176	145085	96474	491385
29	21096	0	73979	100824	66483	199	262581
30	0	54284	0	249	181	31423	86137
31	40084	0	35007	45238	2105	15317	137751
32	25208	20823	60	93	26601	910	73695
33	3404	921	15038	20518	60	18901	58842
34	3349	23	26	31	11730	576	15735
35	6073	10222	131	9997	64	8927	35414
36	550	6	7583	5128	48	64	13299
37	3544	4966	6	10	5354	1422	15302
38	954	2558	3590	2497	17	3341	12957
39	148	7	1989	29	2614	2110	6897
40	1680	668	2	229	1416	125	4120
41	485	795	899	1263	14	1220	4676
42	964	1	253	20	0	37	1275
43	777	887	9	968	735	558	3934
44	287	2	684	6	3	174	1156
45	34	409	0	465	291	53	1252
46	190	1	312	1	79	260	843
47	108	131	0	219	0	46	504
48	46	80	83	0	166	159	534
49	97	0	47	120	3	0	267
50	12	81	0	0	28	72	193
51	25	0	42	37	19	14	137
52	11	15	0	5	0	4	35
53	0	0	7	0	12	13	32
54	17	4	0	2	0	4	27
55	5	1	1	1	2	7	17
56	4	0	3	7	1	1	16
57	1	8	0	0	0	0	9
58	0	0	3	4	3	1	11
59	3	1	0	0	0	0	4
60	1	0	1	0	0	1	3
61	0	0	0	0	0	0	0
62	2	0	1	0	0	3	6
63	0	0	2	3	0	0	5
64	0	0	0	0	0	0	0
65	2	1	0	0	0	0	3
66	0	0	0	0	0	0	0
67	0	2	0	1	0	0	3
68	0	0	0	0	0	2	2
69	1	0	0	1	1	0	3
70	1	0	0	1	0	0	2
71	0	0	0	0	0	0	0
72	0	0	1	1	0	0	2
73	1	0	0	0	0	0	1
74	0	1	0	0	0	1	2
75	1	1	1	0	0	1	4
76	2	0	0	0	0	0	2
77	0	0	0	0	0	0	0

Figure 3.1-6. Detector-specific Histograms for Calibrated Scene Data from MSS Band 1 after Type al Radiometric Processing

3.2 EVALUATION BY VISUAL INSPECTION

A comparative evaluation among images of MSS Band 1 was made using radiometrically uncalibrated data processed by the type a1, a2, and a3 destriping procedures and the type b1 and b2 MSS calibration procedures. The method of evaluation was visual inspection of film recordings of the radiometrically processed images. The images were ranked on the basis of the visually apparent striping which they exhibited.

Photographic prints of the scene data used in this visual evaluation are presented as Plates 1 through 6. The actual evaluation was made from the negatives used to produce these prints, in order to avoid any variations which might be introduced in producing prints from the negatives, and to provide the best possible presentation of the data during evaluation. Negatives of image data for the five radiometrically processed versions of the scene for MSS band 1 (0.5 to 0.6 micrometers), together with a negative of the unprocessed, uncalibrated data, were arranged randomly in a two-wide by three-high array and uniformly illuminated from behind. Five experienced members of IBM's digital image processing group were then asked to rank the six images on the basis of the visually apparent striping.

The rankings which were obtained are presented in Table 3.2-1, together with an overall ranking obtained by summing the individual rankings. On the basis of this overall ranking, the type a2 processing of uncalibrated scene data is clearly preferred.

Table 3.2-1. Results of Visual Evaluation of Radiometrically Processed Scene Data for Landsat MSS Scene 2183 - 16433, MSS Band 1

Image Number	Image Description	Rankings Obtained*					Overall Ranking
		Case 1	Case 2	Case 3	Case 4	Case 5	
1	Uncalibrated scene data, type b1 radiometric processing	1	2	4	3	3	13
2	Uncalibrated scene data, type a1 radiometric processing	1	5	5	2	1	14
3	Uncalibrated scene data, type b2 radiometric processing	1	1	1	5	5	13
4	Uncalibrated scene data, type a2 radiometric processing	1	3	2	1	2	9
5	Uncalibrated scene data, type a3 radiometric processing	1	4	3	4	4	16
6	Uncalibrated, unprocessed scene data	6	6	6	6	6	30

* 1 = best
  6 = worst

3.3 EVALUATION BY POWER SPECTRA ANALYSIS

A comparative evaluation among images of one spectral band was made using radiometrically uncalibrated data processed by the type a1, a2, and a3 destriping procedures. The method of evaluation was power spectra comparison.

Power spectra for two 128-line by 50 sample subimages were generated for each of these radiometrically processed images. The subimages were chosen to provide power spectra of a low frequency and a high frequency region. Power spectra were taken only in the "along track" direction of the image, since the linear gain and offset radiometric transformations employed by the destriping and calibration procedures have known effects on the power spectra in the along scan direction. The specific subimages are identified in Plate 7, which is an overlay for Plates 1 through 6.

The power spectra obtained for this evaluation for regions in the uncalibrated scene data and in the three radiometrically processed scenes are presented in Figures 3.3-1 through 3.3-12. In these figures, the abscissa is the unnormalized squared value of the discrete Fourier coefficient, while the ordinate is the index of the coefficient, and ranges from 0 to the index corresponding to the folding frequency, which is 64 for the 128-line transforms used in this evaluation.

In engineering terms, the spacing between the Fourier components is:

$$\Delta F = \frac{1}{(128 \text{ lines})(80 \text{ meters})} = 9.766 \times 10^{-5} \text{ cycles/meter}$$

while the frequency range of the plotted spectra is:

$$F_f = 64(\Delta F) = 6.25 \times 10^{-3} \text{ cycles/meter.}$$

Components of the power spectra which correspond to striping would be expected to occur at intervals of:

$$F_{st} = \frac{1}{6\ (80\ \text{meters})} = 2.083\ X\ 10^{-3}\ \text{cycles/meter},$$

corresponding to index values $i = n\,[(1/480)] \Big/ [(128)(80)]$ where n is an integer. For the frequency range of the plotted spectra, i = 21.3, 42.7, and 64.

In the power spectra of the high frequency region presented in Figures 3.3-1 through 3.3-4, there is only minimal evidence in the uncalibrated scene data of greater power concentration at those frequencies which would correspond to striping than at other points in the spectra, and there is less evidence of this effect for the processed data. The peak in spectral power which is seen at the folding frequency, in the absence of lower frequency striping-related harmonics, cannot justifiably be attributed to striping, since power at this frequency alone corresponds to a two-line periodicity rather than a six-line periodicity. In the power spectra of the low frequency region presented in Figures 3.3-5 through 3.3-8, the expected concentration of power at the frequencies corresponding to striping is evident, in the unprocessed data, as is the suppression of power at these frequencies which results from the three different types of radiometric processing.

A less complex power spectrum comparison of the striping in these images is provided by power spectra which were generated for a smaller (30 sample by 64 line) low frequency region contained entirely within the originally defined low frequency region and containing only image samples of the Missouri River. These spectra are presented as Figures 3.3-9 through 3.3-12. The simple power spectrum of this uniform-level subimage provides a background against which the power concentrations at the striping frequencies are much more apparent than they are for the power

spectra of Figures 3.3-1 through 3.3-8. For this smaller region, the Fourier coefficient indices calculated for the striping frequencies are 10.7, 21.3, and 32.0, and power concentrations are quite apparent near these values in Figure 3.3-9, the power spectrum obtained for the uncalibrated scent data.

A quantitative characterization of the power present at the striping frequencies for this small, low frequency subimage in the uncalibrated data and in the three processed data sets is presented in Table 3.3-1. In this table, the power levels at the striping frequencies are expressed in decibels above the average power level for the particular spectrum in order to normalize the data for this average, which differs among the source data sets. From this table, it is apparent that the type a3 radiometric processing is most effective in suppressing the power at the fundamental striping frequency, and the type a2 radiometric processing is marginally better than type a3 at suppressing the first harmonic. Both of these techniques considerably enhance the relative power present at the folding frequency. An exact explanation for this effect is unknown, but the detector-specific histograms presented in Figures 3.1-1, 3.1-2, and 3.1-3 suggest that the "forbidden" pixel values produced by these two radiometric processing techniques, which are different for each detector, result in an effective increase in the quantization noise present in the image. Since such an increase would be detector-related, it could appear in the power spectrum at the highest frequency, the folding frequency.

Overall, the type a3 radiometric processing provides the most effective combined suppression of the fundamental and first harmonics of striping, and is the most effective technique on this basis.

Figure 3.3-1. Power Spectrum for High Frequency Region in Uncalibrated Scene Data

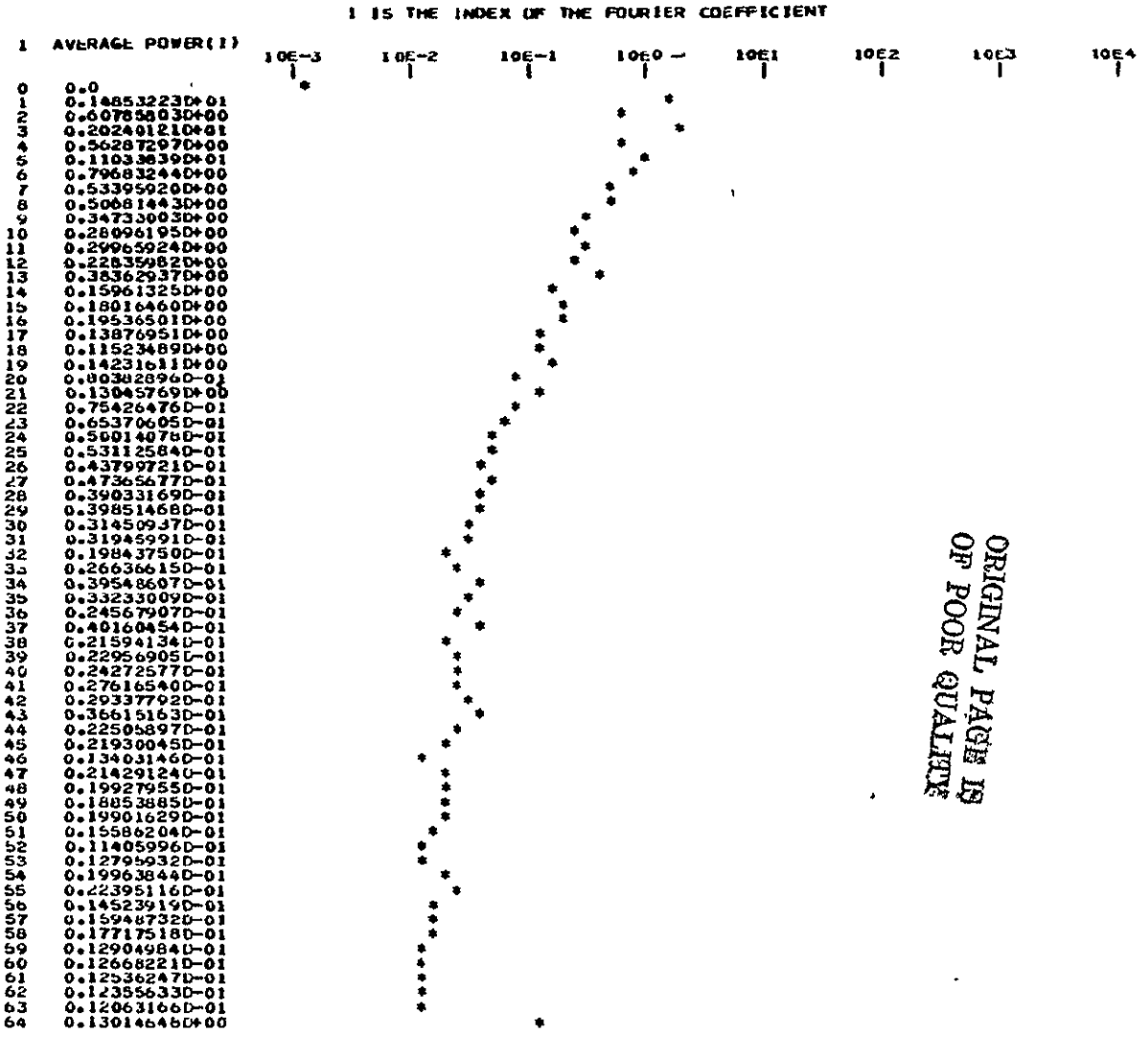

Figure 3.3-2. Power Spectrum for High Frequency Region in Uncalibrated Scene Data after Type al Processing

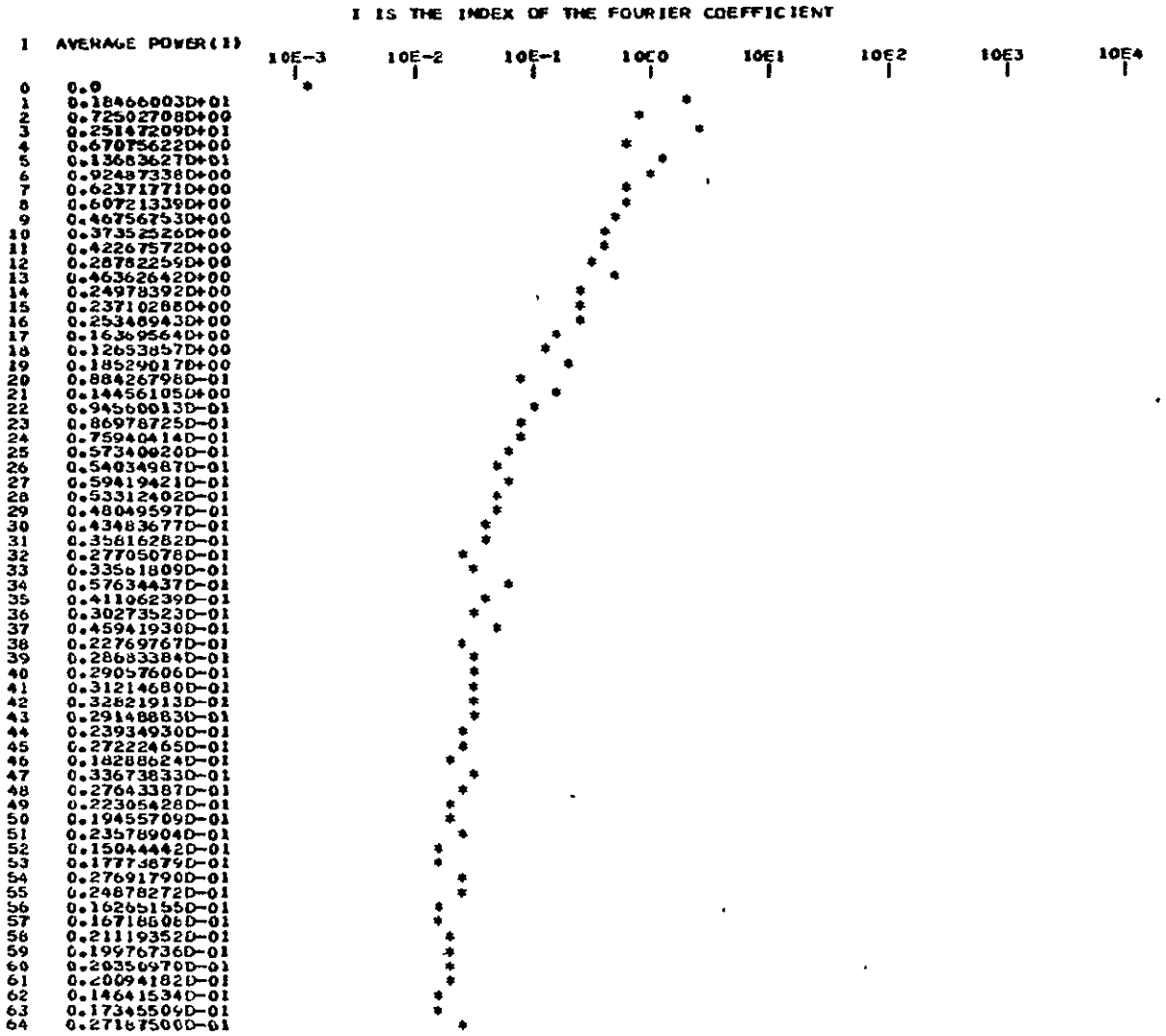

Figure 3.3-3. Power Spectrum for High Frequency Region in Uncalibrated Scene Data after Type a2 Processing

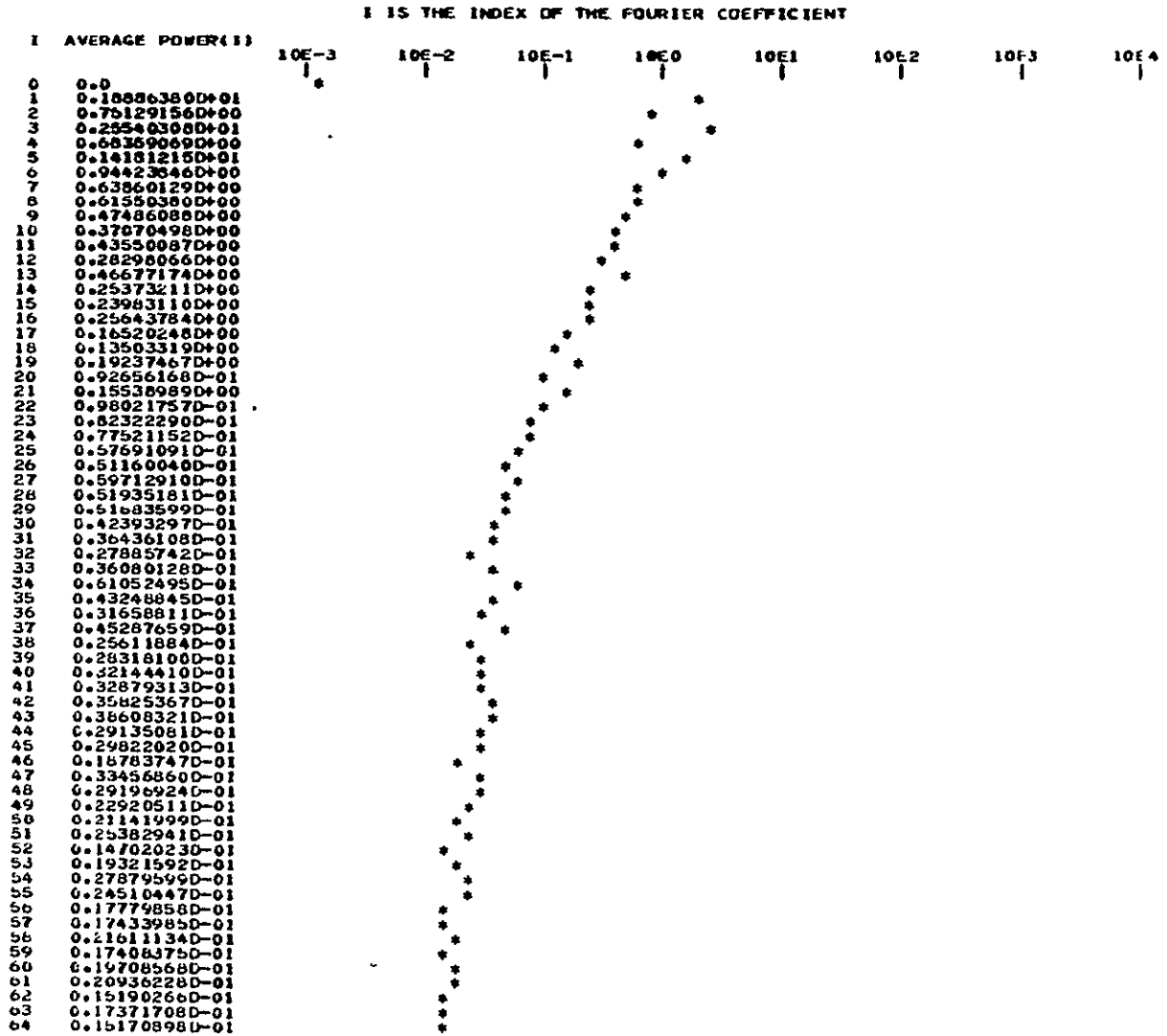

Figure 3.3-4. Power Spectrum for High Frequency Region in Uncalibrated Scene Data after Type a3 Processing

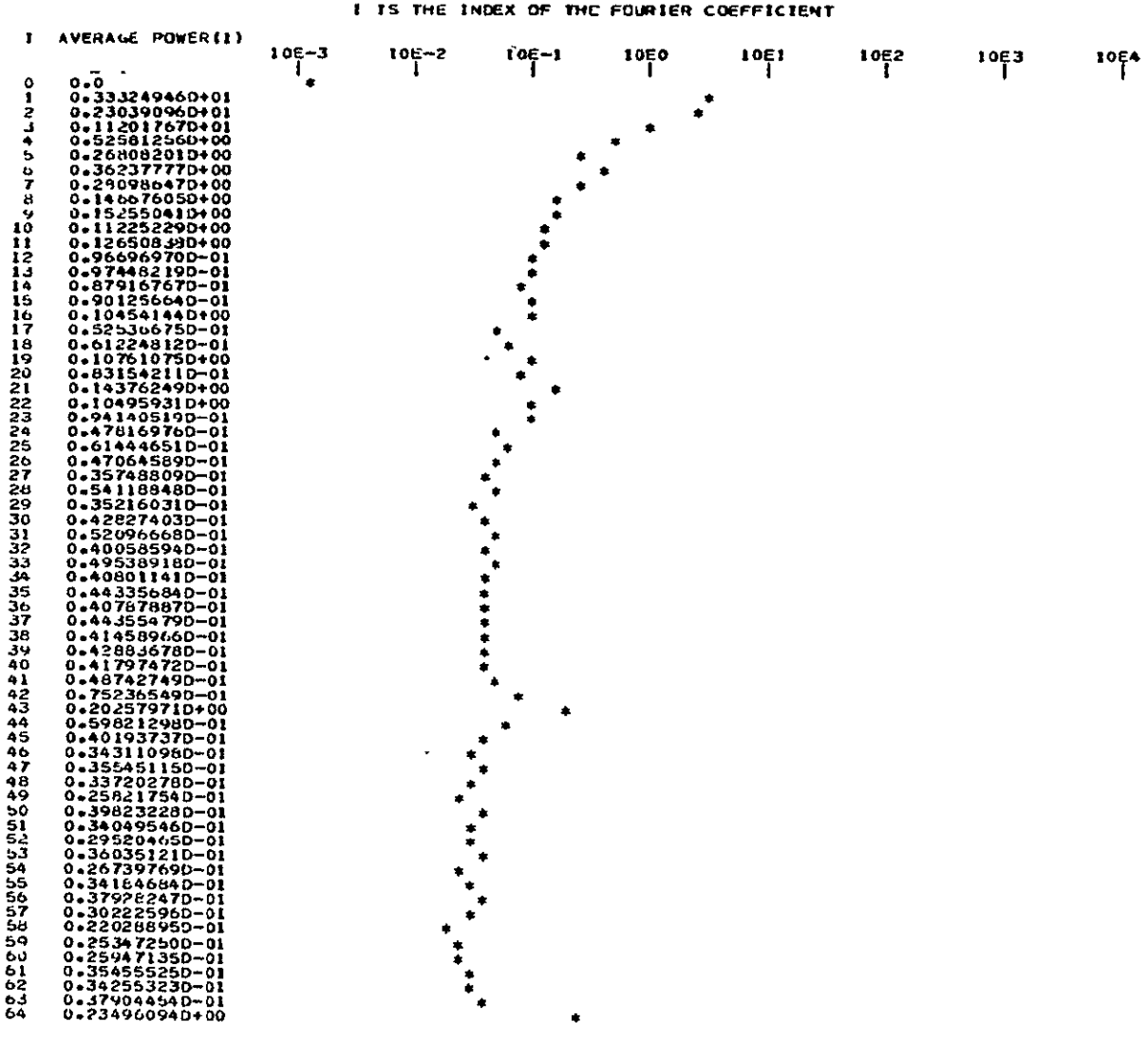

Figure 3.3-5. Power Spectrum for Low Frequency Region in Uncalibrated Scene Data

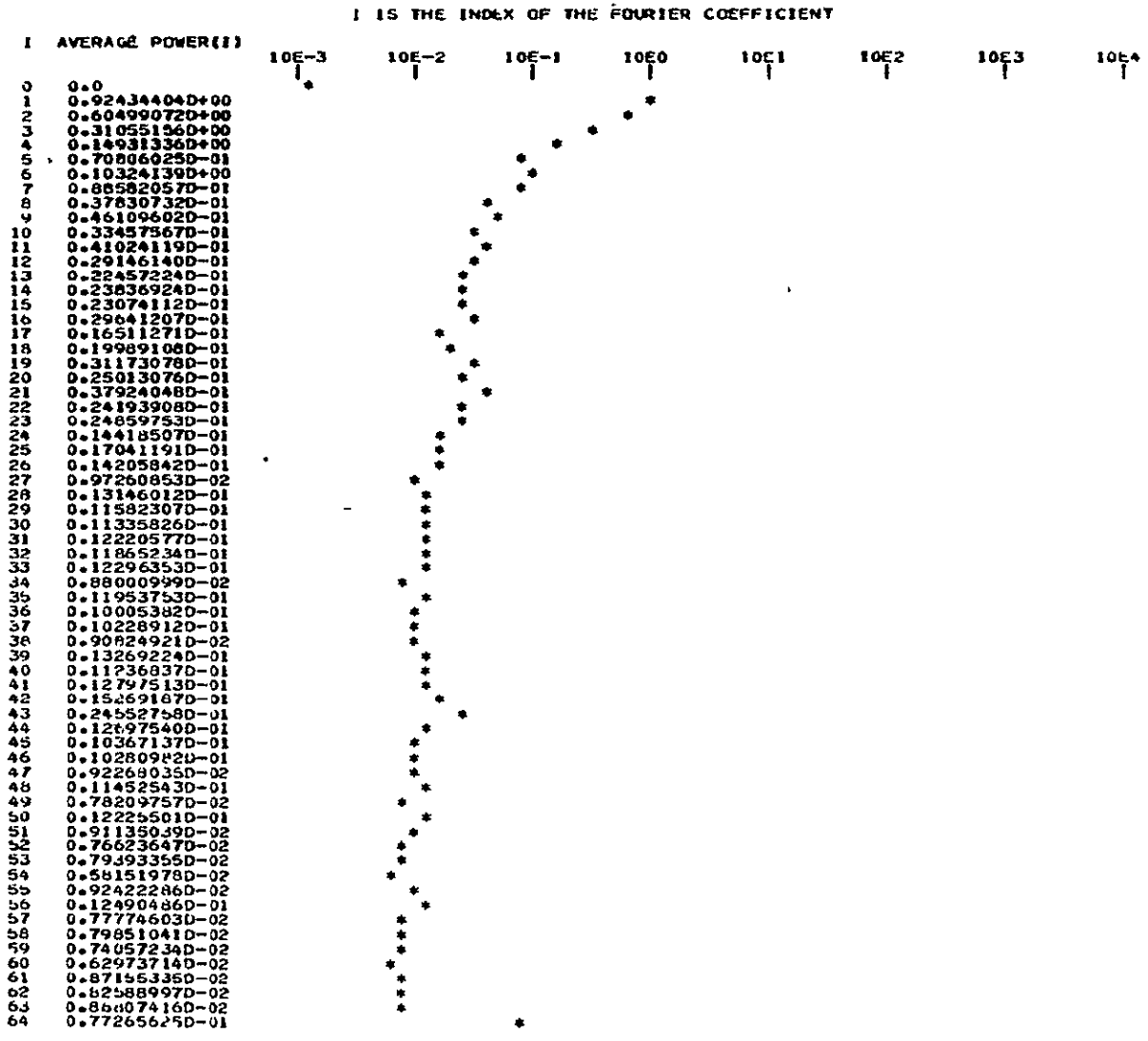

Figure 3.3-6. Power Spectrum for Low Frequency Region in Uncalibrated Scene Data after Type al Processing

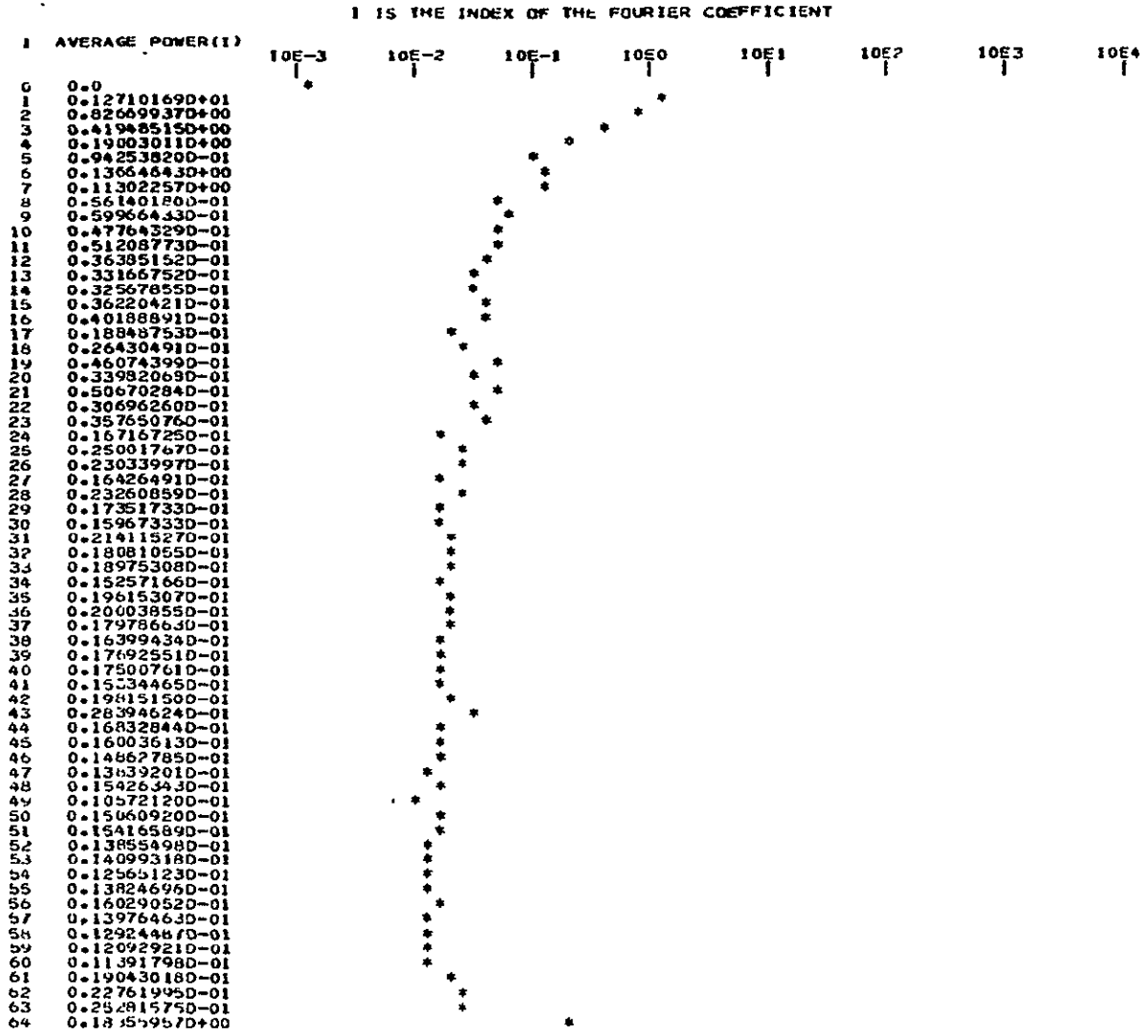

Figure 3.3-7. Power Spectrum for Low Frequency Region in Uncalibrated Scene Data after Type a2 Processing

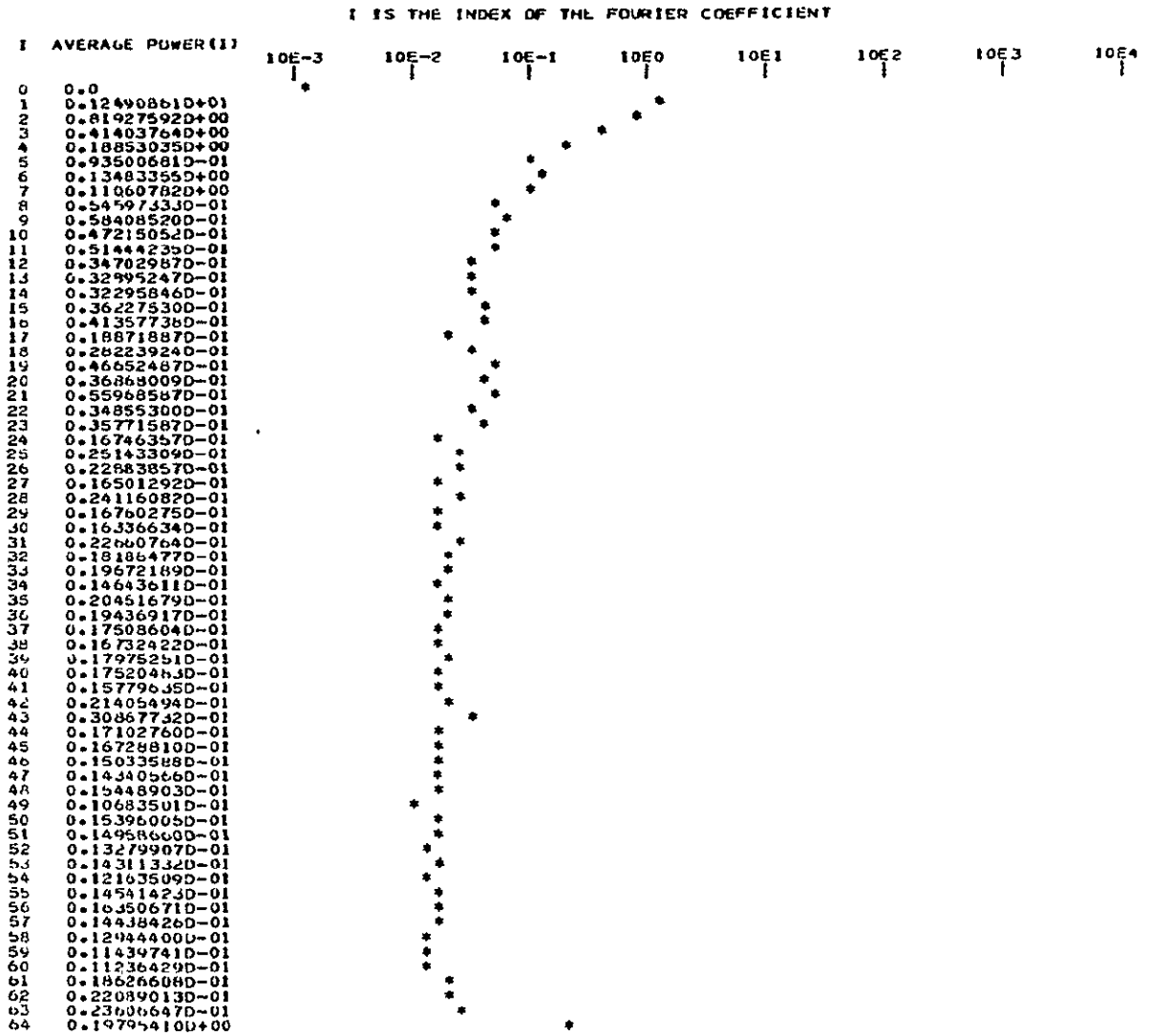

Figure 3.3-8. Power Specturm for Low Frequency Region in Uncalibrated Scene Data after Type a3 Processing

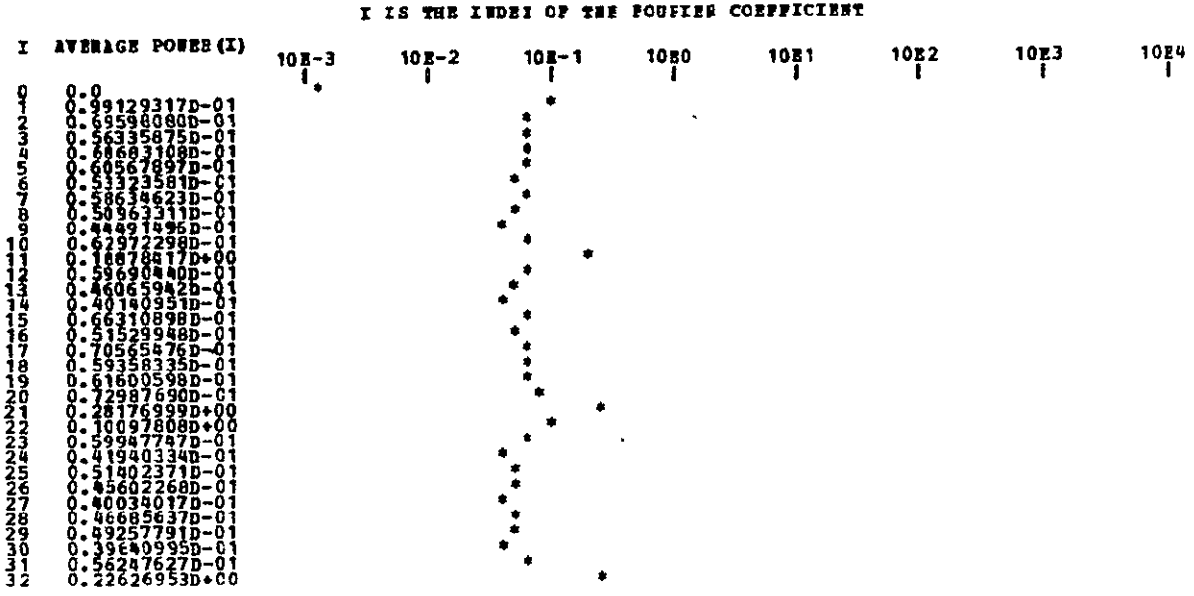

Figure 3.3-9. Power Spectrum for Smaller Low Frequency Region in Uncalibrated Scene Data

Figure 3.3-10. Power Spectrum for Smaller Low Frequency Region in Uncalibrated Scene Data after Type al Processing

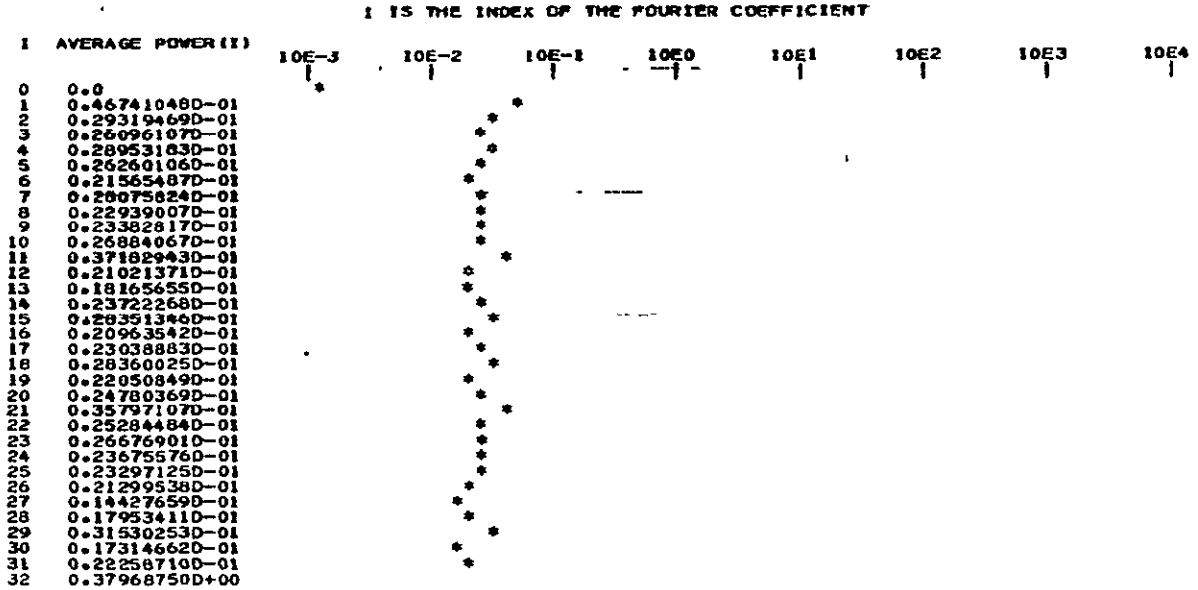

Figure 3.3-11. Power Spectrum for Smaller Low Frequency Region in Uncalibrated Scene Data after Type a2 Processing

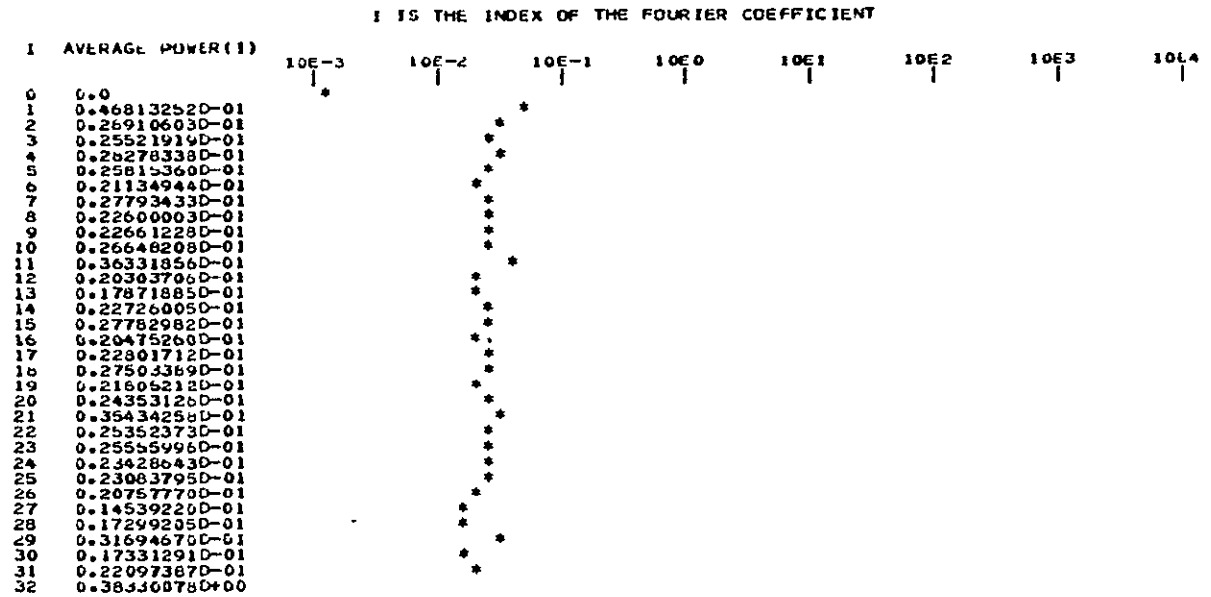

Figure 3.3-12. Power Spectrum for Smaller Low Frequency Region in Uncalibrated Scene Data after Type a3 Processing

Table 3.3-1. Relative (to Average Power) Power Spectrum Values for Restricted Low Frequency Image Region at Frequencies Corresponding to Striping

	Fundamental $i = 11$ $f = 2.15 \times 10^{-3}$ cycles/meter	First Harmonic $i = 21$ $f = 4.10 \times 10^{-3}$ cycles/meter	Second Harmonic $i = 32$ $f = 6.25 \times 10^{-3}$ cycles/meter
Uncalibrated Scene Data	4.04 db	5.78 db	4.83 db
Uncalibrated Scene Data after Type a1 Radiometric Processing	2.42 db	1.80 db	5.87 db
Uncalibrated Scene Data after Type a2 Radiometric Processing	0.08 db	-0.08 db	10.17 db
Uncalibrated Scene Data after Type a3 Radiometric Processing	0.02 db	-0.09 db	10.25 db

3.4 EVALUATION BY MULTISPECTRAL CLASSIFICATION

A comparative evaluation by multispectral classification was performed between two multispectral image data sets, one produced by application of the type b1 MSS calibration procedures to the four bands of uncalibrated MSS data and the other produced by application of type a1 destriping procedure to the four bands of calibrated MSS data.

Each four-band data set was evaluated using a parallelpiped (limit) classifier. For each data set, a training field for each of two classes was selected based on the ground truth data. These training fields were used to determine the class limits. A test field for each of these classes was identified, and the four-vectors within each of these fields were classified against the class limits for the class.

This procedure was then repeated, exchanging the definition of training and testing fields.

Plate 7 is an overlay for Plate 5 which identifies the location in the image data sets of the Hand County LACIE Intensive Study Site 2, which contained the fields employed in this evaluation. Figure 3.4-1 is a diagram of the field structure in this site, and the specific fields employed (5, 50, 204, and 270) are identified on this diagram.

The results obtained in these classification experiments are presented in Table 3.4-1. In all cases, the Type a1 radiometric processing on calibrated scene data has produced image data for which a higher percentage of the field pixels are correctly classified than has the Type b1 radiometric processing on uncalibrated data. However, if the evaluation is based on the volume of the four space parallelpiped which characterizes the classes, a preferred radiometric processing cannot be identified, since for spring wheat this volume is smaller for the Type a1 processing of calibrated data, while for oats this volume is smaller for the Type b1 processing of uncalibrated data.

Because of conflicting conclusions which resulted from this experiment, and because of the lack of spearation of the class regions in four-space which is evident in Table 3.4-1, no reliable conclusions can be drawn for this evaluation.

Table 3.4-1. Results of Evaluation by Multispectral Classification

Class	Field 1 ID	MSS Band	Class 4-Space Range (Counts)	Class Mean Vector (Counts)	No of Pixels	Field 2 ID	MSS Band	Class 4-Space Range (Counts)	Class Mean Vector (Counts)	No of Pixels	Radiometric Processing, Source Data	Percent of Pixels Correctly Classified / Number of Pixels Correctly Classified: Field 1 = Training, Field 2 = Test	Percent of Pixels Correctly Classified / Number of Pixels Correctly Classified: Field 2 = Training, Field 1 = Test
Mature Spring Wheat	204	1	6	23 5	42	270	1	11	26 0	30	Type a 1 Calibrated Data	13%	71%
		2	11	29 0			2	34	38 5			4 Pixels	30 Pixels
		3	12	53 5			3	18	60 5				
		4	7	28 0			4	9	30 0				
		4-Space Volume 5544					4-Space Volume 60588						
Mature Spring Wheat	204	1	7	24 0	42	270	1	14	28 5	30	Type b 1 Uncalibrated Data	3 3%	50%
		2	11	29 0			2	32	44 5			1 Pixel	21 Pixels
		3	11	55 0			3	19	62 0				
		4	7	28 0			4	11	31.0				
		4-Space Volume 5929					4-Space Volume 93622						
Mature Oats	5	1	13	27 0	37	50	1	11	26 0	24	Type a 1 Calibrated Data	83 3%	67 6%
		2	27	37 0			2	20	37 5			20 Pixels	25 Pixels
		3	19	62 0			3	23	56 0				
		4	6	30 5			4	11	28 0				
		4-Space Volume 40014					4-Space Volume 55660						
Mature Oats	5	1	8	29 5	37	50	1	7	29 0	24	Type b 1 Uncalibrated Data	54 2%	54 1%
		2	14	44 5			2	10	42 5			13 Pixels	20 Pixels
		3	12	65 5			3	18	60 5				
		4	6	31 5			4	10	28 5				
		4-Space Volume 8064					4-Space Volume 12600						

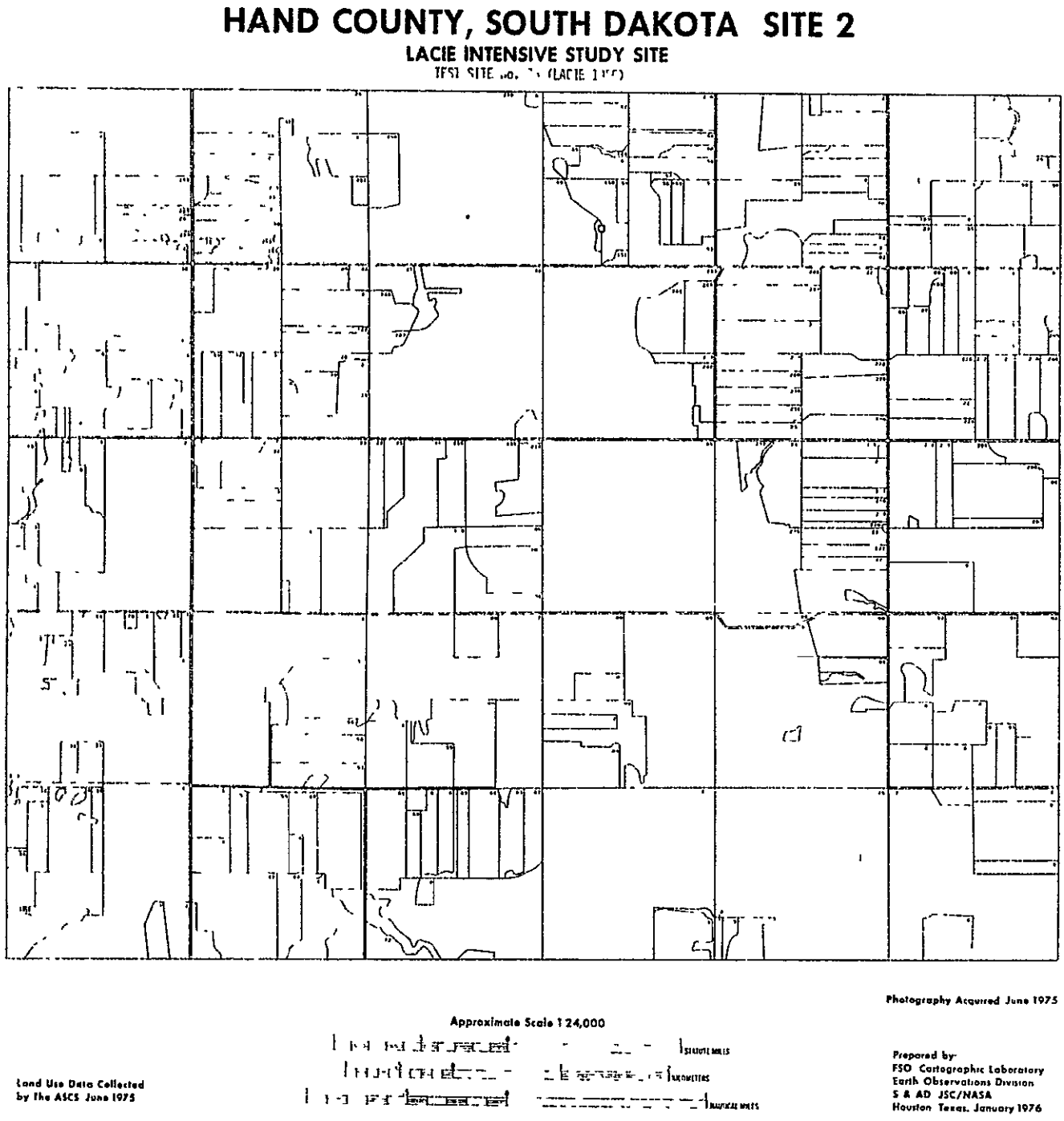

Figure 3.4-1. Field Structure of the Hand County LACIE Intensive Study Site

3.5 SUMMARY OF COMPARATIVE EVALUATION RESULTS

The results obtained in the comparative evaluations of the radiometrically processed image data are summarized in Table 3.5-1. From this table, it is apparent that the Type a2 radiometric processing of uncalibrated scene data has provided the most satisfactory compensation for striping on an overall basis. Scene data produced by this technique was ranked first when evaluated both visually and by means of detector-specific histograms, and was ranked second when evaluated by power spectrum analysis.

Since the multispectral classification evaluation was performed for only the type b1 processing of uncalibrated data and the type a1 processing of calibrated data, the inconclusive results obtained from this evaluation do not compromise the identification of the type a2 processing of uncalibrated scene data as the best overall procedure. Had this evaluation identified a preferred processing technique, one could still not conclude that this processing technique was superior to the type a2 processing of uncalibrated scene data.

Table 3.5-1. Summary of Evaluation Results

(1 = best)

Evaluation Method	Uncalibrated Scene Data Processing Type					Calibrated Scene Data Processing Type
	a1	a2	a3	b1	b2	a1
Detector Specific Histograms	6	1	2	3	4	5
Power Spectrum	3	2	1	-	-	-
Multispectral Classification	inconclusive results					
Visual Evaluation	4	1	5	2	2	-

Section 4
EVALUATION OF MSS CALIBRATION DATA

The calibration wedge data for one MSS band was investigated to characterize its temporal stability, by detector, and the relationship between the calibration data for the various detectors. For this investigation, the full set of MSS band 1 calibration wedge data corresponding to the first 210 mirror sweeps of MSS scene E-2183-16433 was employed.

4.1 TEMPORAL VARIATION OF REPORTED CALIBRATION WEDGE VALUES

For each detector of MSS band 1, plots of the mean and root-mean-squared variation of 50 calibration wedge samples were generated. These plots statistically summarized the temporal variation of a larger number of these values than the six points employed for calibration. These plots are presented as Figures 4.1-1 through 4.1-6. On these plots, the abcissa is the decompressed calibration sample value, and the ordinate is the sample number, counting the first sample of calibration data as 1. For each calibration sample considered, the range of values it assumed is indicated by a string of asterisks, which show the limits of the mean sample value plus and minus the standard deviation. These plots show a stable but non-linear response characteristic over the region of the ordinate where the ordinate scale is linear. (Note that on both ends of the ordinate, the scale of the plot is compressed with respect to the central region. This was done in order to display calibration sample values over the full range of the wedge without producing an excessively large plot.) Over the low value range of the calibration data, and for all detectors, the calibration sample values are stable to within a standard deviation of plus or minus one count, and there is evident no characteristic which suggests that the calibration data is inadequate or inferior for any particular detector.

Figure 4.1-1. Plot of Decompressed Calibration Wedge Data Values and their Standard Deviations for Detector 1, Band 1

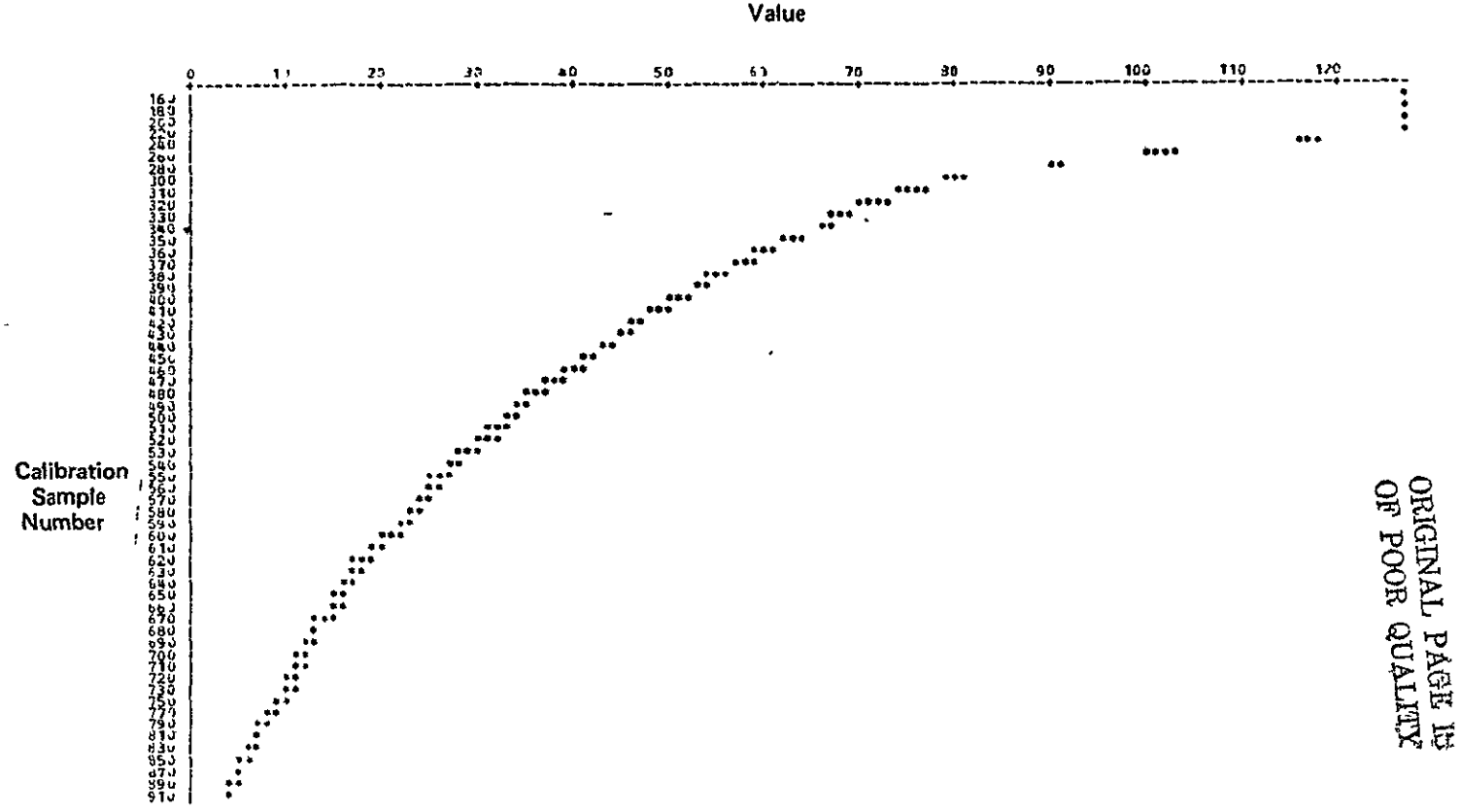

Figure 4.1-2. Plot of Decompressed Calibration Wedge Data Values and their Standard Deviations for Detector 2, Band 1

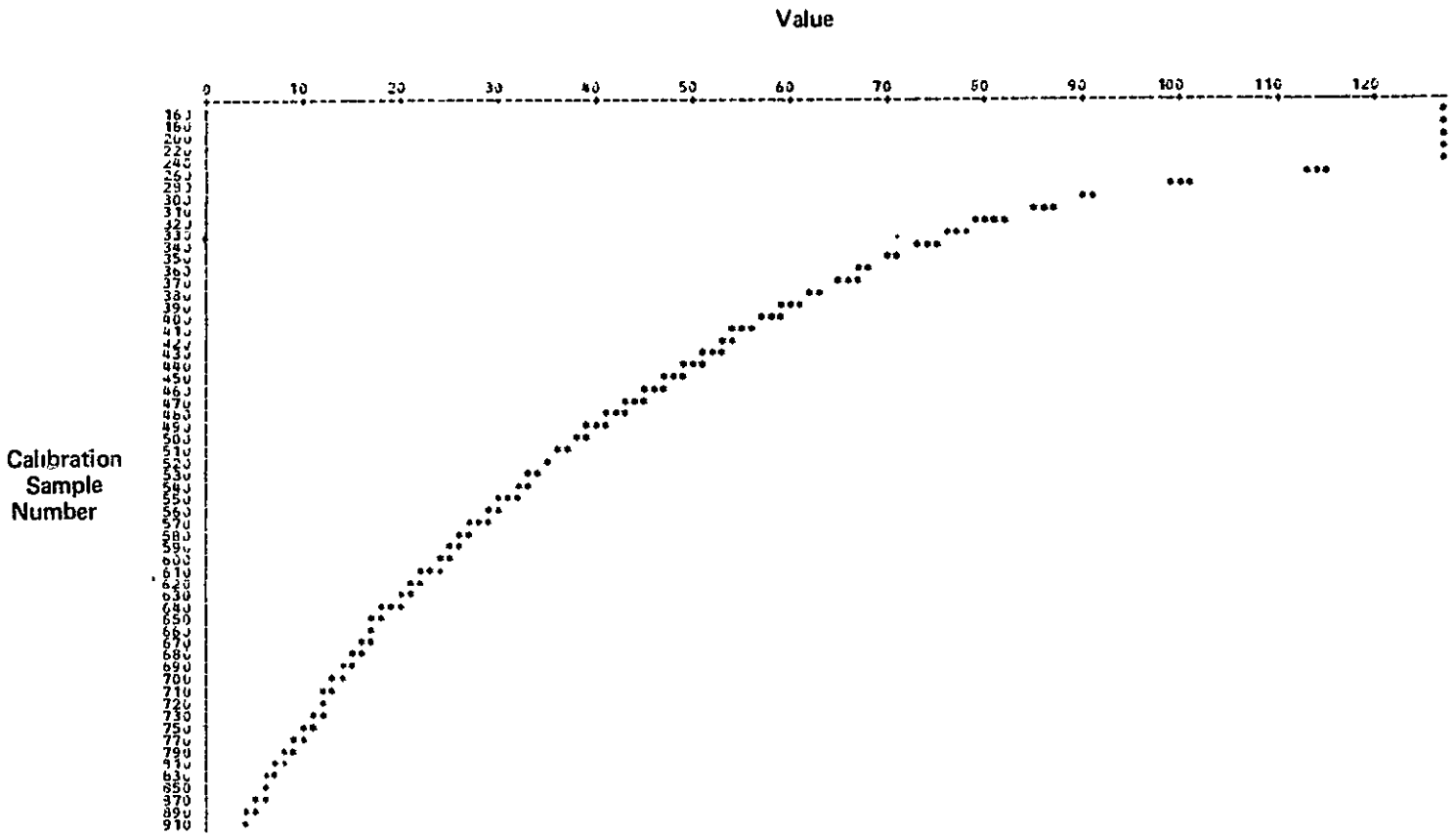

Figure 4.1-3. Plot of Decompressed Calibration Wedge Data Values and their Standard Deviations for Detector 3, Band 1

Figure 4.1-4. Plot of Decompressed Calibration Wedge Data Values and their Standard Deviations for Detector 4, Band 1

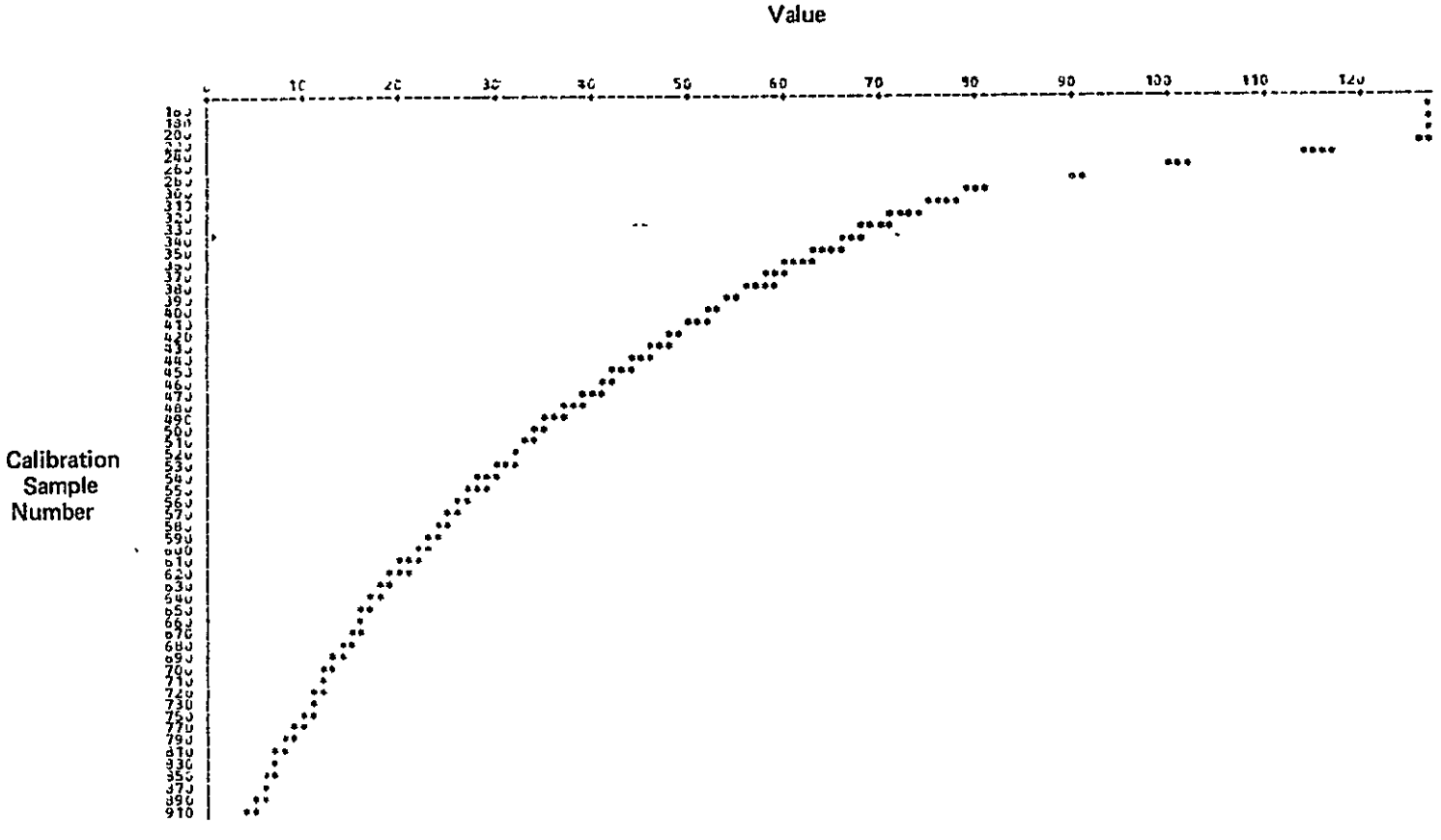

Figure 4.1-5. Plot of Decompressed Calibration Wedge Data Values and their Standard Deviations for Detector 5, Band 1

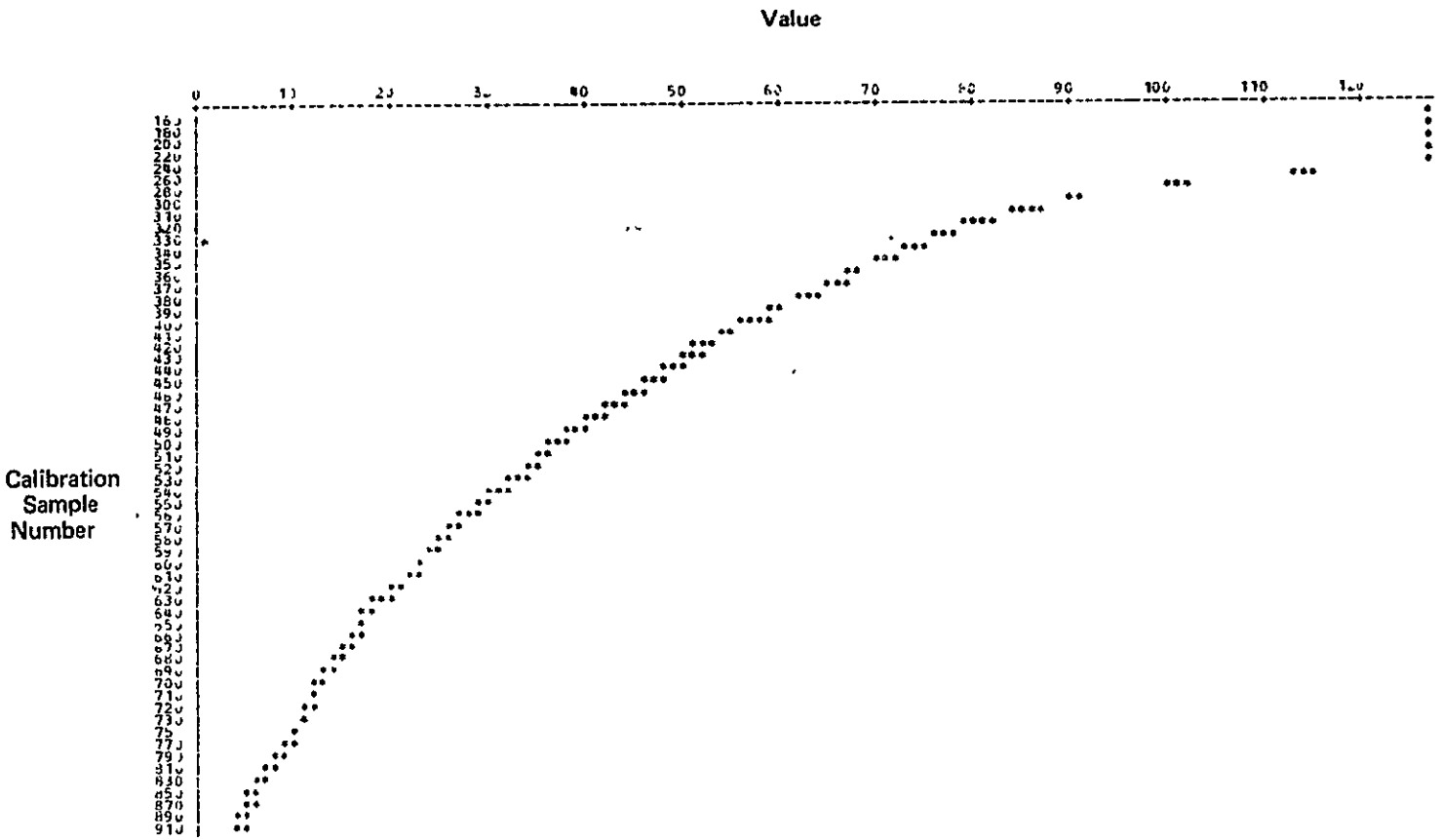

Figure 4.1-6. Plot of Decompressed Calibration Wedge Data Values and their Standard Deviations for Detector 6, Band 1

4.2 GAIN AND BIAS COEFFICIENT TIME SERIES

The MSS calibration procedure was applied to the standard six points from the calibration wedge data, and the resulting time series of gain and bias coefficients was plotted. These plots are presented in Figures 4.2-1 through 4.2-12. In these plots, the scale of the abscissa is the same among all the individual gain plots and among all the individual bias plots, so that visual comparison among corresponding plots for different detectors is not deceptive.

For the gain coefficient plots, the plotted values have been normalized into the range 0 to 1, where 0 corresponds to an actual gain value of 95.52, and 1 corresponds to an actual gain value of 122.64. Thus, the quantization of the plotting for the abscissa is an interval of 0.27 in the value of the gain coefficient.

For the bias coefficient plots, a similar normalization has been employed In this case, the minimum plot value of zero corresponds to a bias value of -47.670563, and the maximum plot value of 1 corresponds to a bias coefficient value of 52.329422. Thus, the quantization of the plotting on the abscissa is an interval of 1.00.

To provide an intuitive appreciation for the meaning of the fluctuations observed in these plots, the way in which the gain and bias coefficients are employed in radiometric calibration of MSS data must be considered The equation which is used to calibrate the data is:

$$V_c = \frac{KV_{Max}}{\Delta R}\left[\frac{V-pa_s}{q\ b_s} - R_{Min}\right] - r$$

where the symbols are defined in Appendix B. This can be rewritten in the form:

$$V_c = GV + B$$

where

$$G = \left(\frac{K}{\Delta R\ q}\right)\left(\frac{V_{Max}}{b_s}\right)$$

and

$$B = -\left\{\left(\frac{K}{\Delta R\ q}\right)\left(\frac{V_{Max}\ a_s}{b_s}\right)\ p + \left[\left(\frac{K\ V_{Max}}{\Delta R}\right) R_{Min} + r\right]\right\}$$

For the radiometric calibration implemented in the MDP for MSS band 1 (0.5 to 0.6 micrometers), the nominal values for the constants in these expressions are:

$$\frac{K}{\Delta R\ q} = 1$$

$$p = 1$$

$$\left[\frac{K\ V_{Max}}{\Delta R} R_{Min} + r\right] = \emptyset$$

$$V_{Max} = 127$$

Using these values for the constants in the calibration function, the expressions for G and B become:

$$G = \frac{127}{b_s}$$

$$B = -\frac{127}{b_s}\ a_s$$

Since we are using unsmoothed values for the gain and bias values in the present investigation, the subscript 's' will be dropped, yielding as the expression for the calibration function:

$$V_c = \frac{127}{b}\ (V-a)$$

The effect of the observed variations in the gain and bias coefficient values in the plots can be demonstrated by means of a Taylor series expansion of the calibration function about nominal coefficient values. The variation in the calibrated sample value is given by:

$$\Delta V_c = -\left[\frac{127}{b^2}(V-a)\right]\Bigg|_{\substack{\Delta b \\ b=b_o \\ a=a_o}} - \frac{127}{b}\Bigg|_{\substack{\Delta a \\ b=b_o}}$$

$$= -\frac{127}{b_o^2}(\Delta b)V + \frac{127}{b_o^2}\left[a_o\Delta b - b_o\Delta a\right]$$

$$= (\Delta G)V + \Delta B$$

where a_o and b_o are typical values for the MSS calibration coefficients and

$$\Delta G = -\frac{127}{b_o^2}(\Delta b)$$

and

$$\Delta B = \frac{127}{b_o^2}\left[a_o\Delta b - b_o\Delta a\right]$$

Table 4.2-1 presents a compilation of the maximum and minimum gain coefficient values observed in the gain coefficient plots, together with the corresponding bias coefficient values, typical coefficient values obtained by averaging the values from the plots, and deviations from the typical values obtained by taking one-half the difference of the values obtained from the plots. The effect of these typical values and the observed deviations is shown in Table 4.2-2, which presents the values of the coefficients of the calibration function and series expansion of the calibration function, taking into account the observed inverse relation between variations in the gain coefficient and variations in the bias coefficient.

Note that the variation in the additive constant is limited to approximately $\pm$ 1, and this for the unsmoothed data. Thus, the variations in calibrated sample values attributable to this term in the calibration function are at most of this magnitude. The amount of variation in calibrated sample values attributable to the multiplicative factor depends on the value of the uncalibrated sample, but for a typical uncalibrated sample value of 20, is of the same magnitude as that due to the additive term.

Pairwise comparison of the gain plots (or bias plots) for the detectors (e.g., detector 1 against detector 5) reveals no apparent correlation in the variation of the coefficient values along the time series. If striping, which on close inspection exhibits a six-line periodicity and is therefore necessarily, even if non-causally, detector related, were attributable to a systematic, detector-related variation in the calibration function, one would expect to observe a consistency in these variations across detectors (e.g., the bias value for detector 1 varying in synchronization with that for detector 5).

Thus, while there exist fluctuations in the calibration coefficient values which are of sufficient magnitude to produce a striping effect, these variations do not have the interdetector correlation which would be necessary to identify inadequate radiometric calibration processing procedures as the cause of the striping of MSS images.

Table 4.2-1. Summary of Variations in Gain and Bias Coefficients Obtained with Mss Calibration Procedure

Detector	Minimum Gain	Bias	Record	Maximum Gain	Bias	Record	Gain		Bias	
							Typical b_o	Deviation from Typical Δb	Typical a_o	Deviation from Typical Δa
1	95.51874	1.72894	123	102.64764	0.76947	115	99.08	$\pm$3 56	1.25	$\mp$0.48
2	104.12521	3.38972	8	114.47604	2.86726	71	109.30	$\pm$5.18	3.13	$\mp$0.26
3	104.42088	2.57248	37	112.57640	0.98093	47	108.50	$\pm$4.08	1.78	$\mp$0.80
4	112.91699	3.32911	127	122.64281	1.55055	49	117.78	$\pm$4.86	2.44	$\mp$0.89
5	97.20721	4.04221	146	105.33539	2.26438	205	101.27	$\pm$4 06	3.15	$\mp$0.89
6	106.34644	2.89016	40	114.60645	1.52419	197	110.48	$\pm$4.13	2.21	$\mp$0.68

Table 4.2-2. Variations of Calibration Function Coefficients

	MSS Calibration Coefficient Values				Calibration Function Coefficients			
	Gain		Bias		Gain		Bias	
Detector	Typical Value b_o	Deviation from Typical Δb	Typical Value a_o	Deviation from Typical Δa	Typical Value G	Deviation from Typical ΔG	Typical Value B	Deviation from Typical ΔB
1	99.08	± 3.56	1.25	∓ 0.48	1.282	$\mp 4.60 \times 10^{-2}$	-1.602	± 0.673
2	109.30	± 5.18	3.13	∓ 0.26	1.162	$\mp 5.51 \times 10^{-2}$	-3.637	± 0.474
3	108.50	± 4.08	1.78	∓ 0.80	1.170	$\mp 4.40 \times 10^{-2}$	-2.084	± 1.014
4	117.78	± 4.86	2.44	∓ 0.89	1.078	$\mp 4.50 \times 10^{-2}$	-2.631	± 1.068
5	101.27	± 4.06	3.15	∓ 0.89	1.254	$\mp 5.03 \times 10^{-2}$	-3.950	± 1.274
6	110.48	± 4.13	2.21	∓ 0.68	1.150	$\mp 4.30 \times 10^{-2}$	-2.540	± 0.877

$$G = + \frac{127}{b_o} \qquad B = - \frac{127}{b_o} a_o$$

$$\Delta G = -\Delta b \frac{127}{b_o^2} \qquad \Delta B = \frac{127}{b_o^2} \left[a_o \Delta b - b_o \Delta a \right]$$

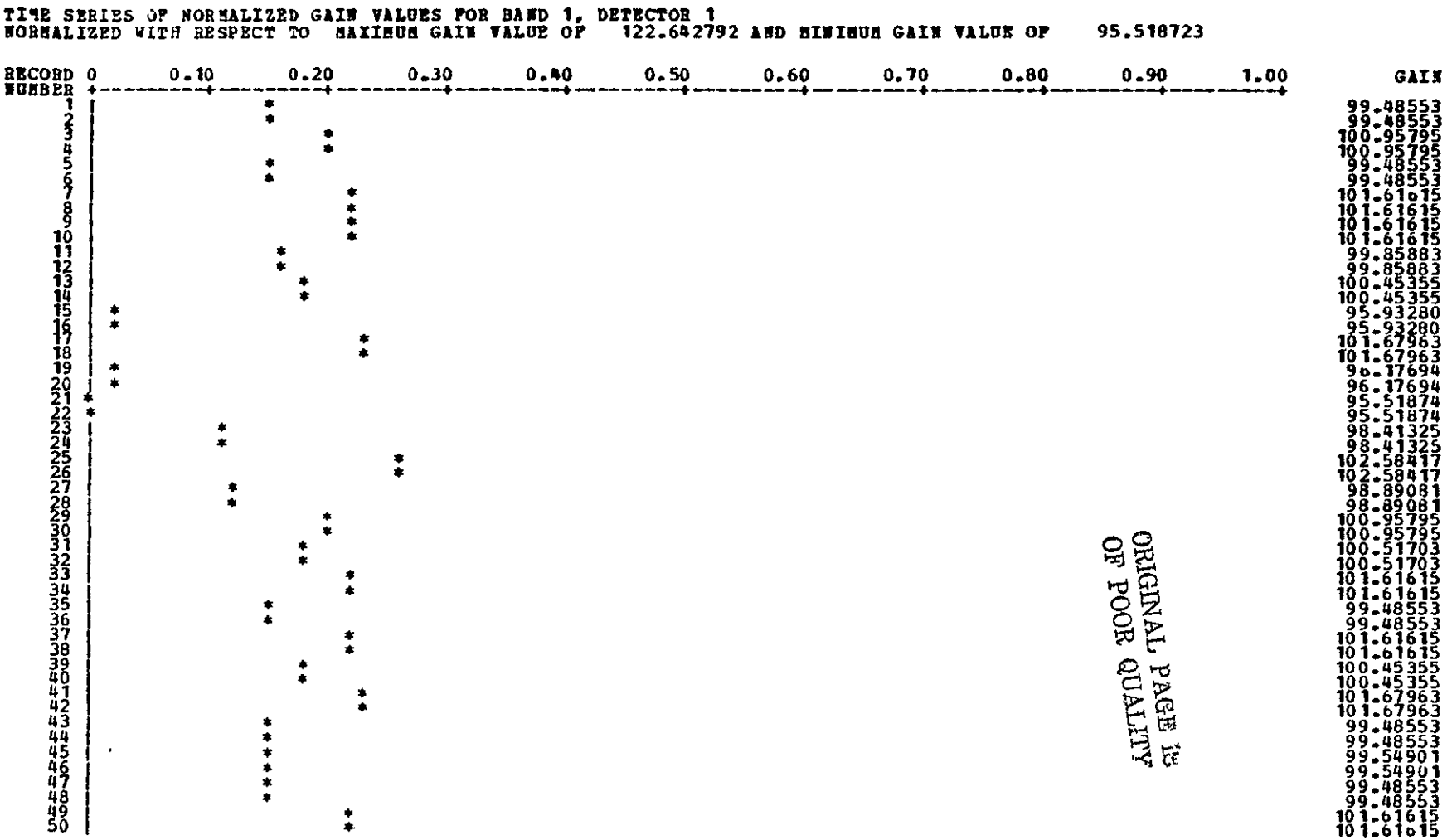

Figure 4.2-1 (Sheet 1 of 5)

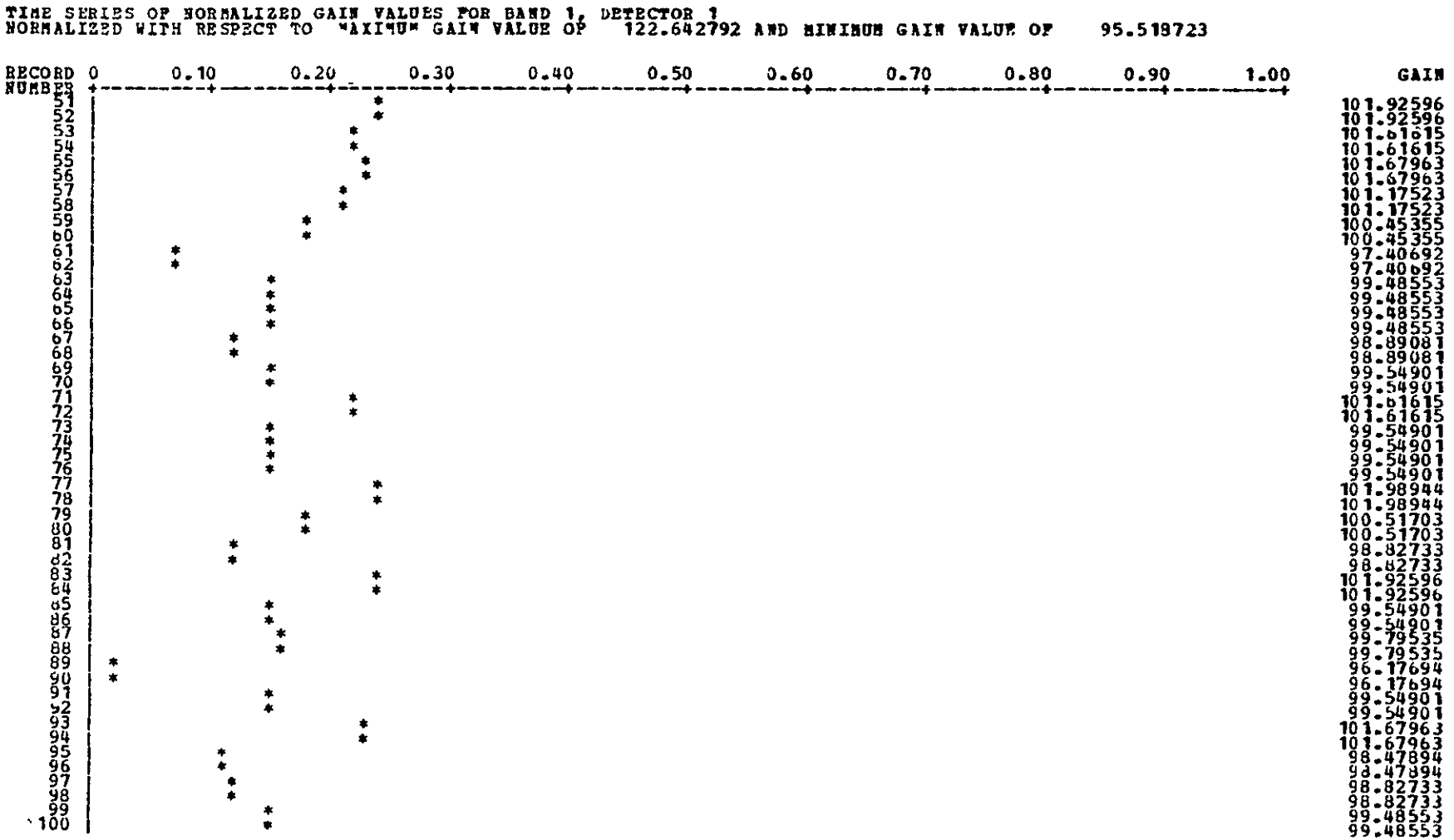

Figure 4.2-1 (Sheet 2 of 5)

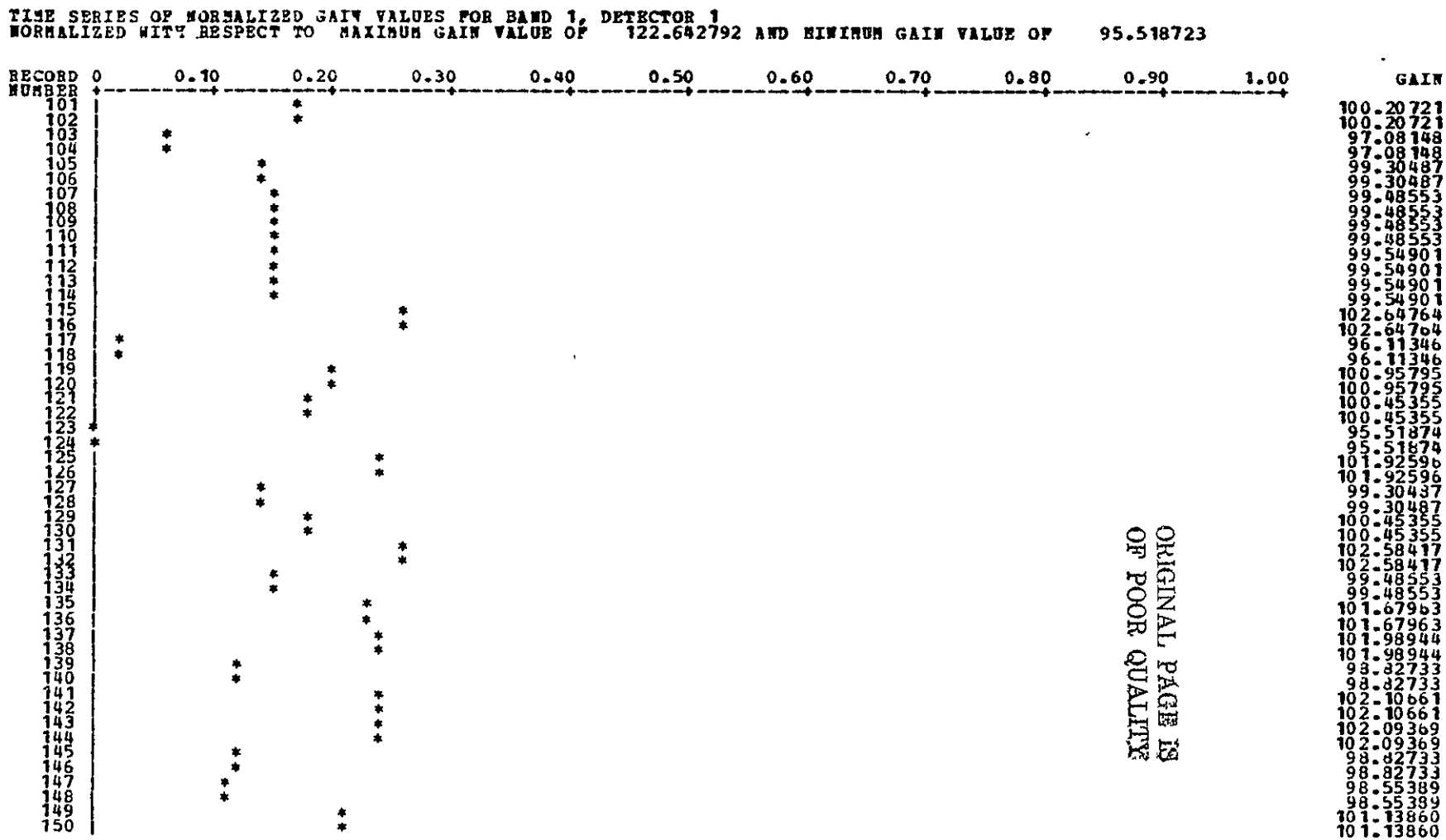

Figure 4.2-1 (Sheet 3 of 5)

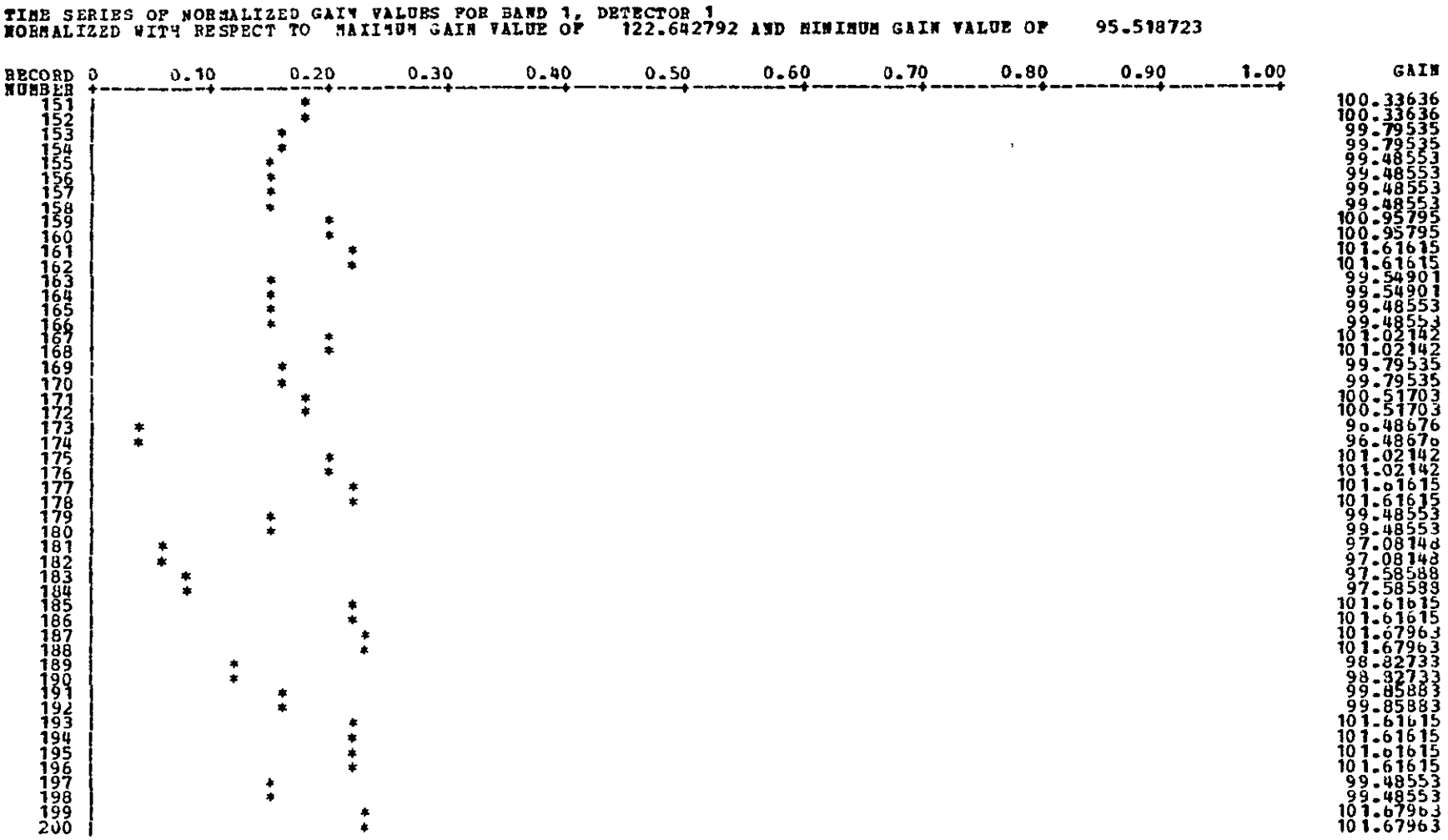

Figure 4.2-1 (Sheet 4 of 5)

TIME SERIES OF NORMALIZED GAIN VALUES FOR BAND 1, DETECTOR 1
NORMALIZED WITH RESPECT TO MAXIMUM GAIN VALUE OF 122.642792 AND MINIMUM GAIN VALUE OF 95.518723

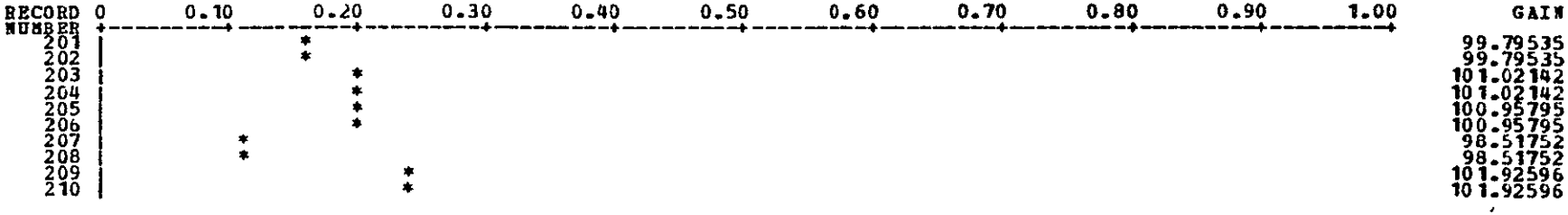

Figure 4.2-1 (Sheet 5 of 5)

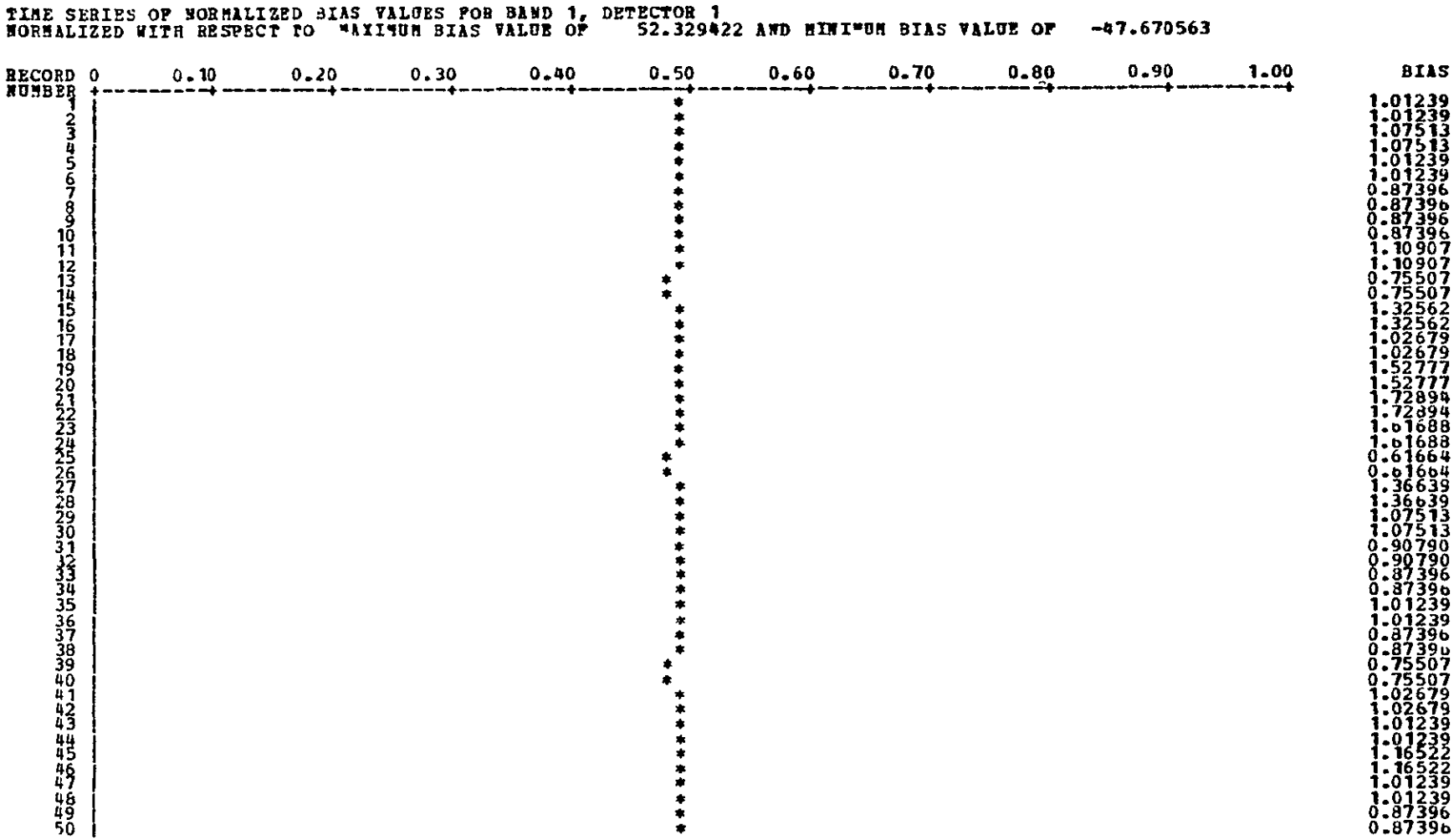

Figure 4.2-2 (Sheet 1 of 5)

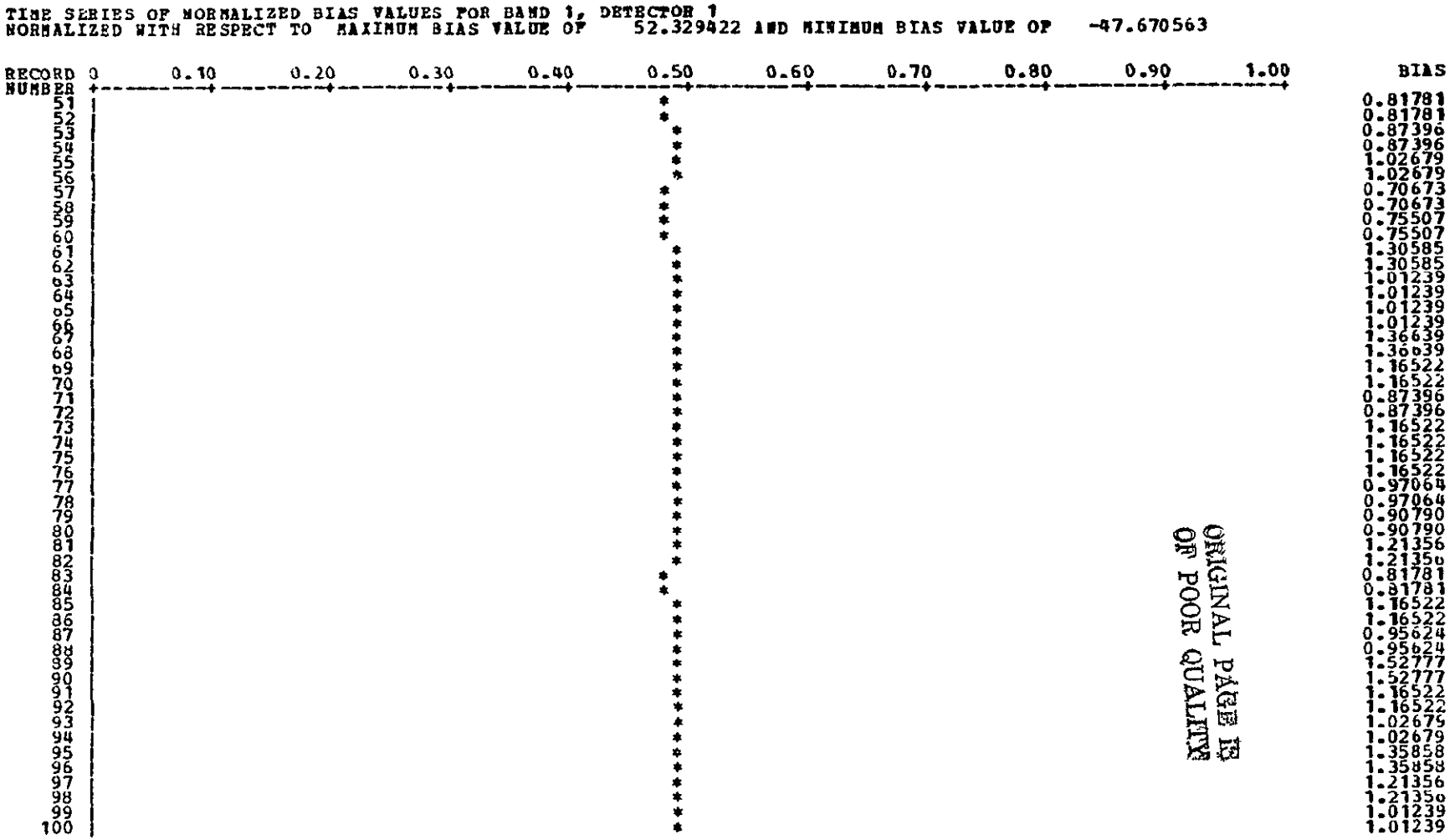

Figure 4.2-2 (Sheet 2 of 5)

TIME SERIES OF NORMALIZED BIAS VALUES FOR BAND 1, DETECTOR 1
NORMALIZED WITH RESPECT TO MAXIMUM BIAS VALUE OF 52.329422 AND MINIMUM BIAS VALUE OF -47.670563

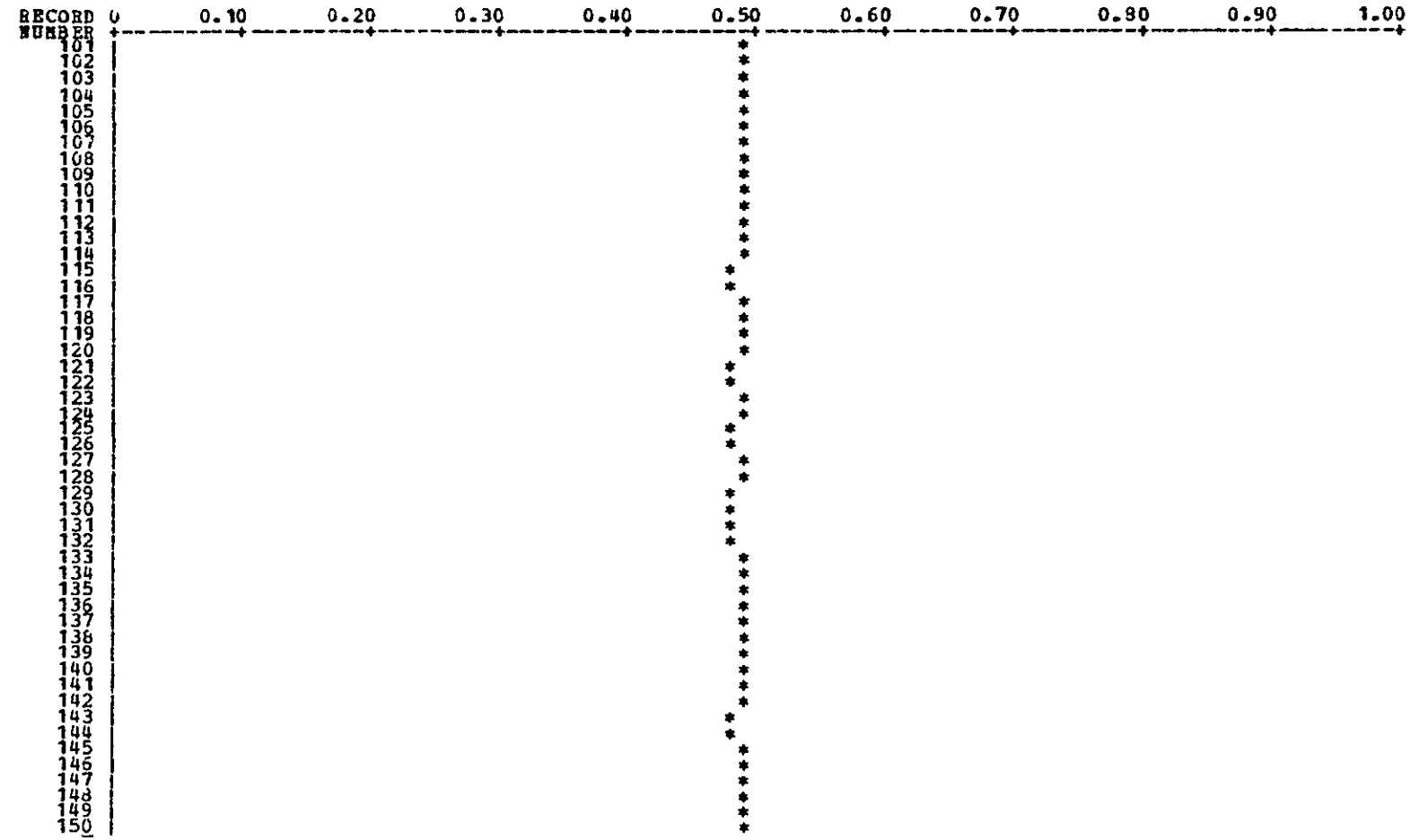

Figure 4.2-2 (Sheet 3 of 5)

TIME SERIES OF NORMALIZED BIAS VALUES FOR BAND 1, DETECTOR 1
NORMALIZED WITH RESPECT TO MAXIMUM BIAS VALUE OF 52.329422 AND MINIMUM BIAS VALUE OF -47.670563

RECORD NUMBER	0 0.10 0.20 0.30 0.40 0.50 0.60 0.70 0.80 0.90 1.00	BIAS
151	*	0.85858
152	*	0.85858
153	*	0.95624
154	*	0.95624
155	*	1.01239
156	*	1.01239
157	*	1.01239
158	*	1.01239
159	*	1.07513
160	*	1.07513
161	*	0.87396
162	*	0.87396
163	*	1.16522
164	*	1.16522
165	*	1.01239
166	*	1.01239
167	*	1.22797
168	*	1.22797
169	*	0.95624
170	*	0.95624
171	*	0.90790
172	*	0.90790
173	*	1.47162
174	*	1.47162
175	*	1.22797
176	*	1.22797
177	*	0.87396
178	*	0.87396
179	*	1.01239
180	*	1.01239
181	*	1.11762
182	*	1.11762
183	*	1.43768
184	*	1.43768
185	*	0.87396
186	*	0.87396
187	*	1.02679
188	*	1.02679
189	*	1.21356
190	*	1.21356
191	*	1.10907
192	*	1.10907
193	*	0.87396
194	*	0.87396
195	*	0.87396
196	*	0.87396
197	*	1.01239
198	*	1.01239
199	*	1.02679
200	*	1.02679

Figure 4.2-2 (Sheet 4 of 5)

TIME SERIES OF NORMALIZED BIAS VALUES FOR BAND 1, DETECTOR 1
NORMALIZED WITH RESPECT TO MAXIMUM BIAS VALUE OF 52.329422 AND MINIMUM BIAS VALUE OF -47.670563

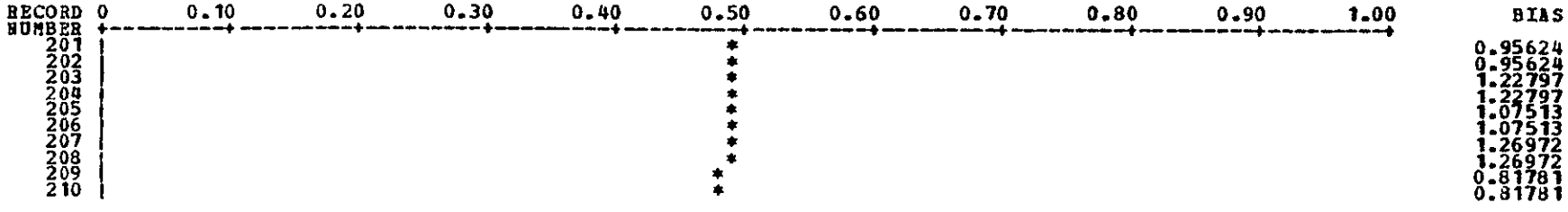

Figure 4.2-2 (Sheet 5 of 5)

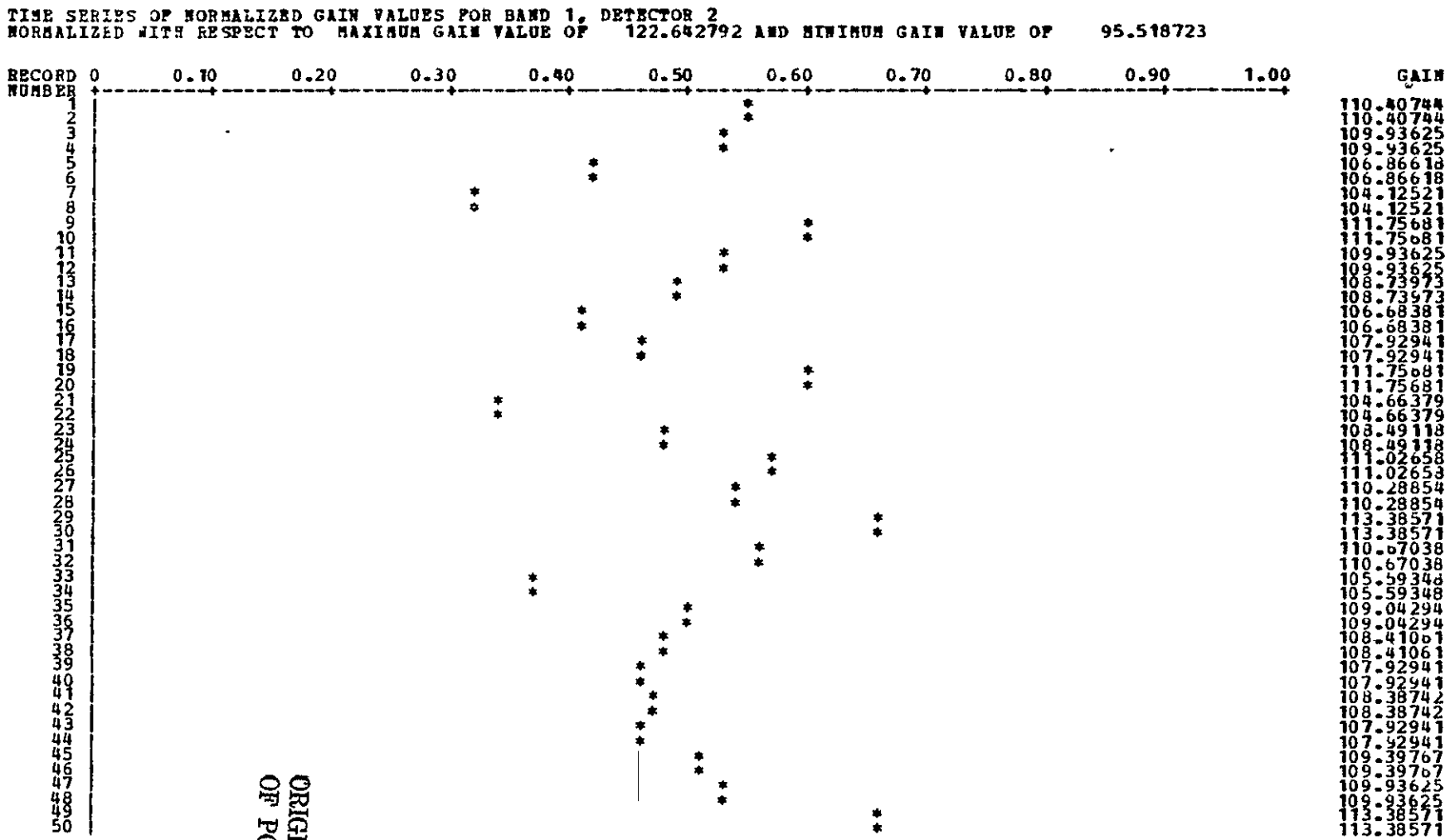

Figure 4.2-3 (Sheet 1 of 5)

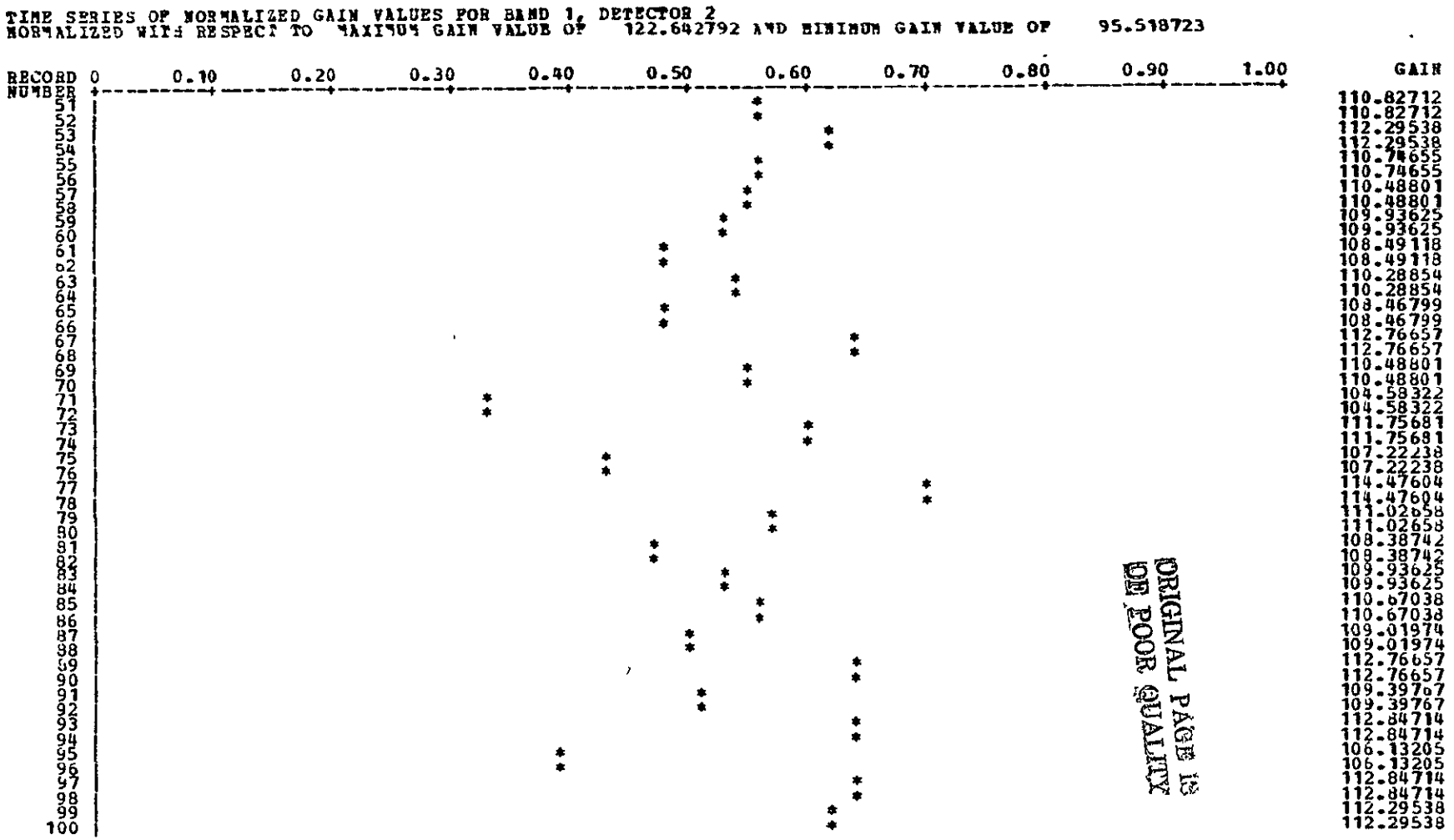

Figure 4.2-3 (Sheet 2 of 5)

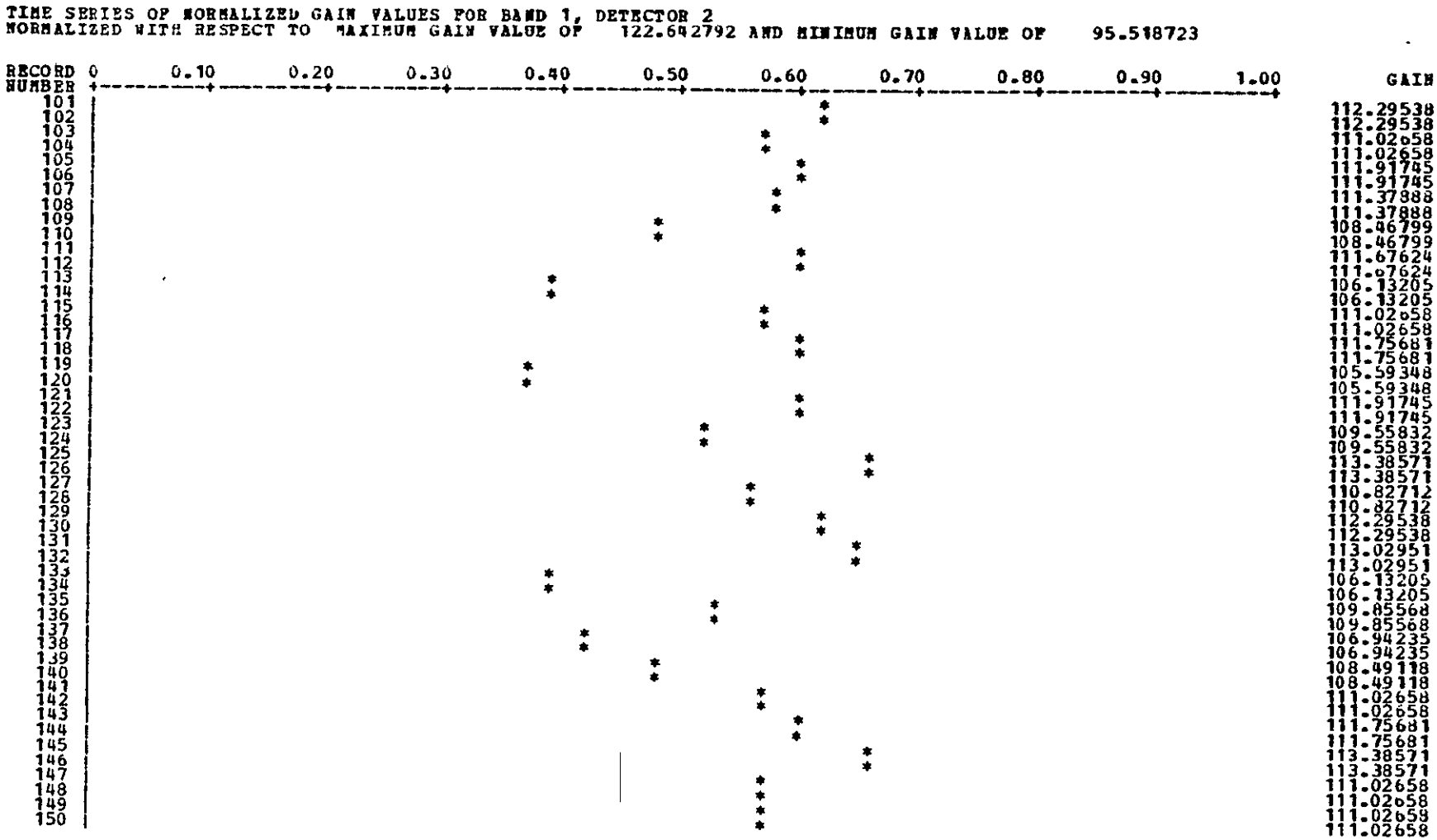

Figure 4.2-3 (Sheet 3 of 5)

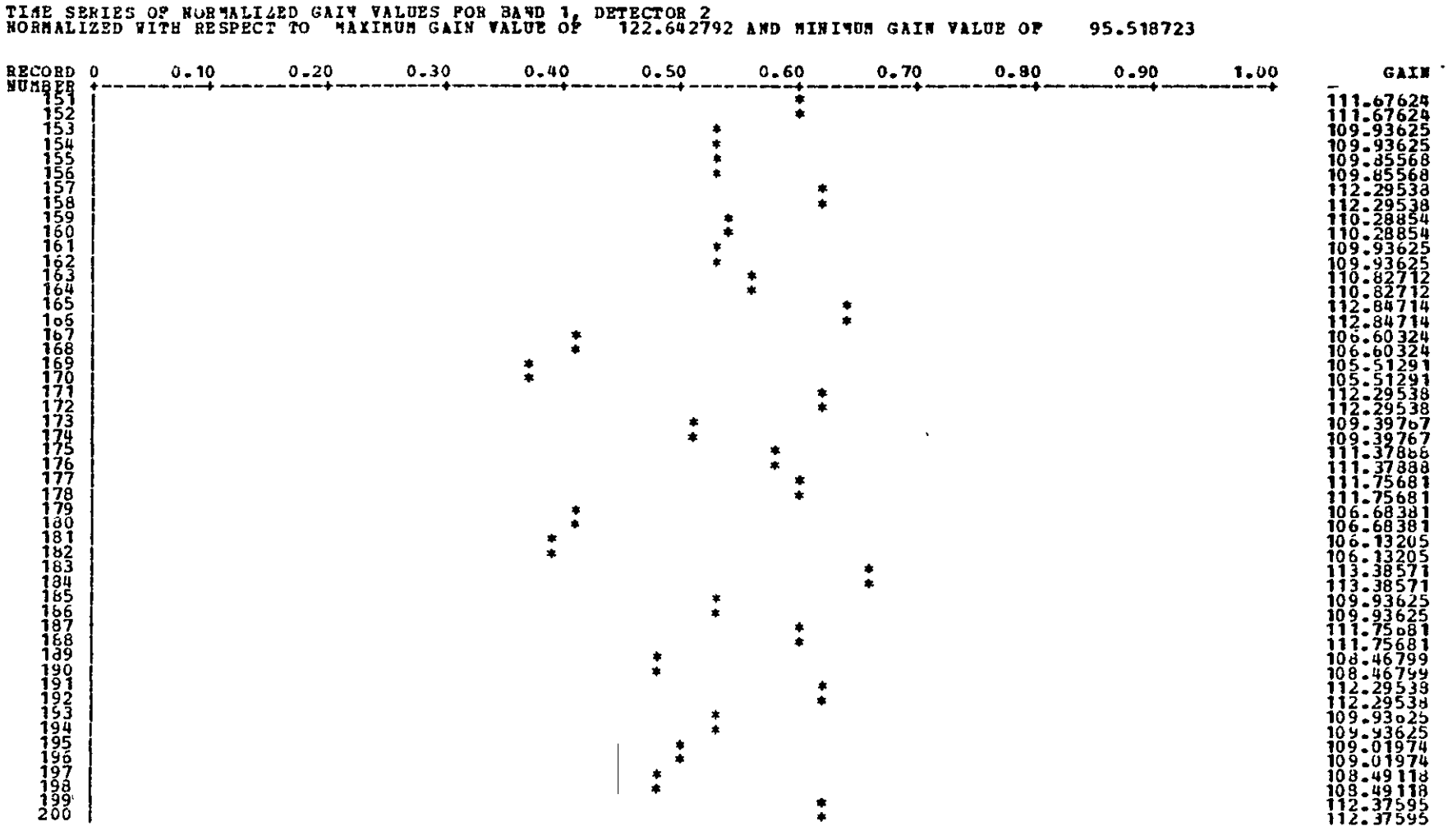

Figure 4.2-3 (Sheet 4 of 5)

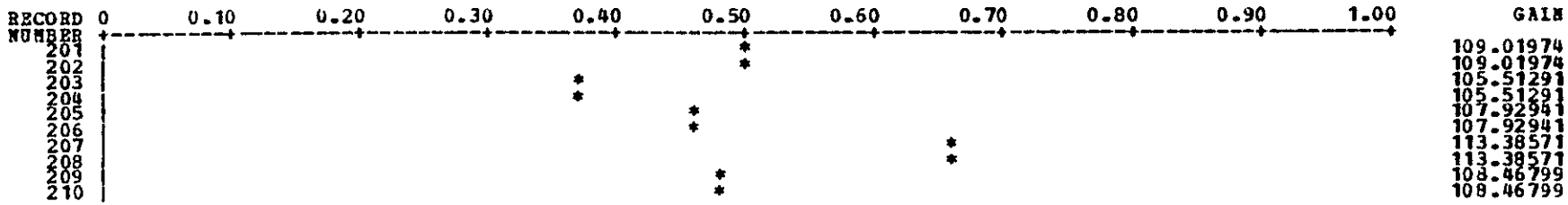

Figure 4.2-3 (Sheet 5 of 5)

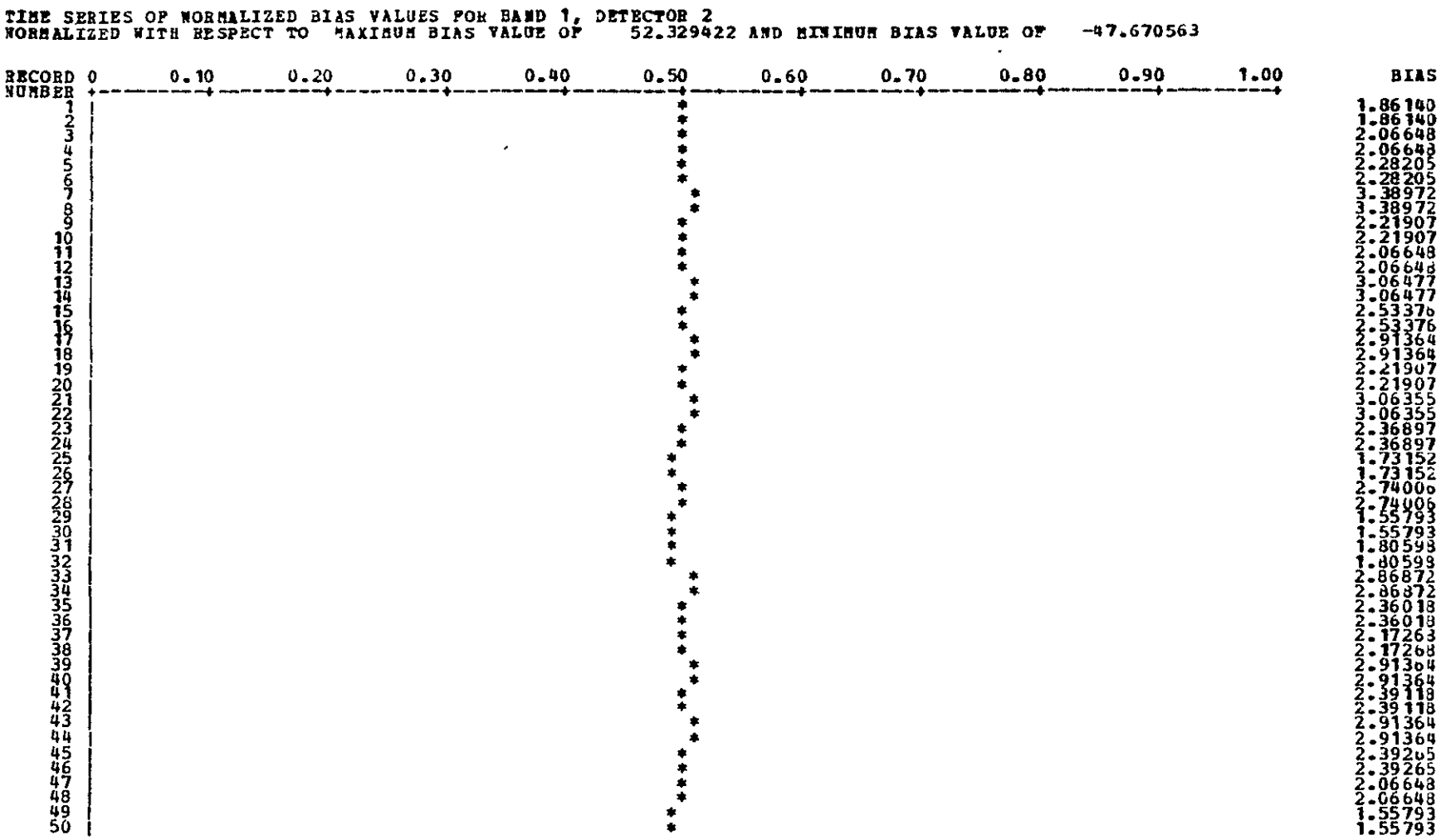

Figure 4.2-4 (Sheet 1 of 5)

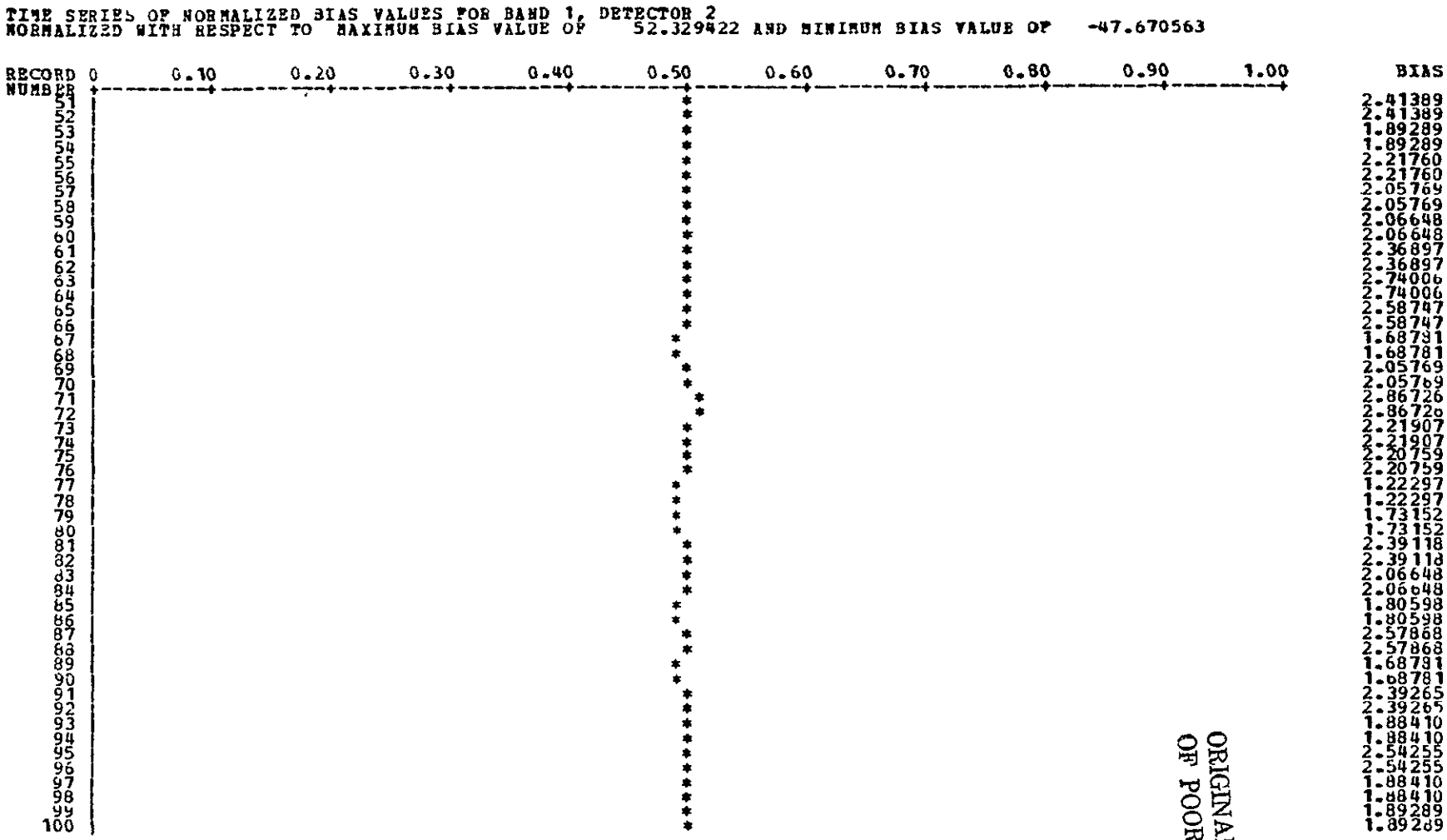

Figure 4.2-4 (Sheet 2 of 5)

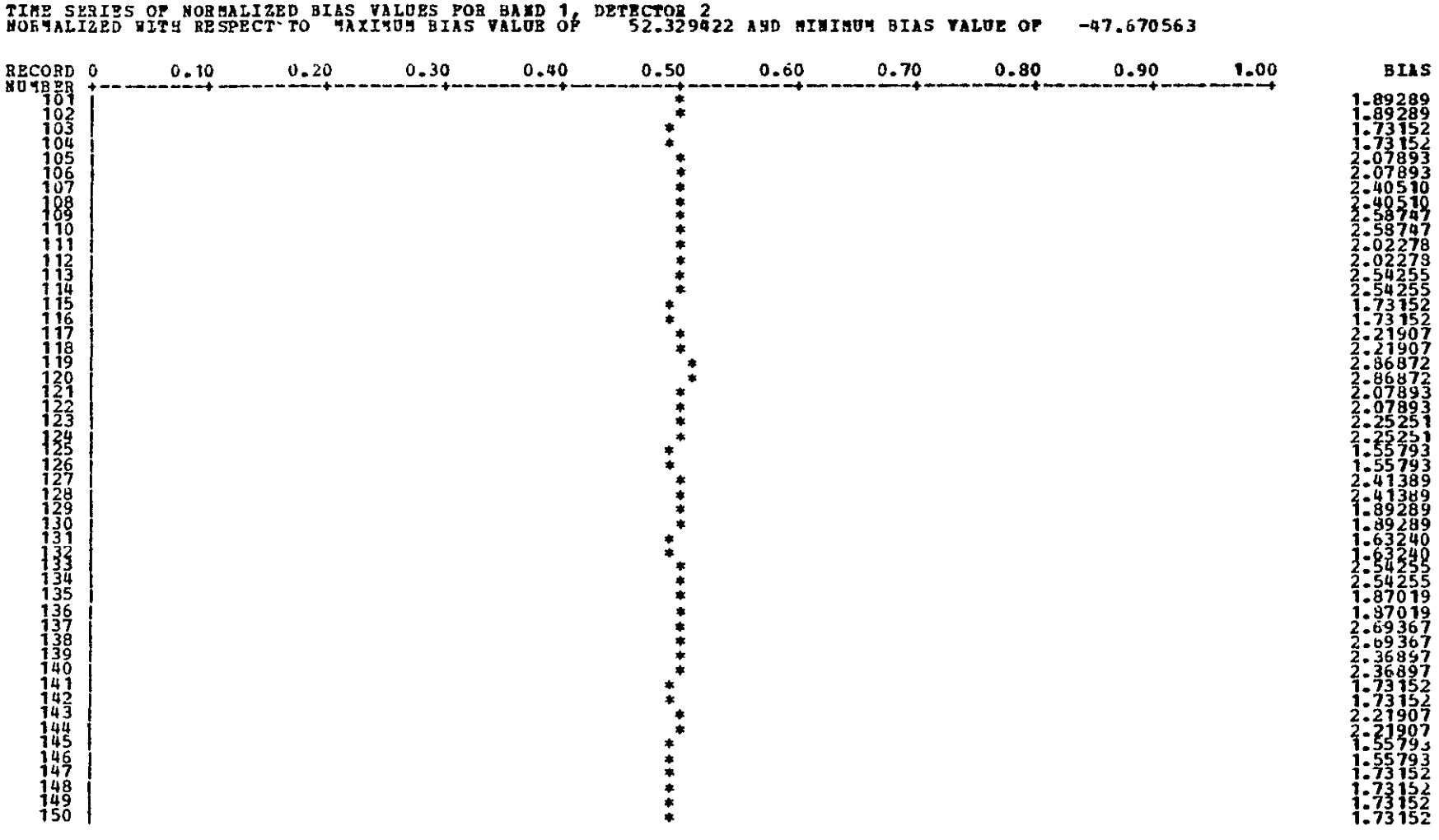

Figure 4.2-4 (Sheet 3 of 5)

TIME SERIES OF NORMALIZED BIAS VALUES FOR BAND 1, DETECTOR 2
NORMALIZED WITH RESPECT TO MAXIMUM BIAS VALUE OF 52.329422 AND MINIMUM BIAS VALUE OF -47.670563

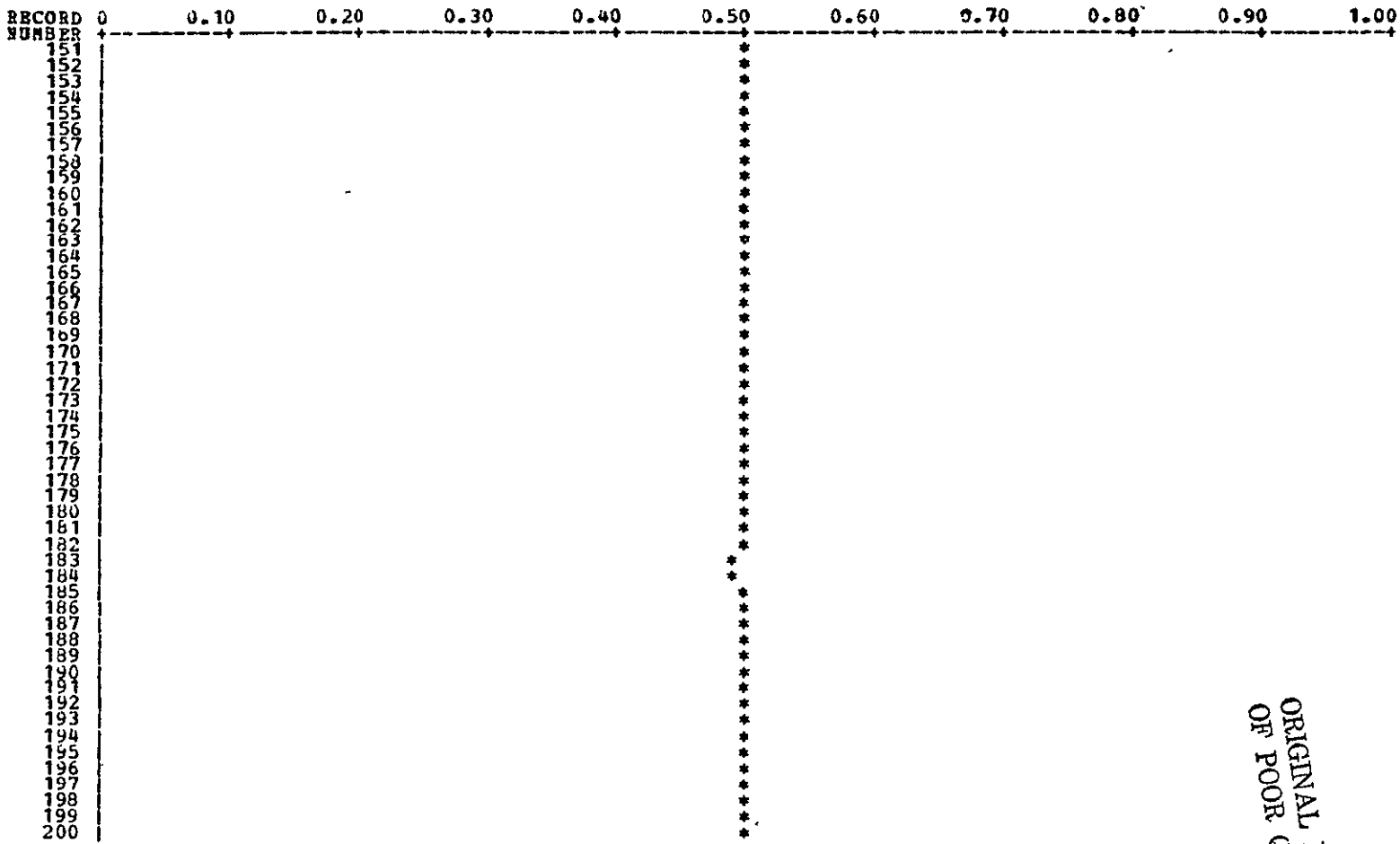

Figure 4.2-4 (Sheet 4 of 5)

TIME SERIES OF NORMALIZED BIAS VALUES FOR BAND 1, DETECTOR 2
NORMALIZED WITH RESPECT TO MAXIMUM BIAS VALUE OF 52.329422 AND MINIMUM BIAS VALUE OF -47.670563

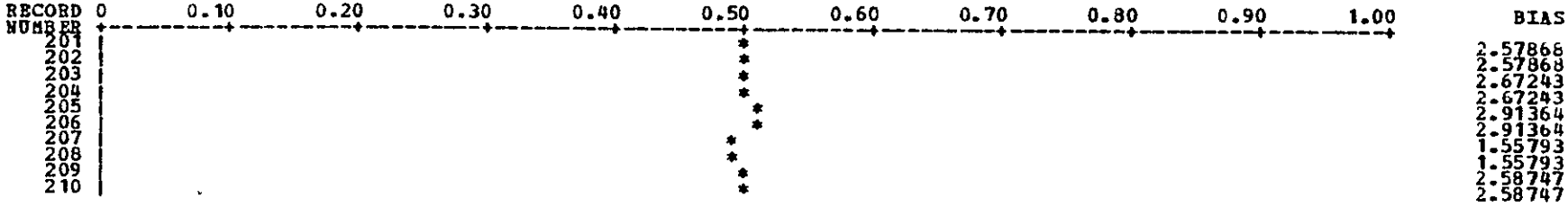

Figure 4.2-4 (Sheet 5 of 5)

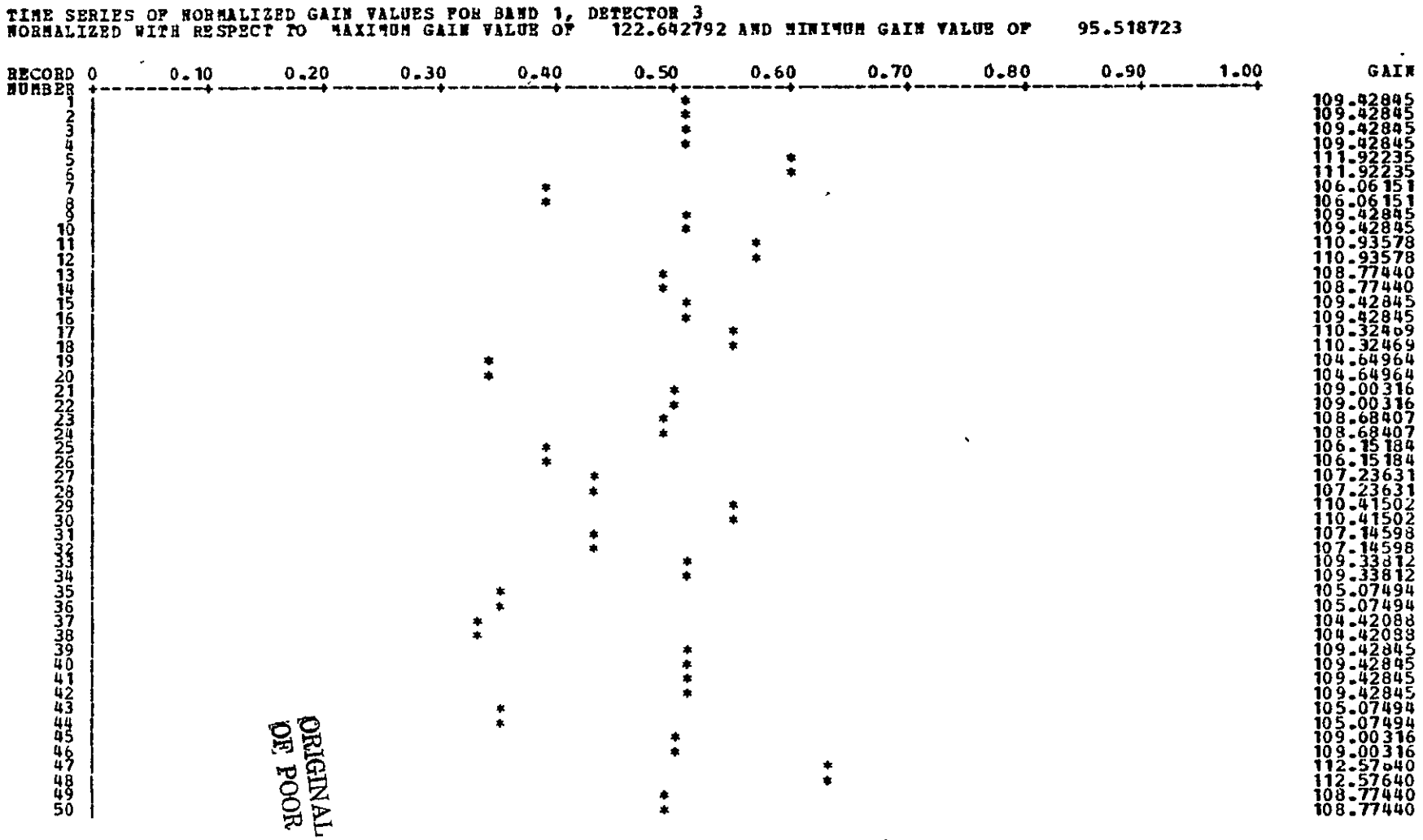

Figure 4.2-5 (Sheet 1 of 5)

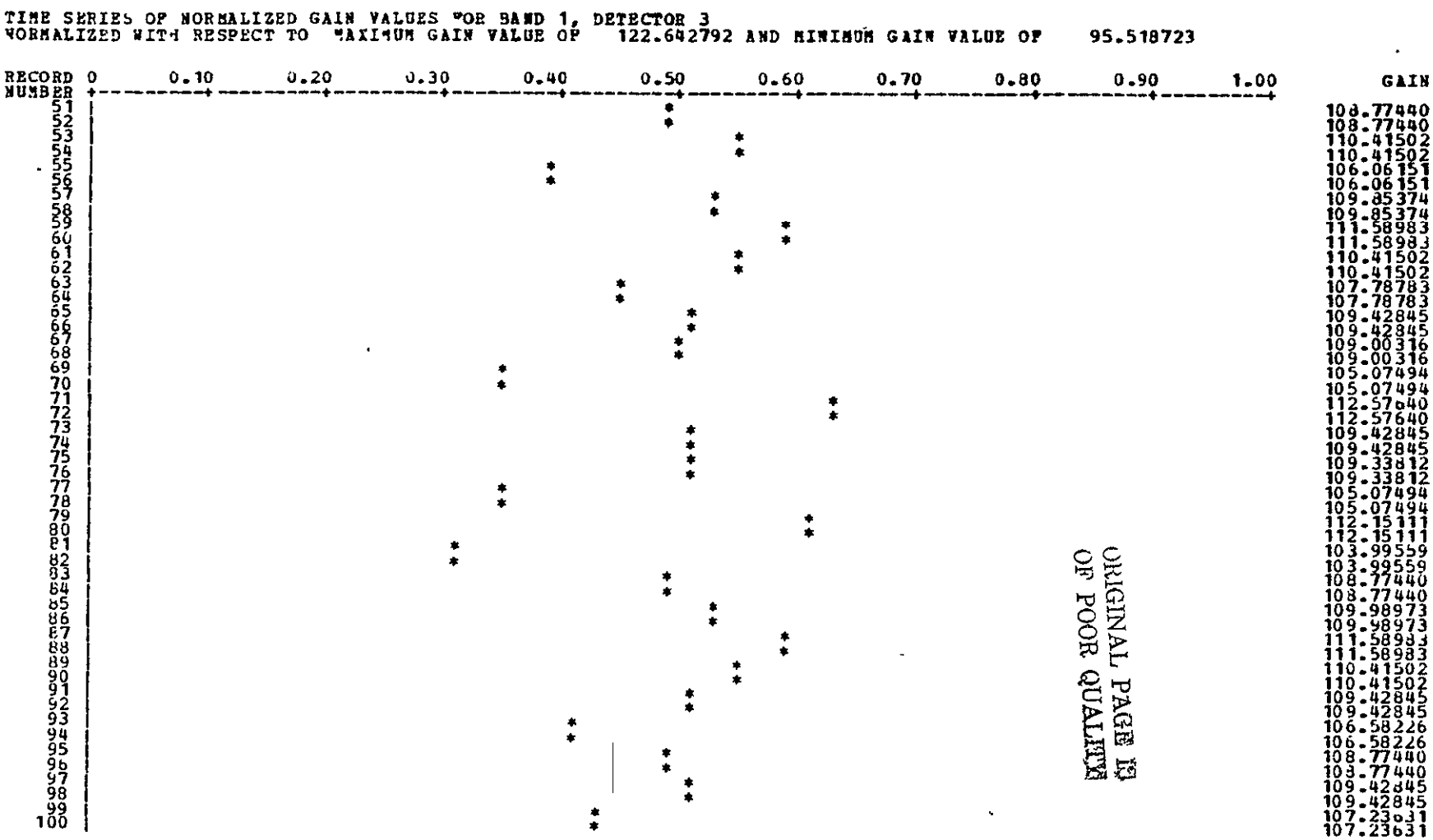

Figure 4.2-5 (Sheet 2 of 5)

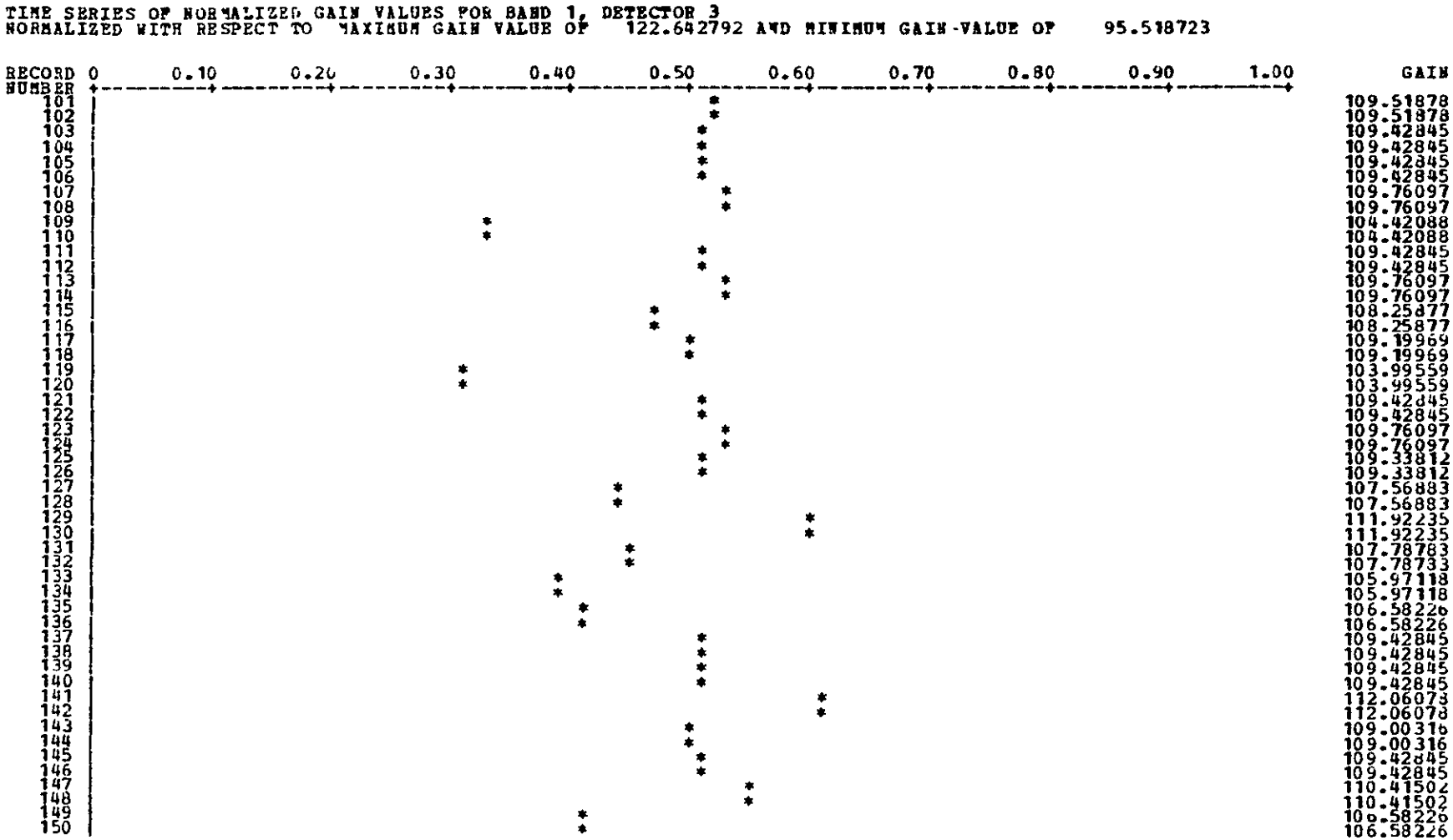

Figure 4.2-5 (Sheet 3 of 5)

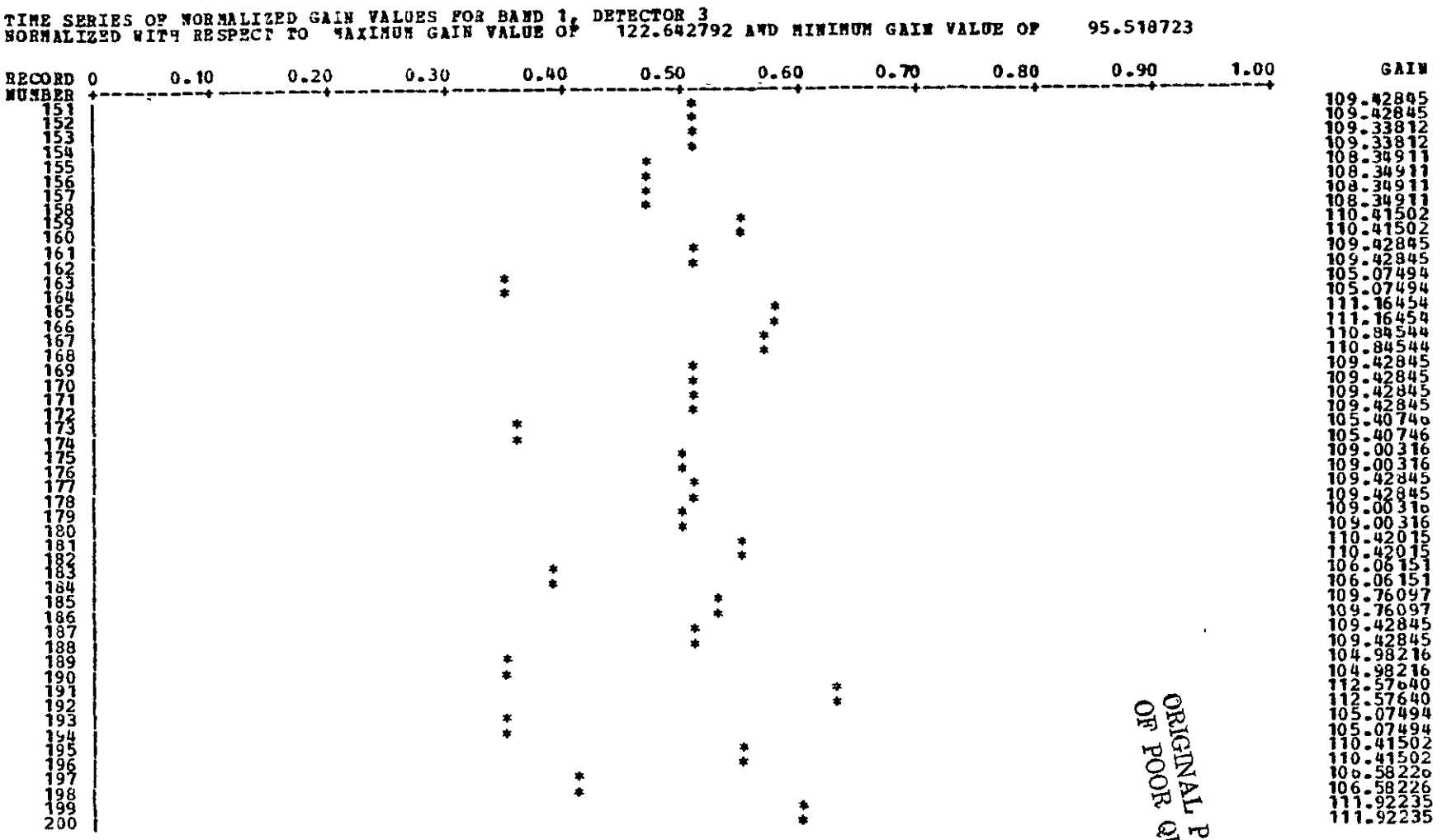

Figure 4.2-5 (Sheet 4 of 5)

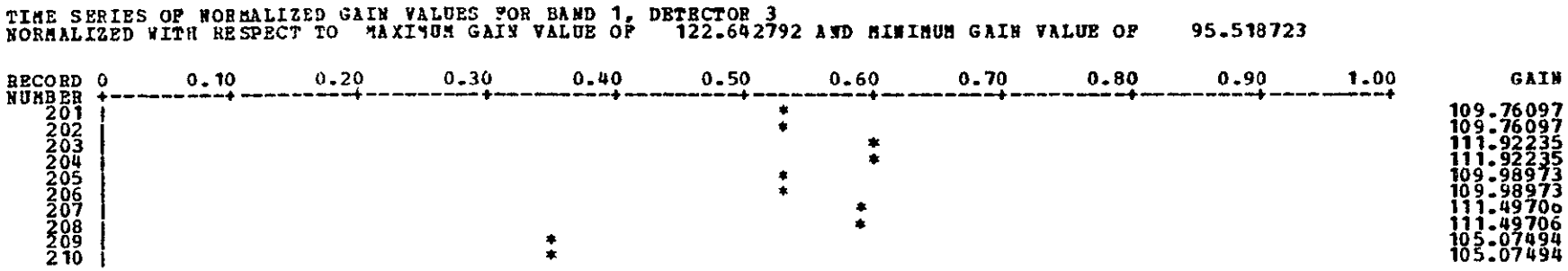

Figure 4.2-5 (Sheet 5 of 5)

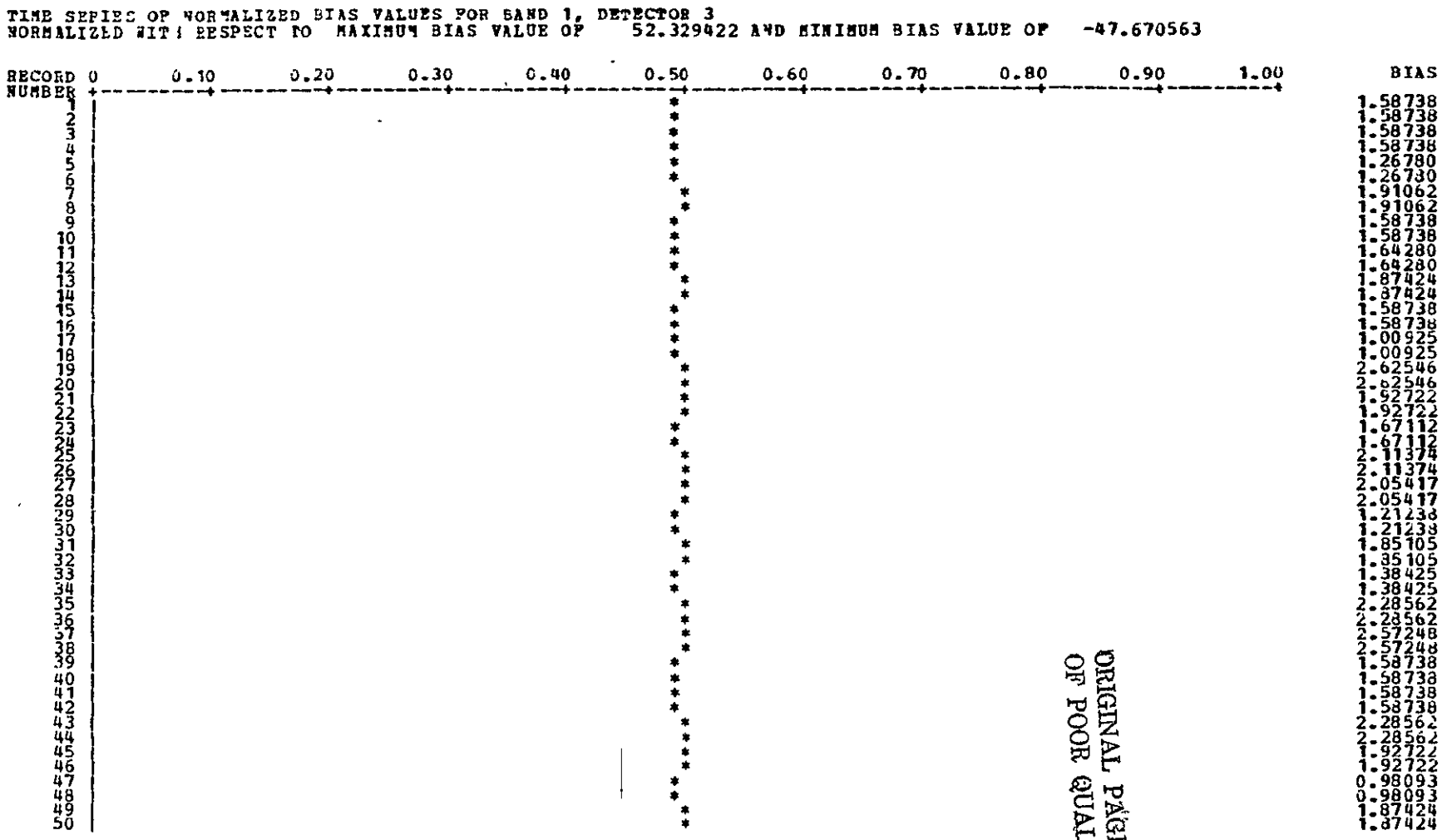

Figure 4.2-6 (Sheet 1 of 5)

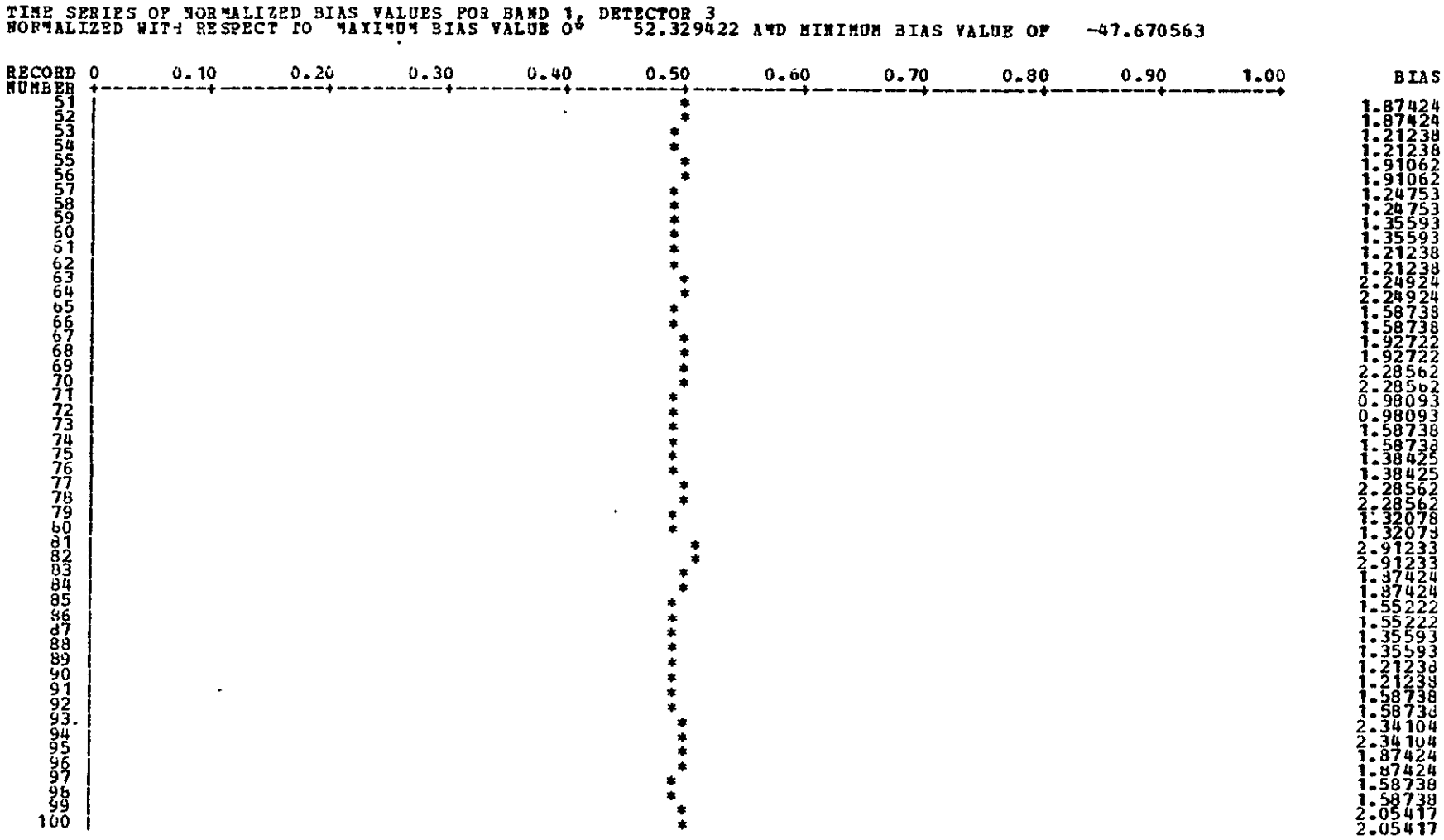

Figure 4.2-6 (Sheet 2 of 5)

TIME SERIES OF NORMALIZED BIAS VALUES FOR BAND 1, DETECTOR 3
NORMALIZED WITH RESPECT TO MAXIMUM BIAS VALUE OF 52.329422 AND MINIMUM BIAS VALUE OF -47.670563

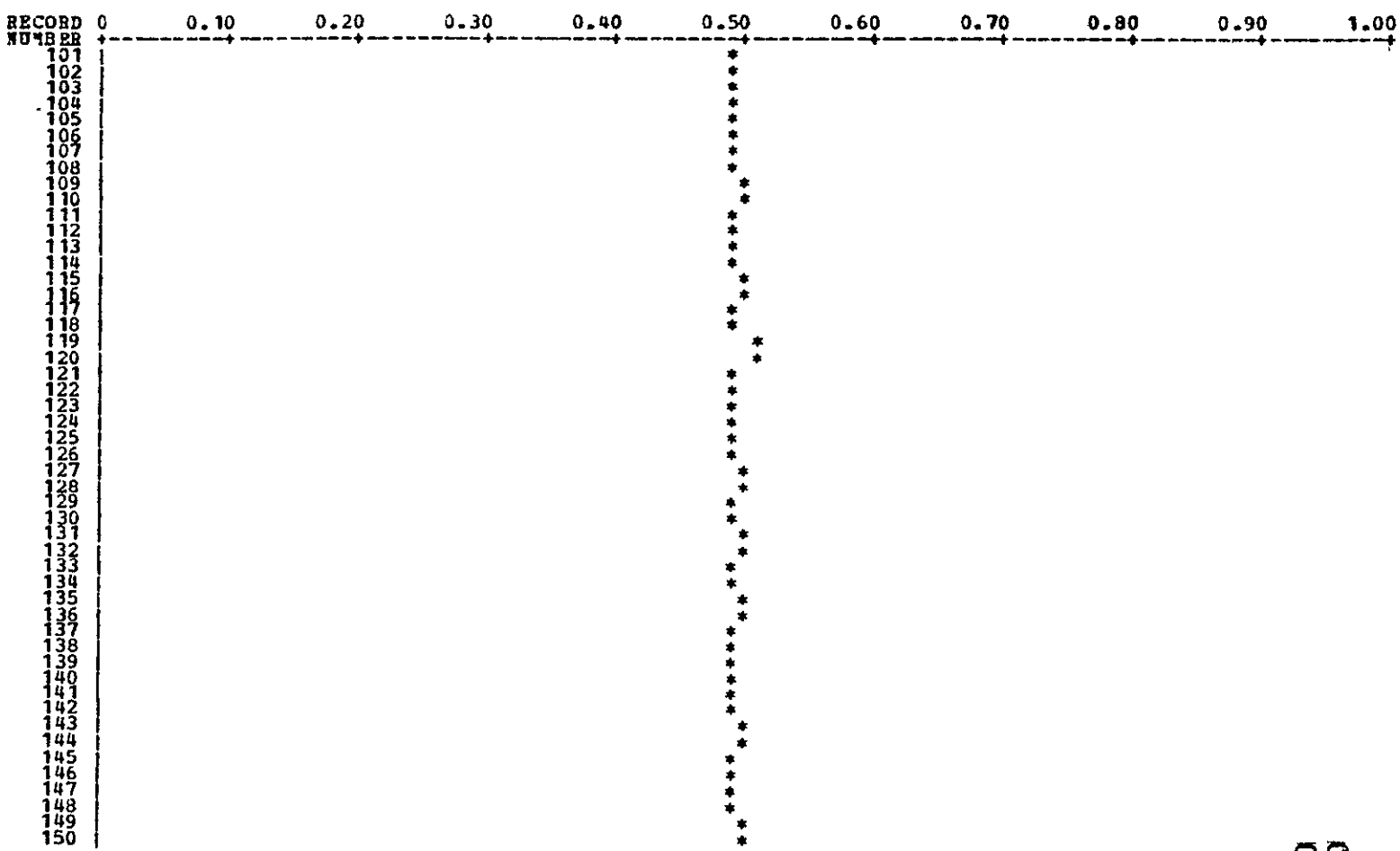

RECORD NUMBER	BIAS
101	1.79050
102	1.79050
103	1.58738
104	1.58738
105	1.58738
106	1.58738
107	1.49924
108	1.49924
109	2.57248
110	2.57248
111	1.58738
112	1.58738
113	1.49924
114	1.49924
115	2.01096
116	2.01096
117	1.53440
118	1.53440
119	2.91233
120	2.91233
121	1.58738
122	1.58738
123	1.49924
124	1.49924
125	1.38425
126	1.38425
127	1.96604
128	1.96604
129	1.26780
130	1.26780
131	2.24924
132	2.24924
133	1.70750
134	1.70750
135	2.34104
136	2.34104
137	1.58738
138	1.58738
139	1.58738
140	1.58738
141	1.11765
142	1.11765
143	1.92722
144	1.92722
145	1.58738
146	1.58738
147	1.21238
148	1.21238
149	2.34104
150	2.34104

Figure 4.2-6 (Sheet 3 of 5)

TIME SERIES OF NORMALIZED BIAS VALUES FOR BAND 1, DETECTOR 3
NORMALIZED WITH RESPECT TO MAXIMUM BIAS VALUE OF 52.329422 AND MINIMUM BIAS VALUE OF -47.670563

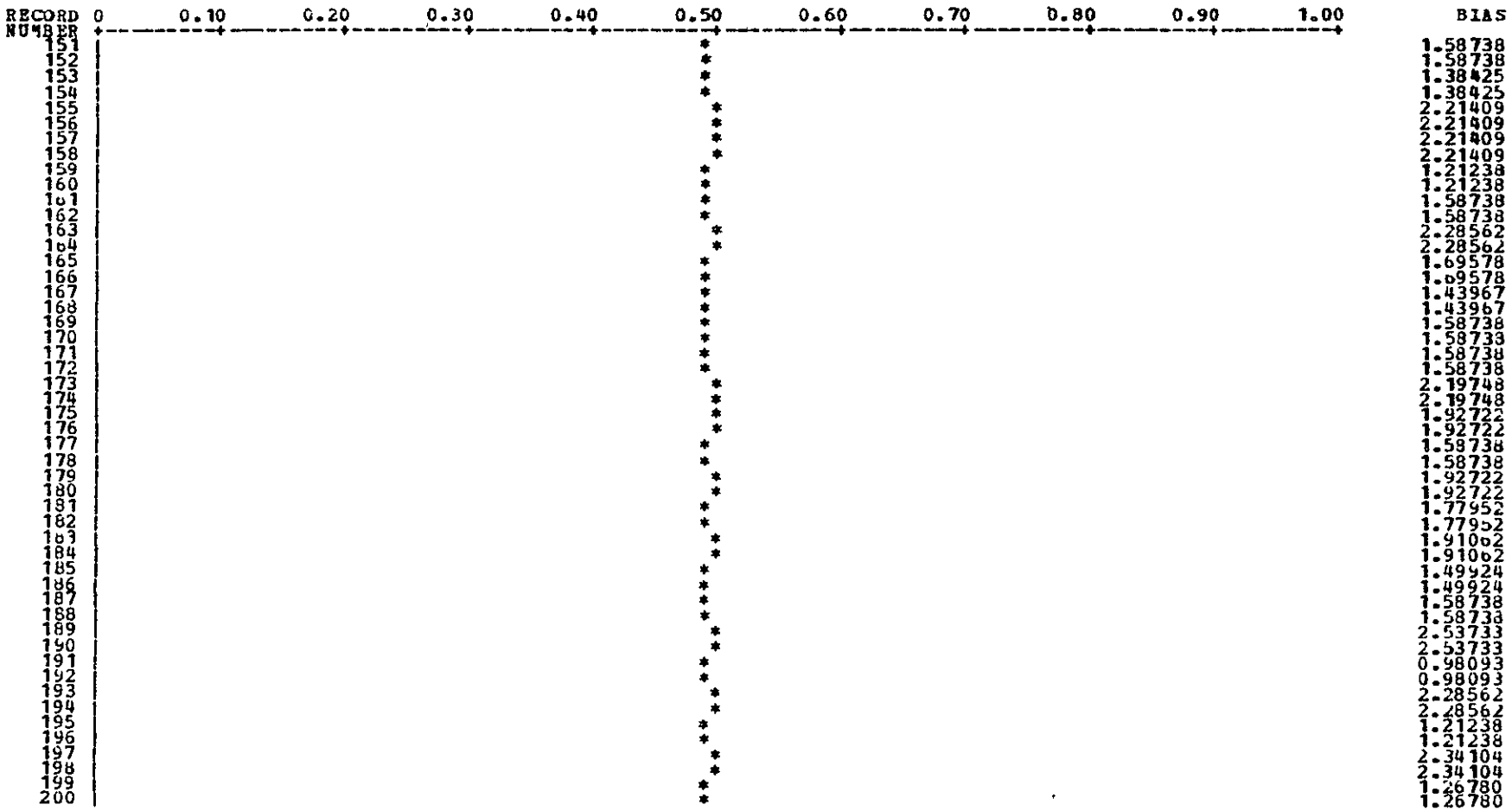

Figure 4.2-6 (Sheet 4 of 5)

TIME SERIES OF NORMALIZED BIAS VALUES FOR BAND 1, DETECTOR 3
NORMALIZED WITH RESPECT TO MAXIMUM BIAS VALUE OF 52.329422 AND MINIMUM BIAS VALUE OF -47.670563

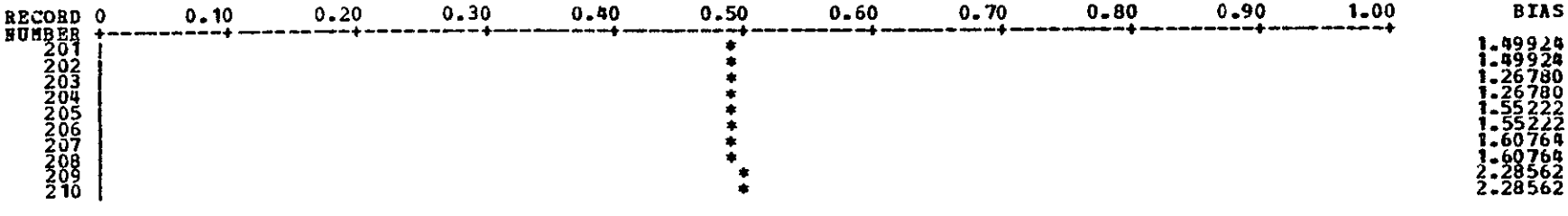

Figure 4.2-6 (Sheet 5 of 5)

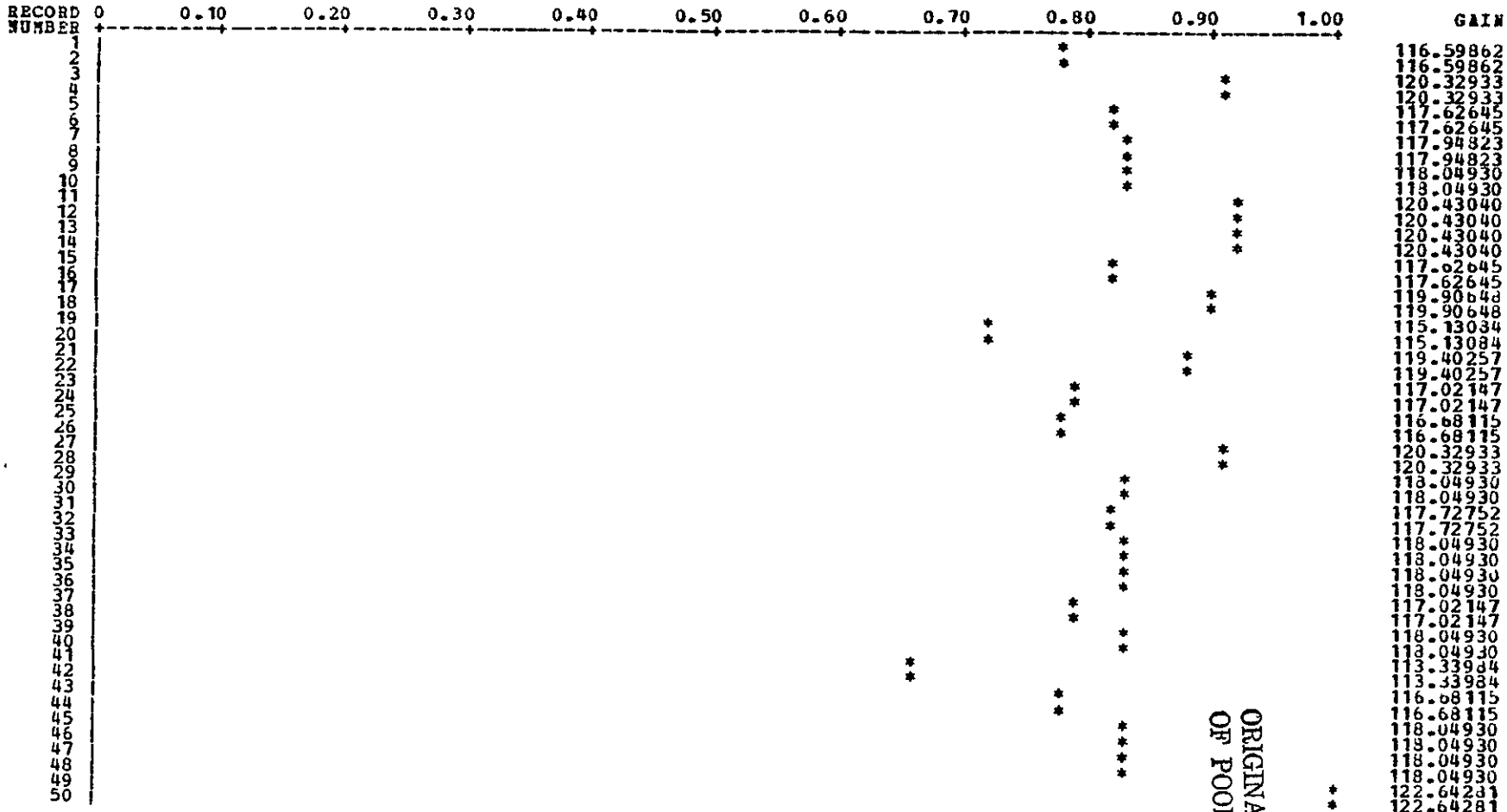

Figure 4.2-7 (Sheet 1 of 5)

TIME SERIES OF NORMALIZED GAIN VALUES FOR BAND 1, DETECTOR 4
NORMALIZED WITH RESPECT TO MAXIMUM GAIN VALUE OF 122.642792 AND MINIMUM GAIN VALUE OF 95.518723

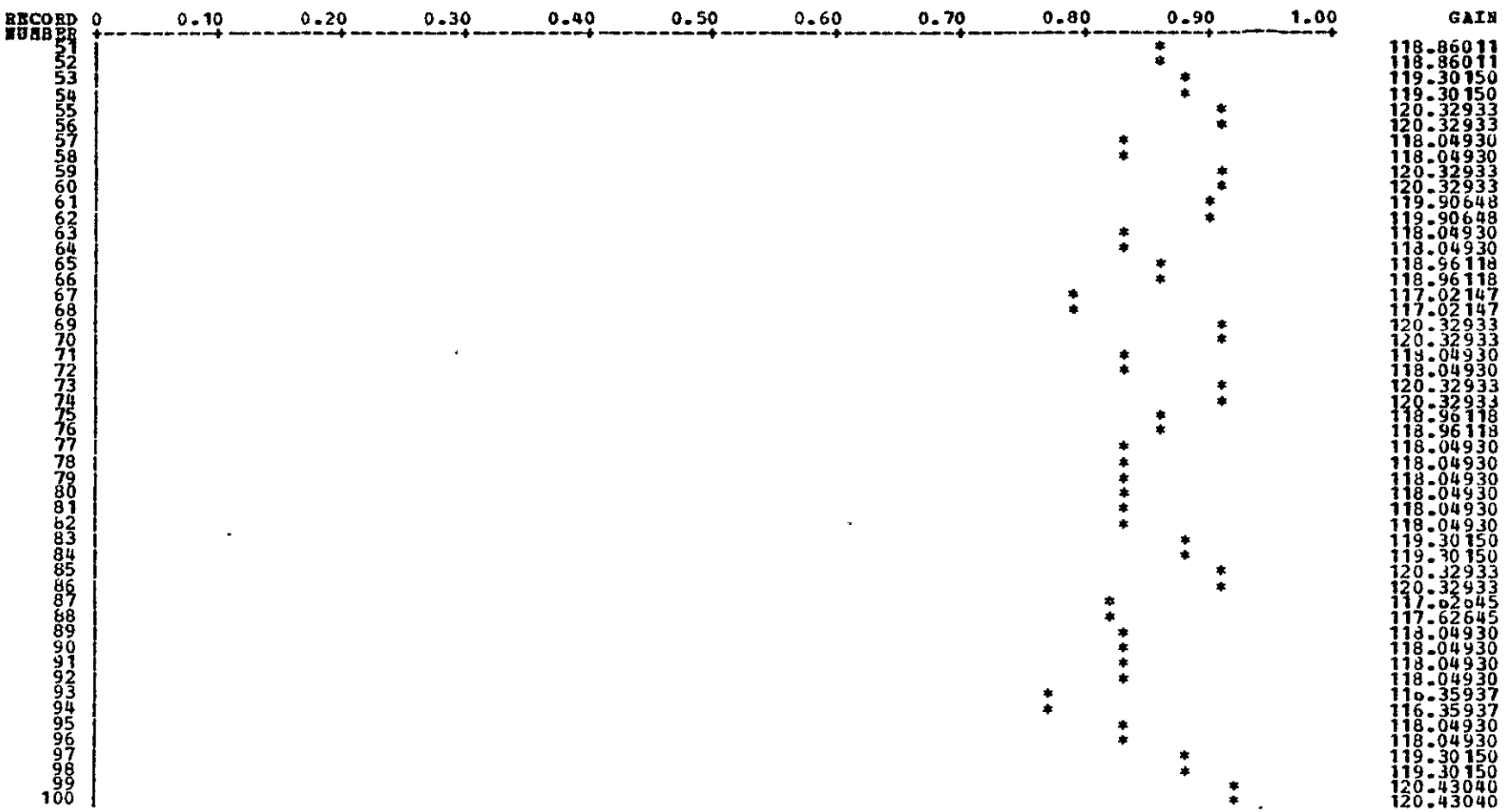

Figure 4.2-7 (Sheet 2 of 5)

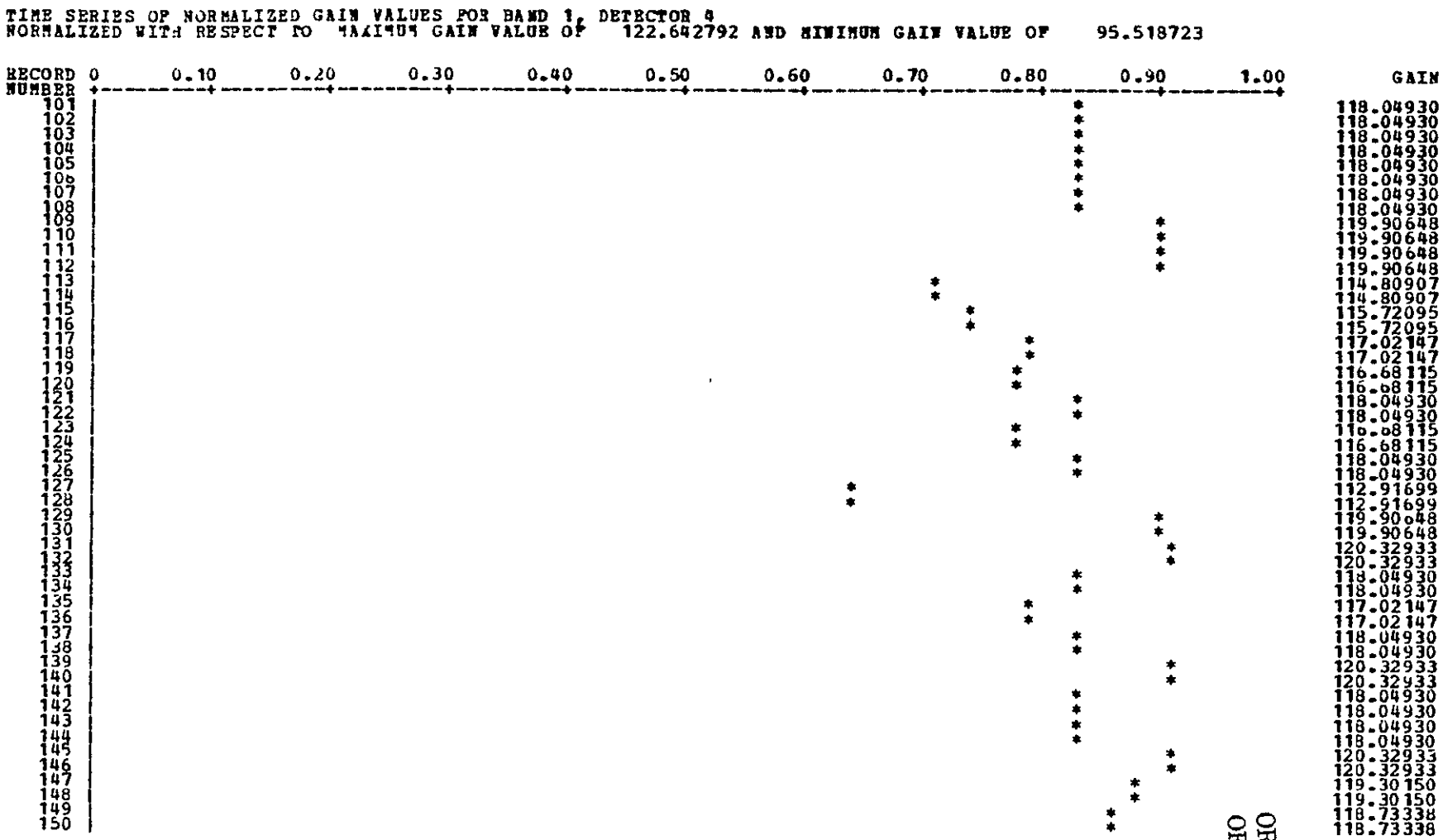

Figure 4.2-7 (Sheet 3 of 5)

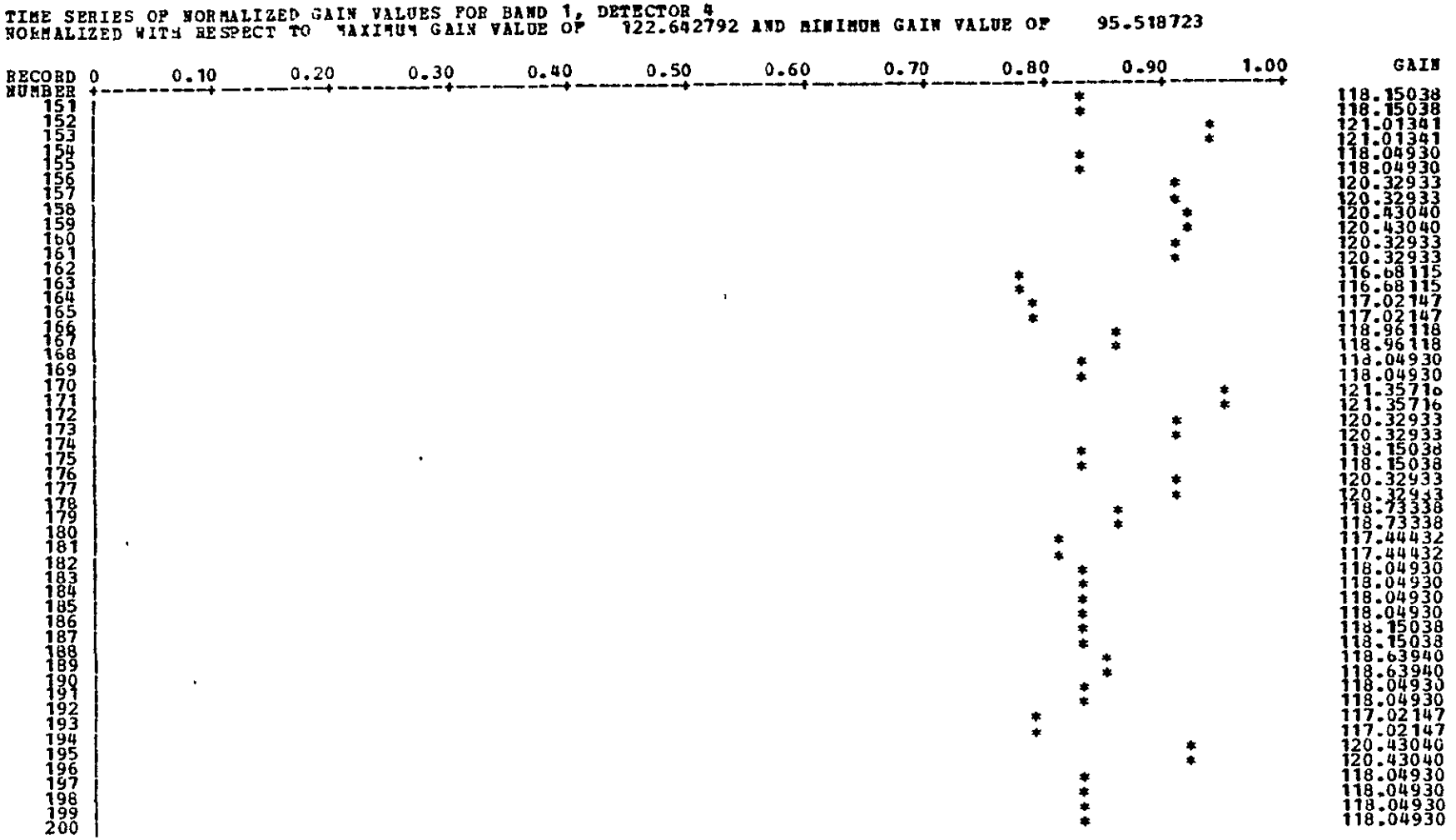

Figure 4.2-7 (Sheet 4 of 5)

TIME SERIES OF NORMALIZED GAIN VALUES FOR BAND 1, DETECTOR 4
NORMALIZED WITH RESPECT TO MAXIMUM GAIN VALUE OF 122.642792 AND MINIMUM GAIN VALUE OF 95.518723

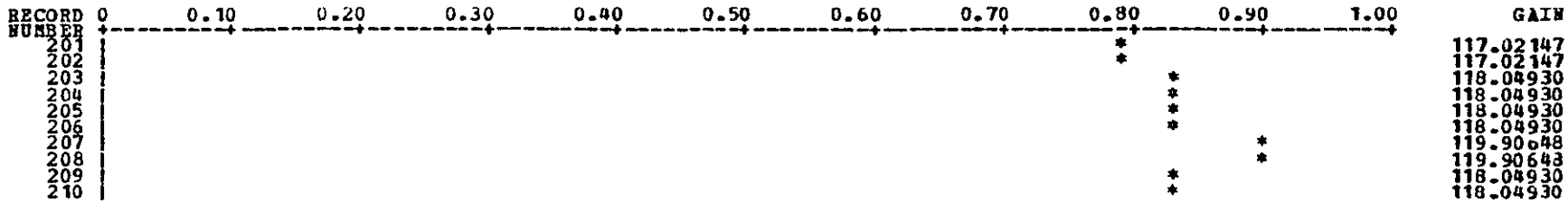

Figure 4.2-7 (Sheet 5 of 5)

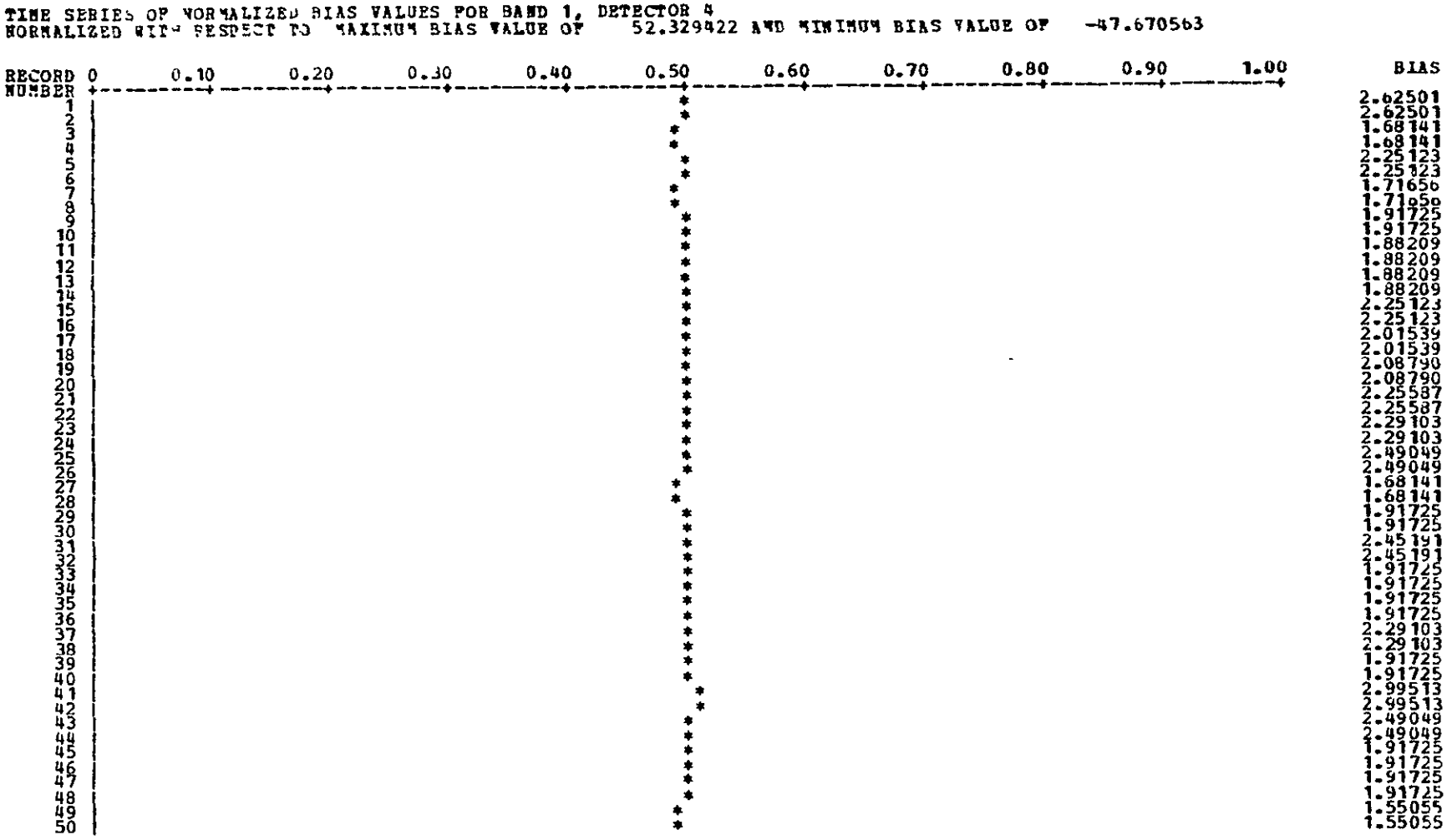

Figure 4.2-8 (Sheet 1 of 5)

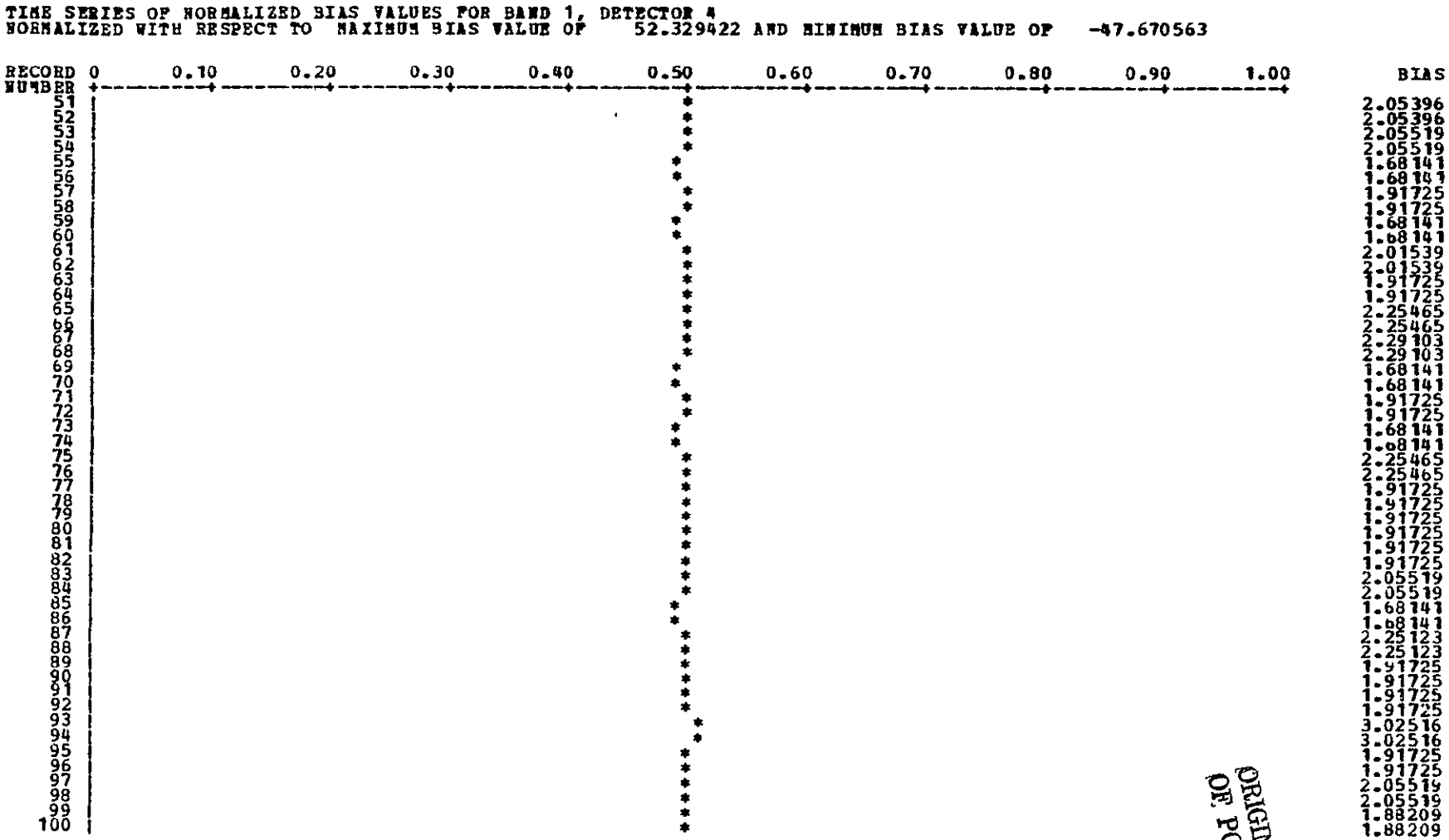

Figure 4.2-8 (Sheet 2 of 5)

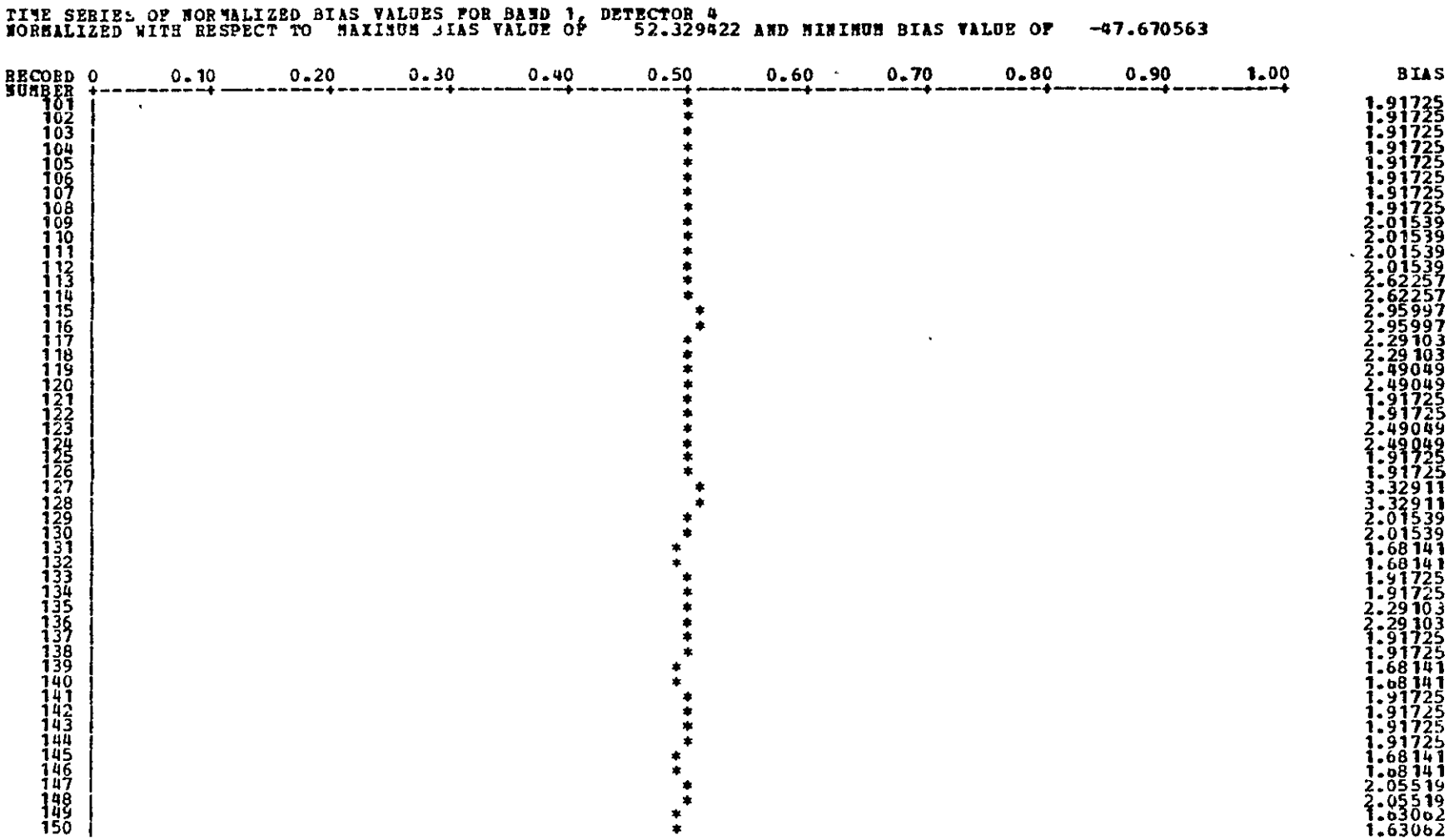

Figure 4.2-8 (Sheet 3 of 5)

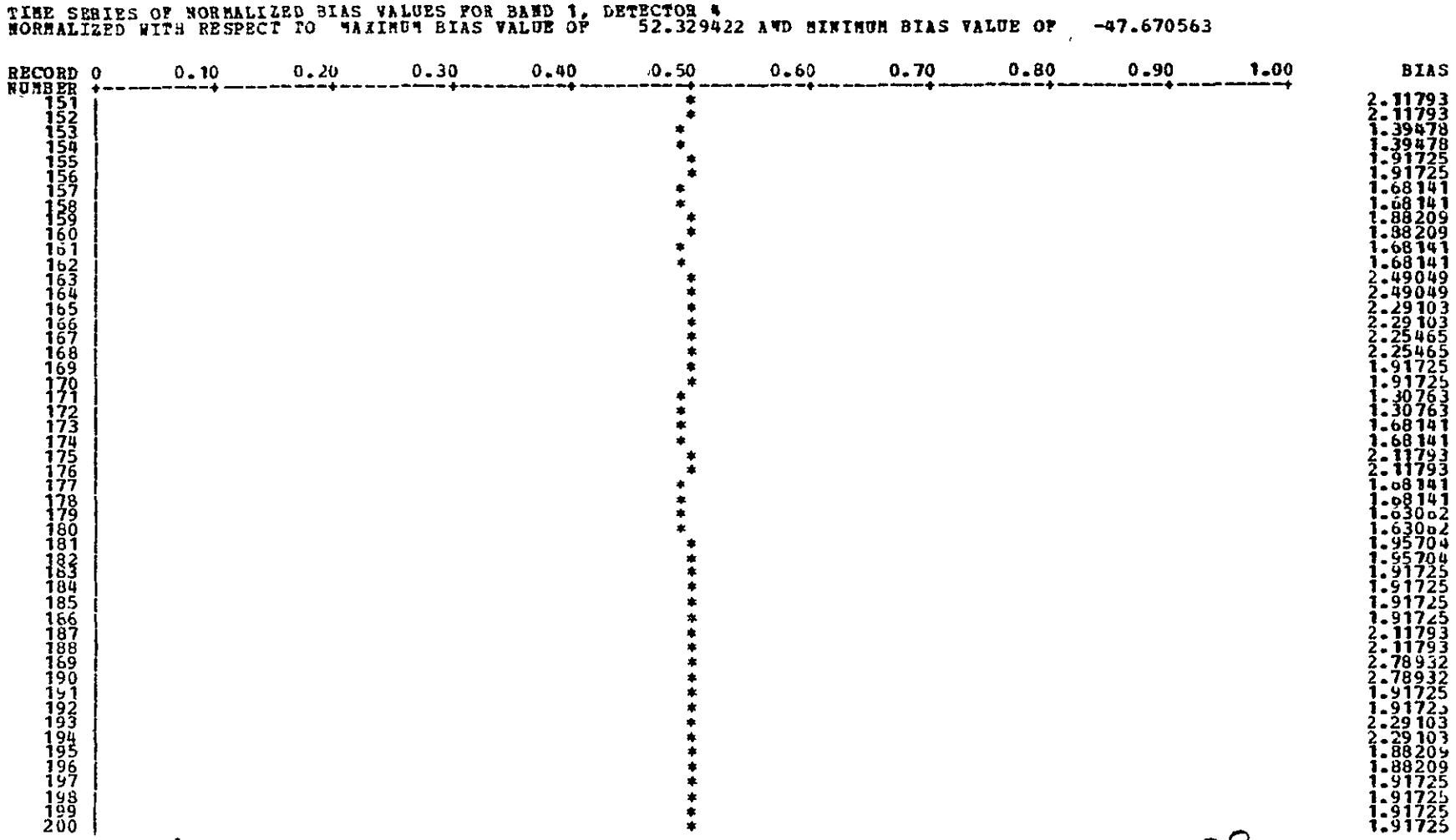

Figure 4.2-8 (Sheet 4 of 5)

TIME SERIES OF NORMALIZED BIAS VALUES FOR BAND 1, DETECTOR 4
NORMALIZED WITH RESPECT TO MAXIMUM BIAS VALUE OF 52.329422 AND MINIMUM BIAS VALUE OF -47.670563

RECORD NUMBER	0 0.10 0.20 0.30 0.40 0.50 0.60 0.70 0.80 0.90 1.00	BIAS
201	*	2.29103
202	*	2.29103
203	*	1.91725
204	*	1.91725
205	*	1.91725
206	*	1.91725
207	*	2.01539
208	*	2.01539
209	*	1.91725
210	*	1.91725

Figure 4.2-8 (Sheet 5 of 5)

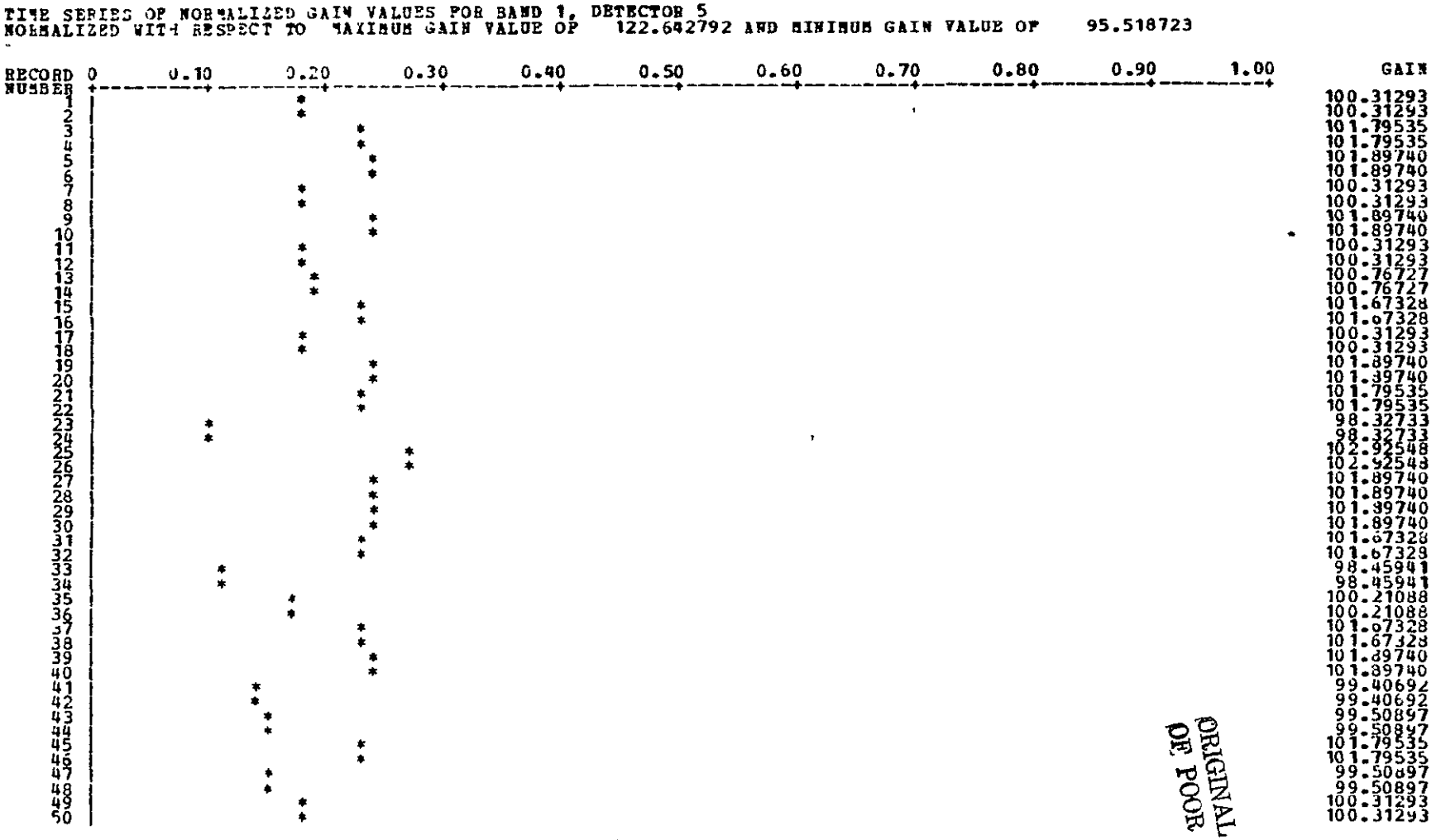

Figure 4.2-9 (Sheet 1 of 5)

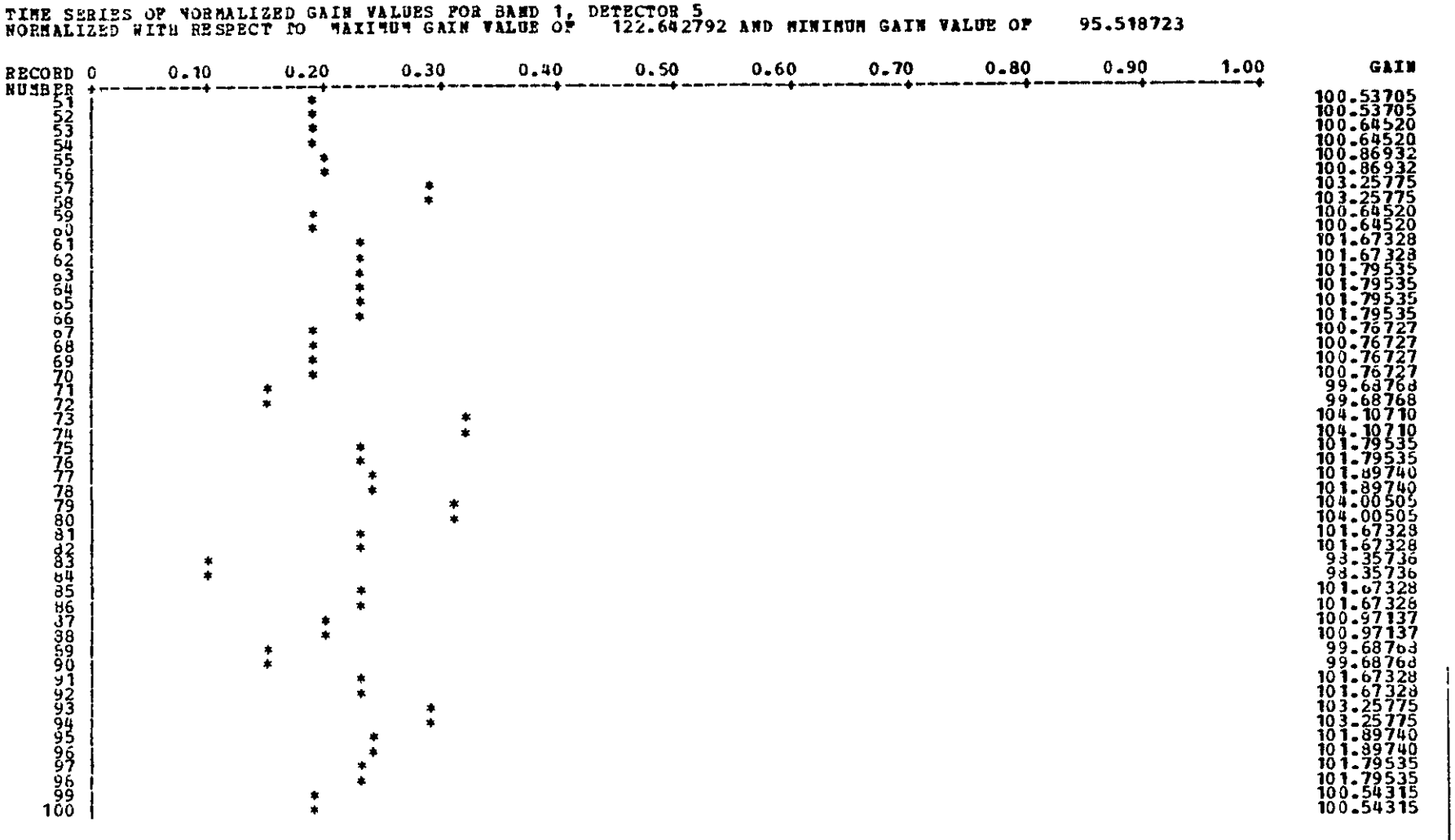

Figure 4.2-9 (Sheet 2 of 5)

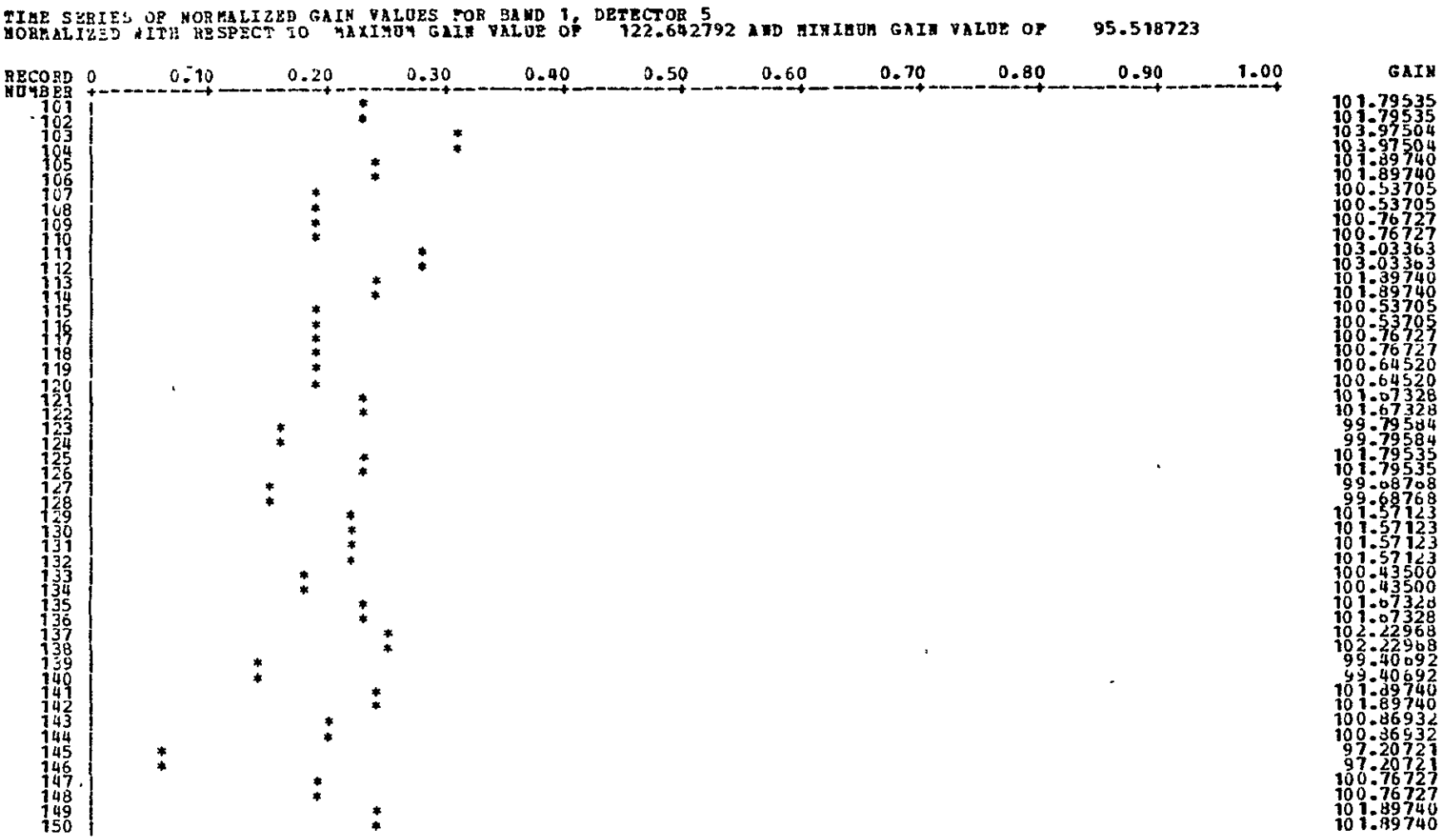

Figure 4.2-9 (Sheet 3 of 5)

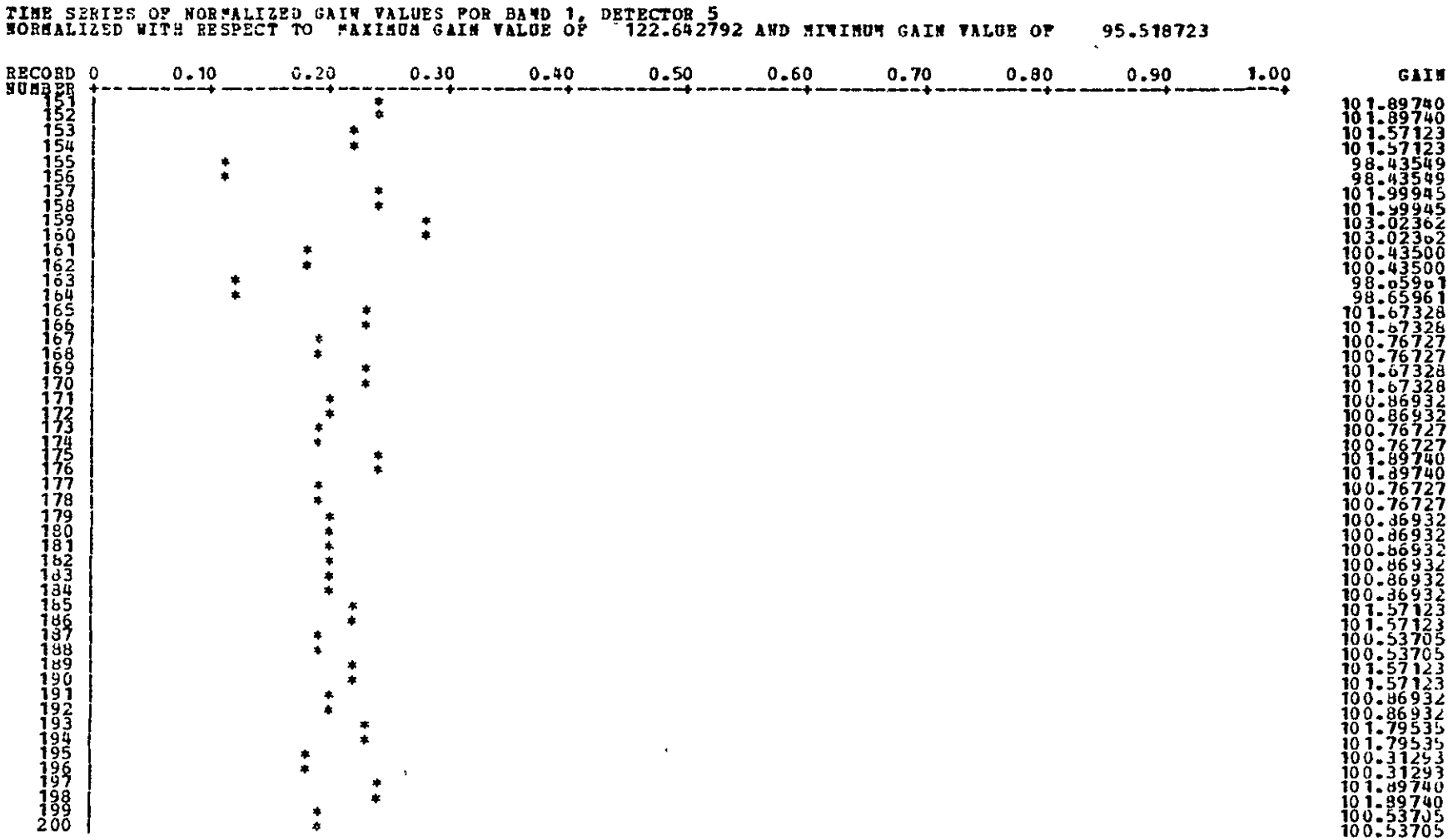

Figure 4.2-9 (Sheet 4 of 5)

TIME SERIES OF NORMALIZED GAIN VALUES FOR BAND 1, DETECTOR 5
NORMALIZED WITH RESPECT TO MAXIMUM GAIN VALUE OF 122.642792 AND MINIMUM GAIN VALUE OF 95.518723

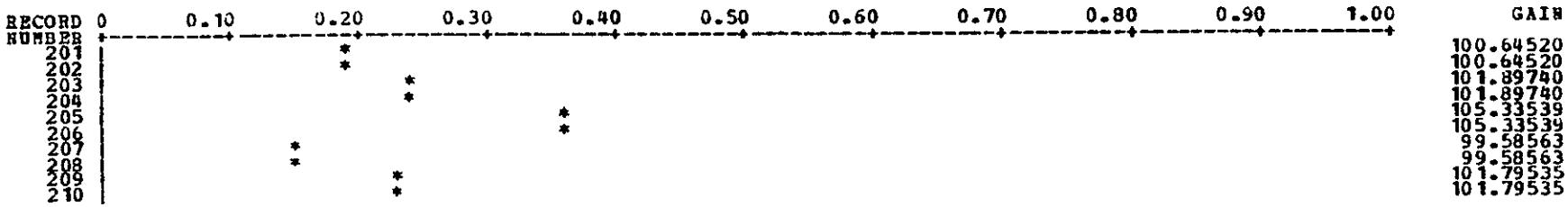

Figure 4.2-9 (Sheet 5 of 5)

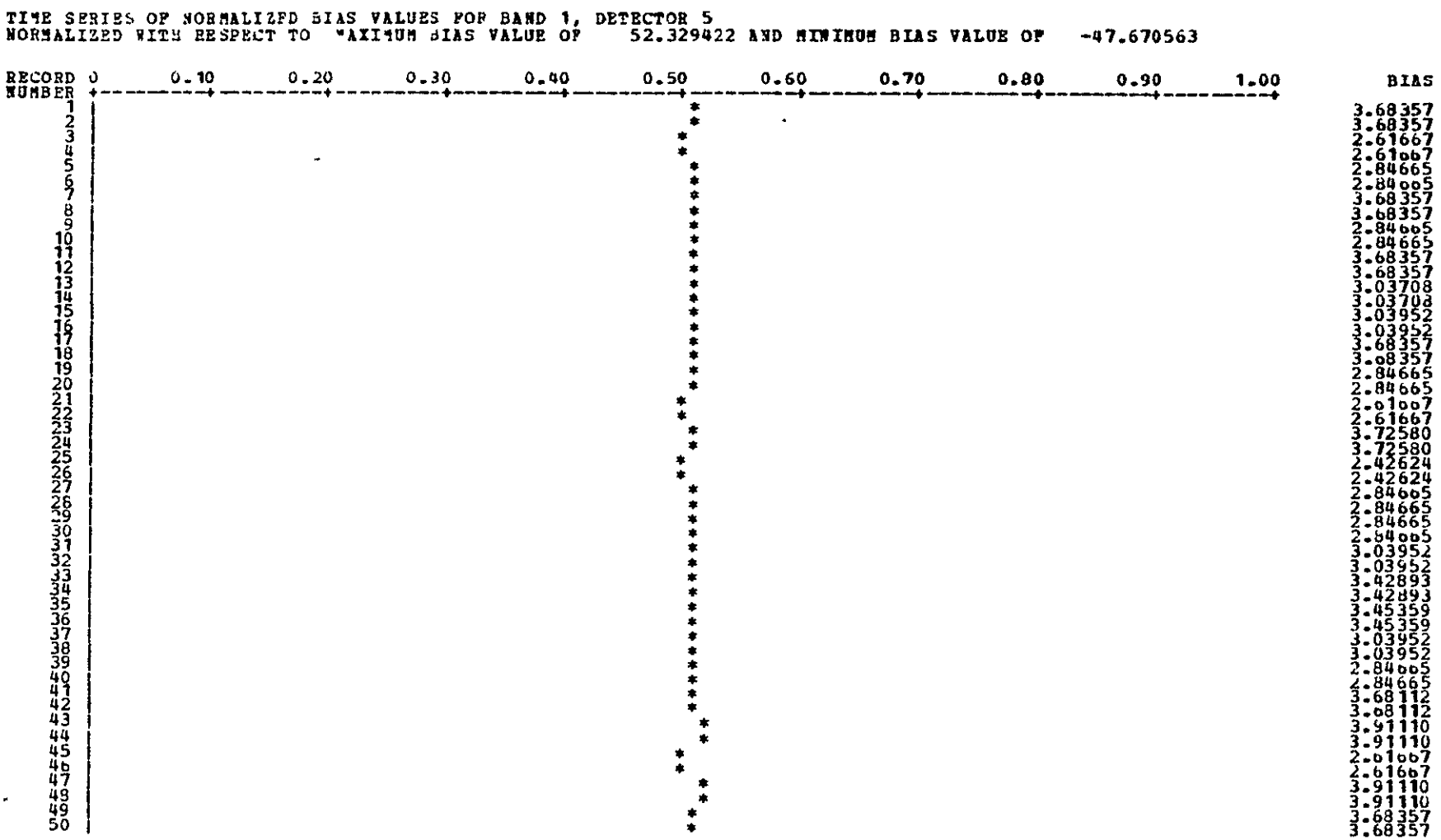

Figure 4.2-10 (Sheet 1 of 5)

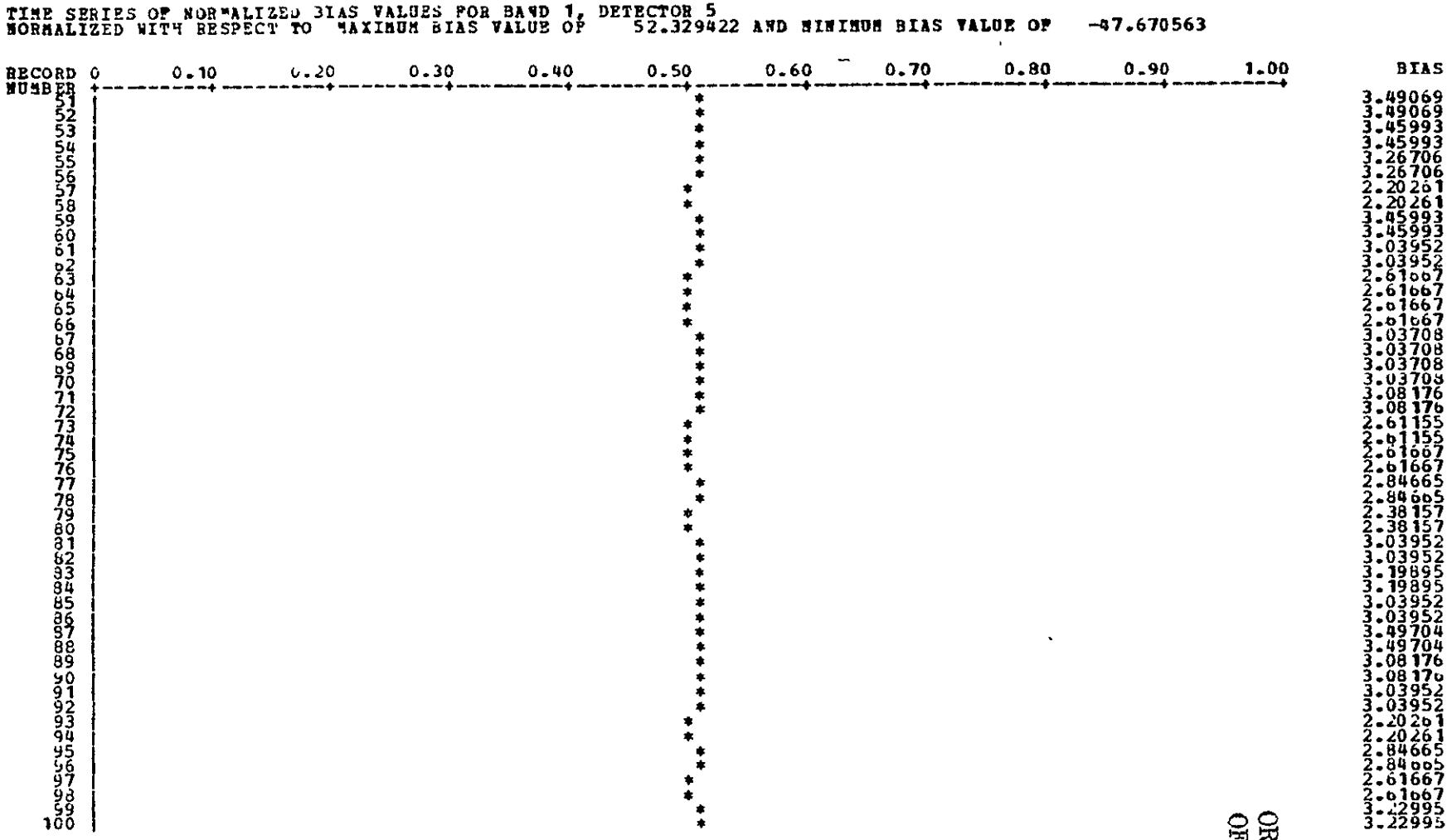

Figure 4.2-10 (Sheet 2 of 5)

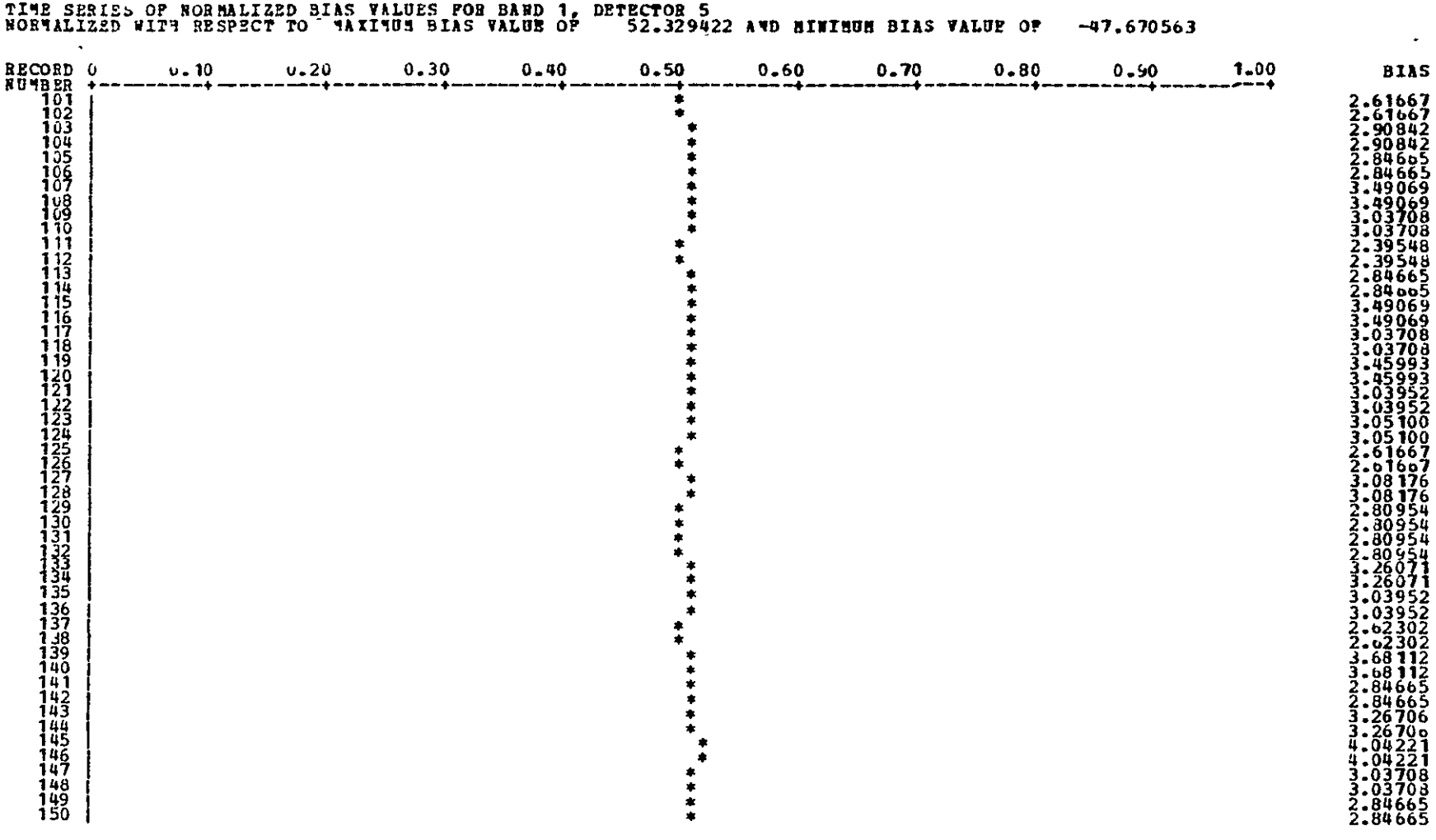

Figure 4.2-10 (Sheet 3 of 5)

TIME SERIES OF NORMALIZED BIAS VALUES FOR BAND 1, DETECTOR 5
NORMALIZED WITH RESPECT TO MAXIMUM BIAS VALUE OF 52.329422 AND MINIMUM BIAS VALUE OF -47.670563

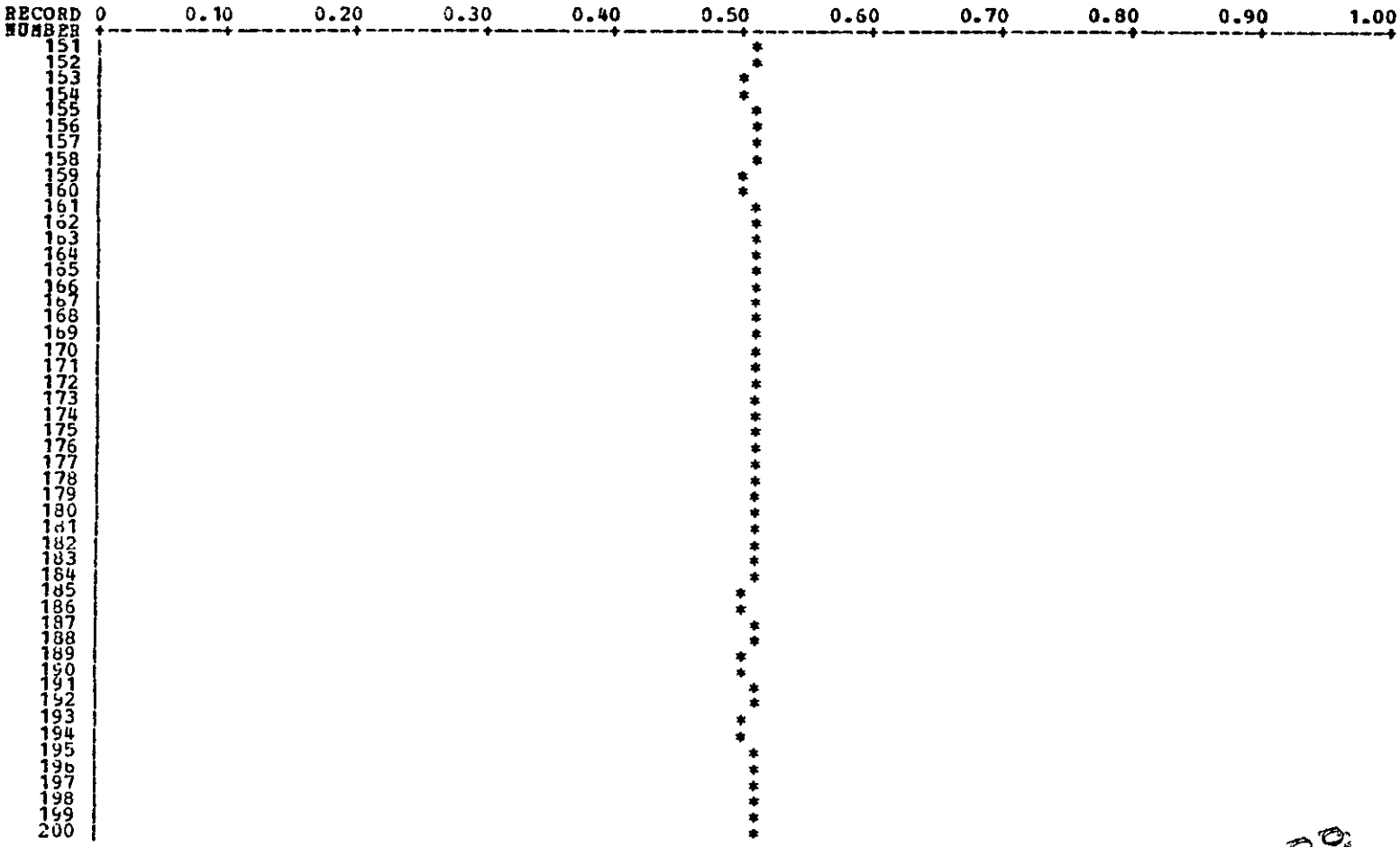

BIAS

2.84665
2.84665
2.80954
2.80954
3.69504
3.69504
3.07663
3.07663
2.26950
2.26950
3.26071
3.26071
3.50217
3.50217
3.03952
3.03952
3.03708
3.03708
3.03952
3.03952
3.26706
3.26706
3.03708
3.03708
2.84665
2.84665
2.84665
3.03708
3.03708
3.26706
3.26706
3.26706
3.26706
3.26706
3.26706
2.80954
2.80954
3.49069
3.49069
2.80954
2.80954
3.26706
3.26706
2.61067
2.61067
3.68357
3.68357
2.84665
2.84665
3.49069
3.49069

Figure 4.2-10 (Sheet 4 of 5)

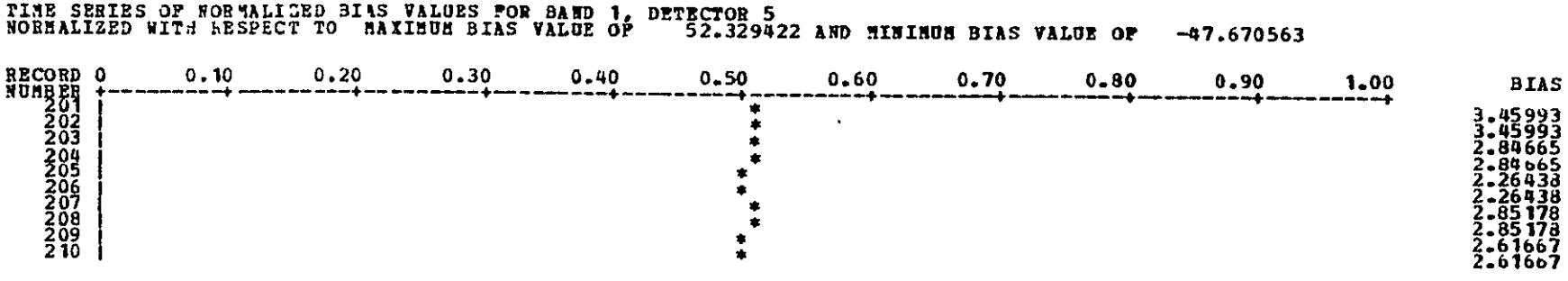

Figure 4.2-10 (Sheet 5 of 5)

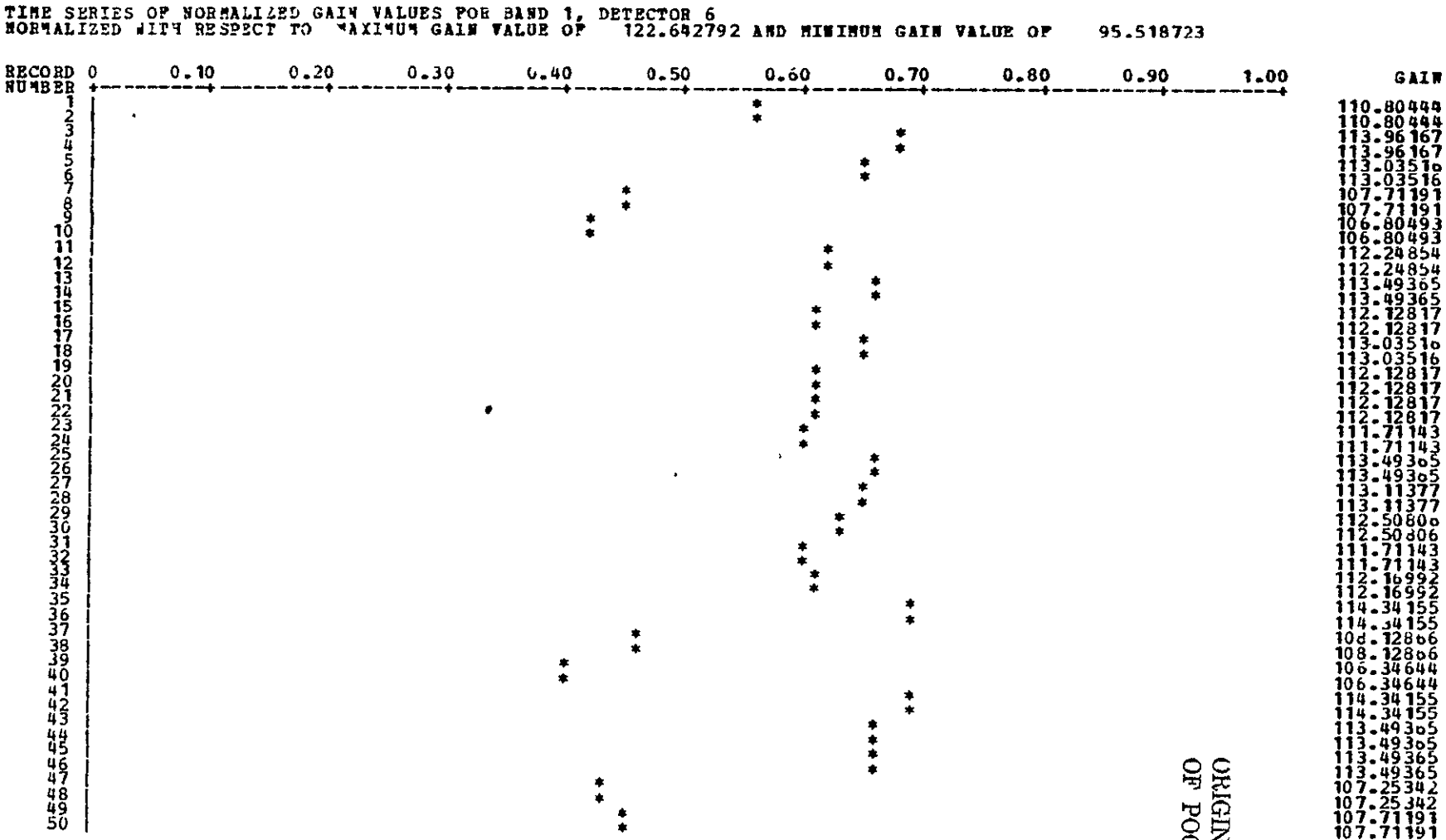

Figure 4.2-11 (Sheet 1 of 5)

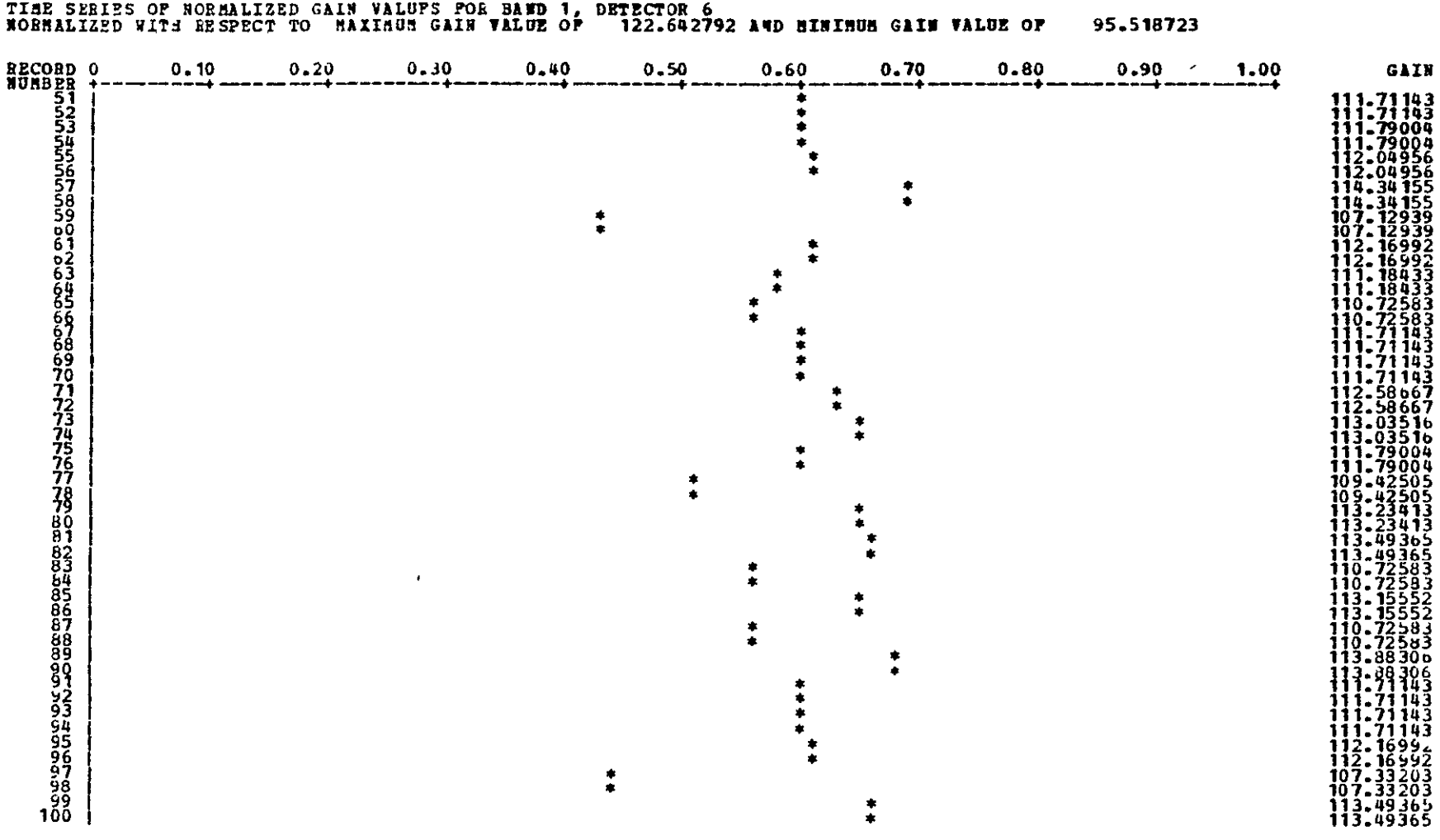

Figure 4.2-11 (Sheet 2 of 5)

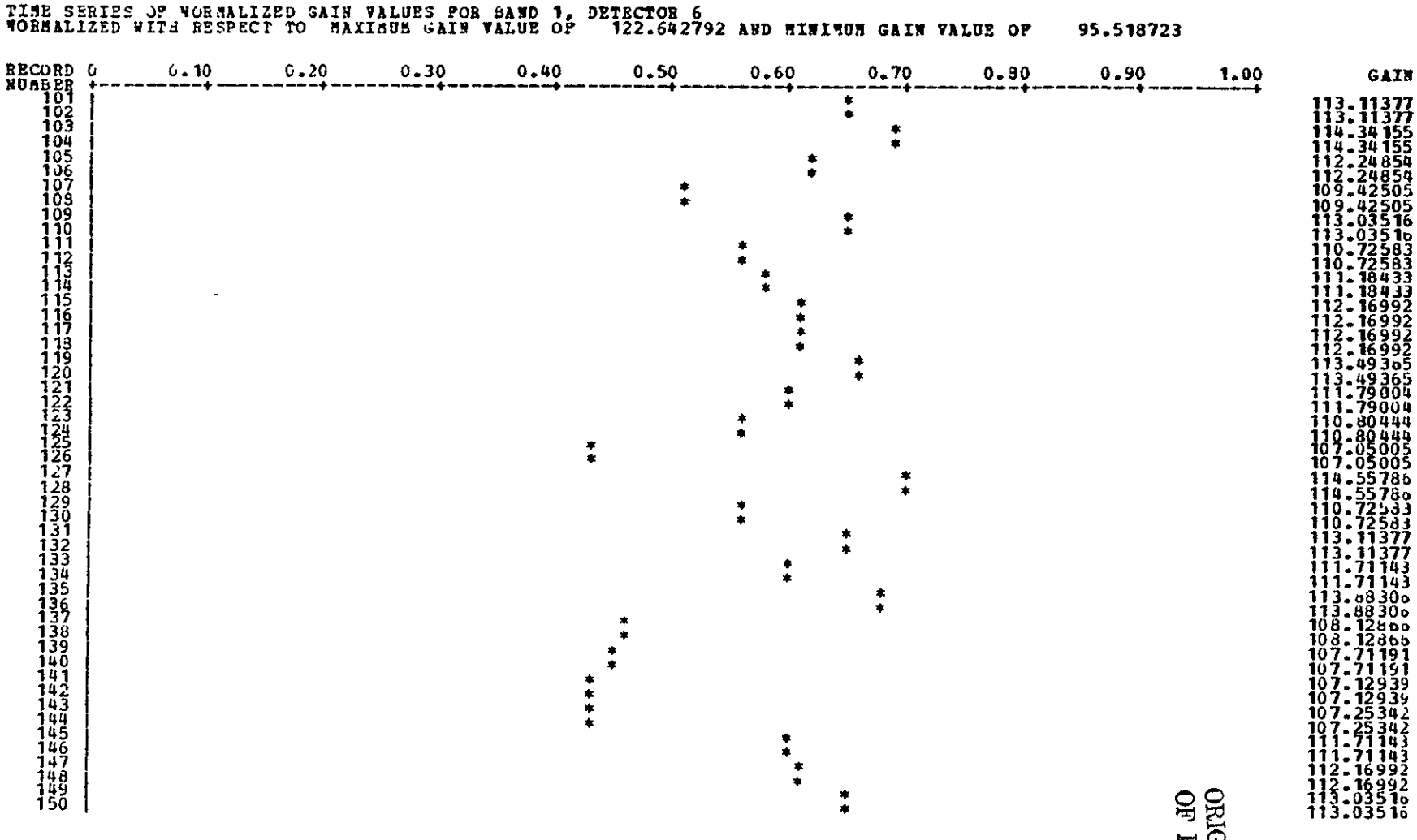

Figure 4.2-11 (Sheet 3 of 5)

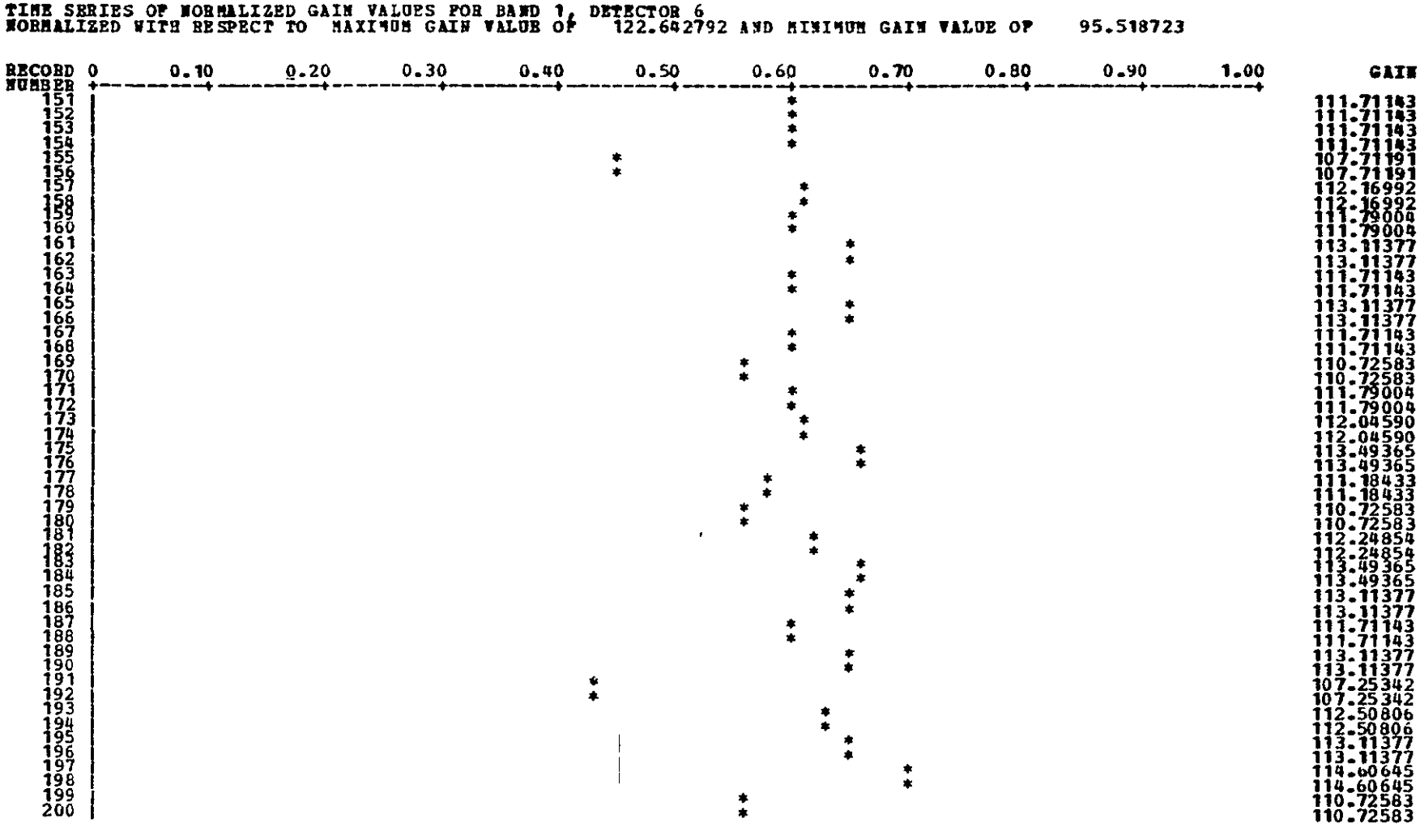

Figure 4.2-11 (Sheet 4 of 5)

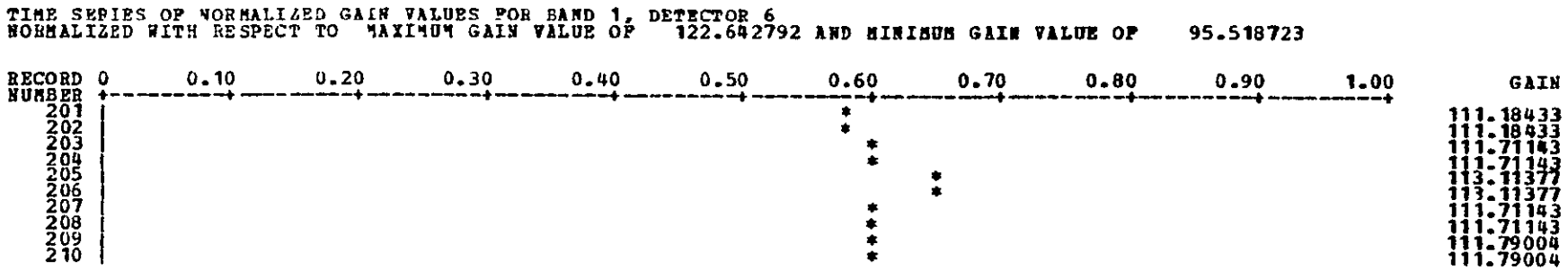

Figure 4.2-11 (Sheet 5 of 5)

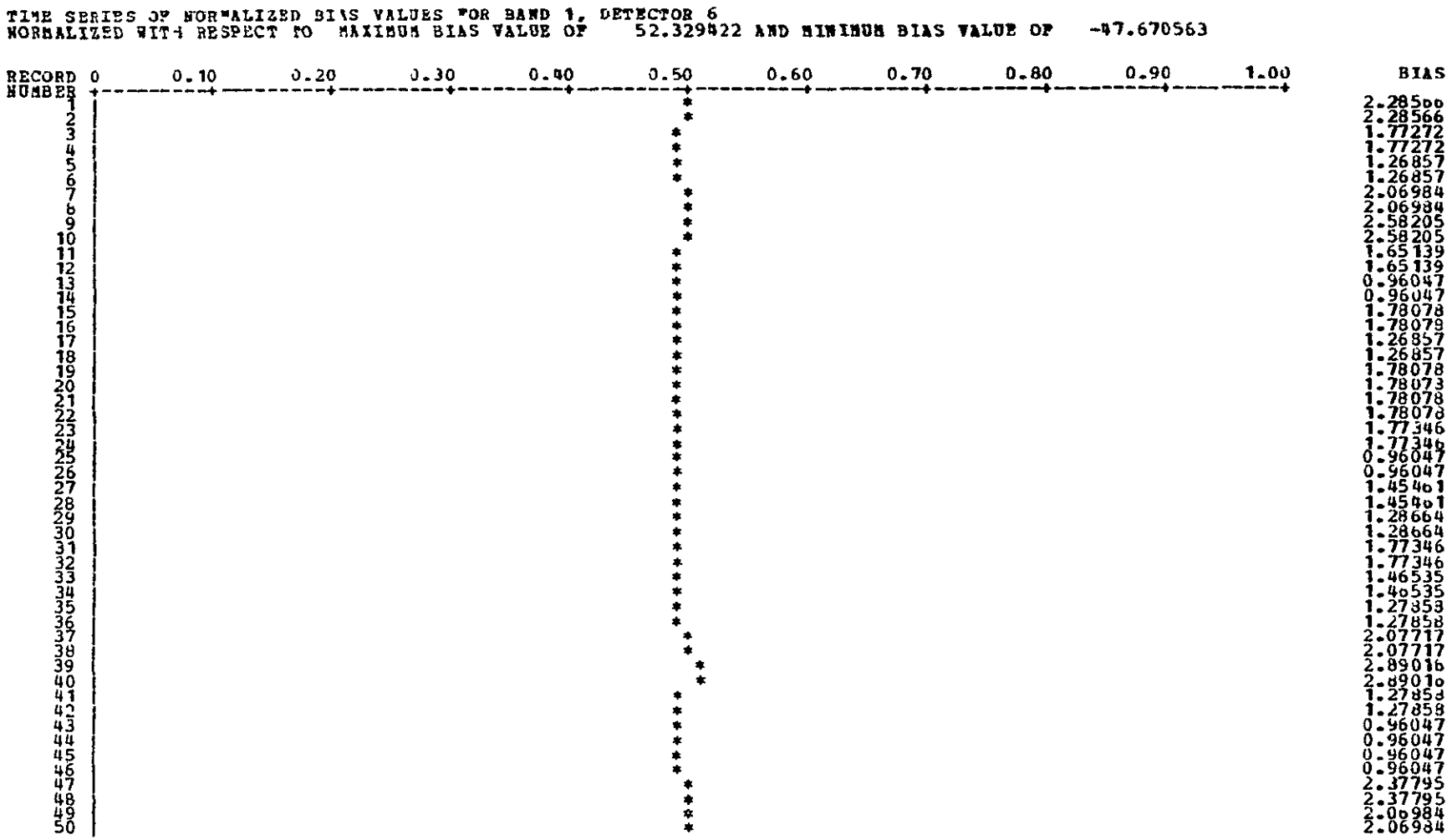

Figure 4.2-12 (Sheet 1 of 5)

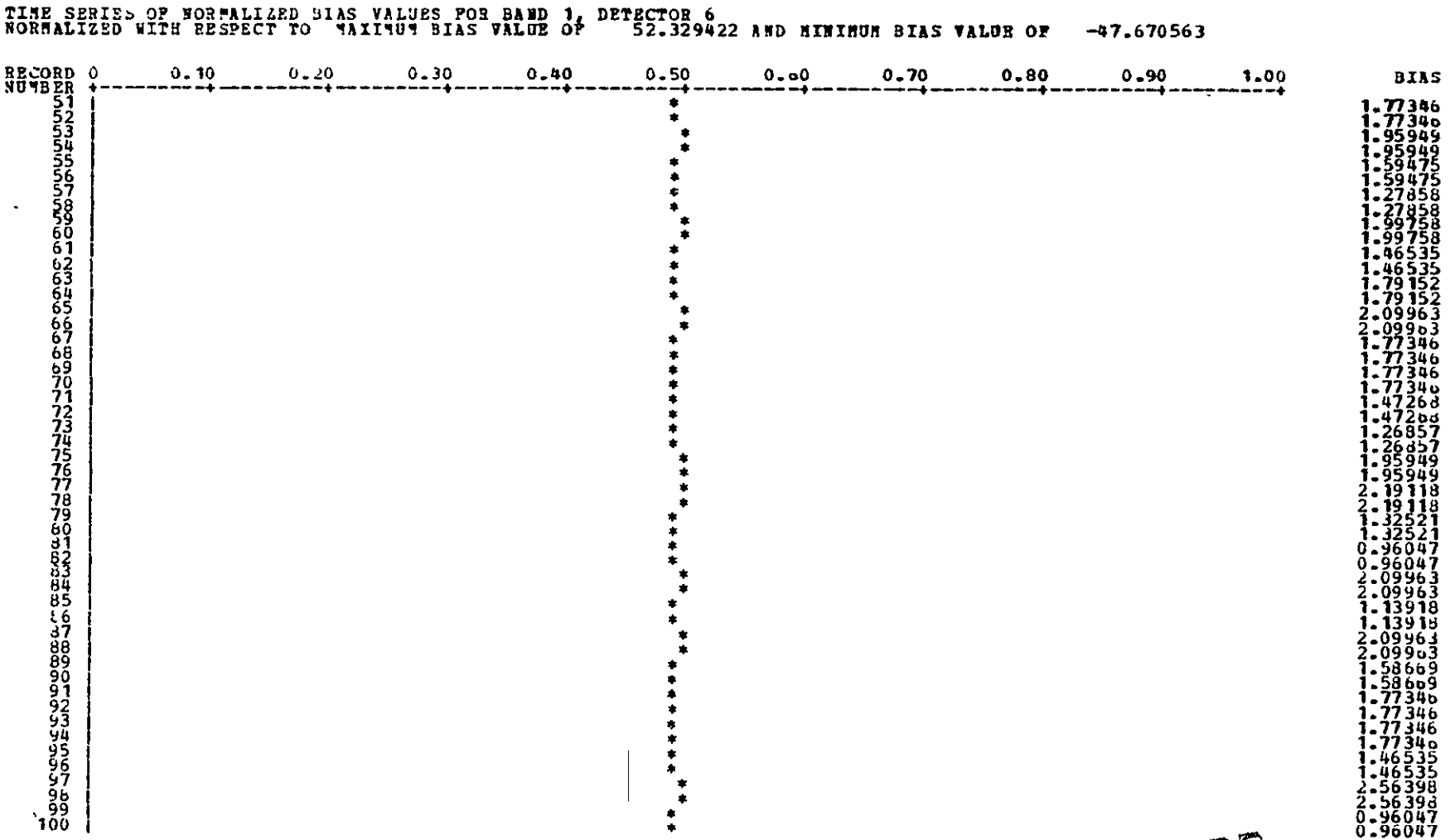

Figure 4.2-12 (Sheet 2 of 5)

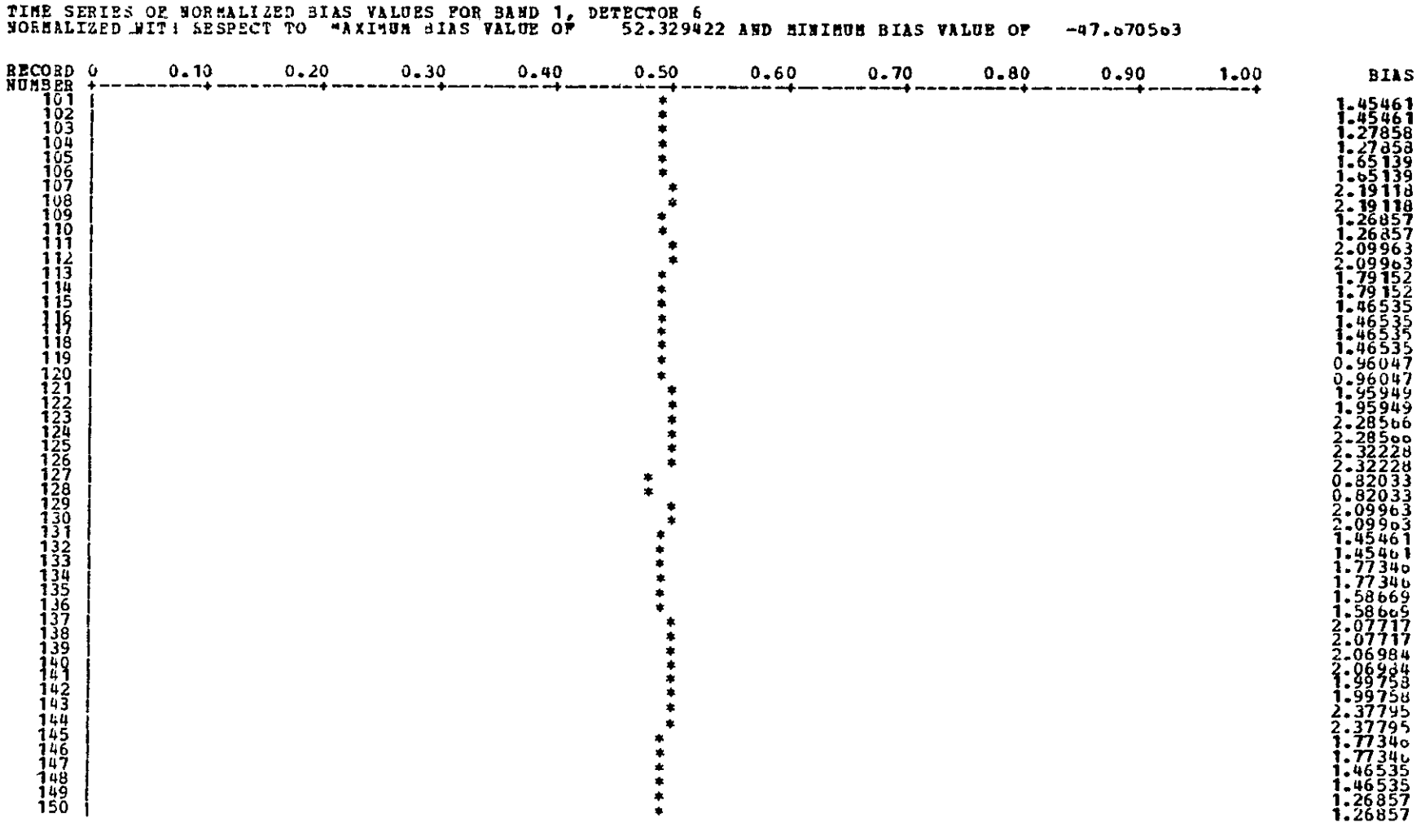

Figure 4.2-12 (Sheet 3 of 5)

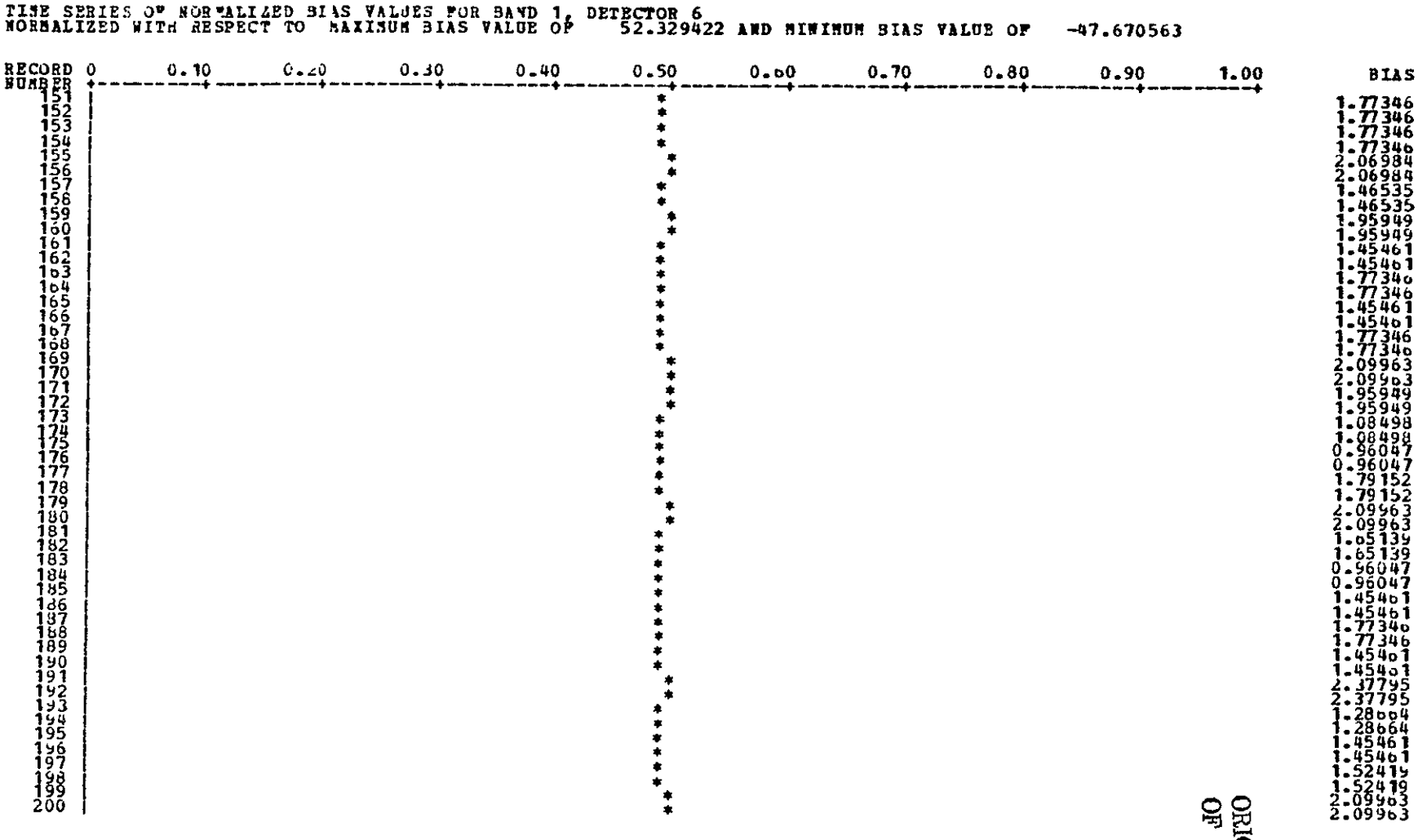

Figure 4.2-12 (Sheet 4 of 5)

TIME SERIES OF NORMALIZED BIAS VALUES FOR BAND 1, DETECTOR 6
NORMALIZED WITH RESPECT TO MAXIMUM BIAS VALUE OF 52.329422 AND MINIMUM BIAS VALUE OF -47.670563

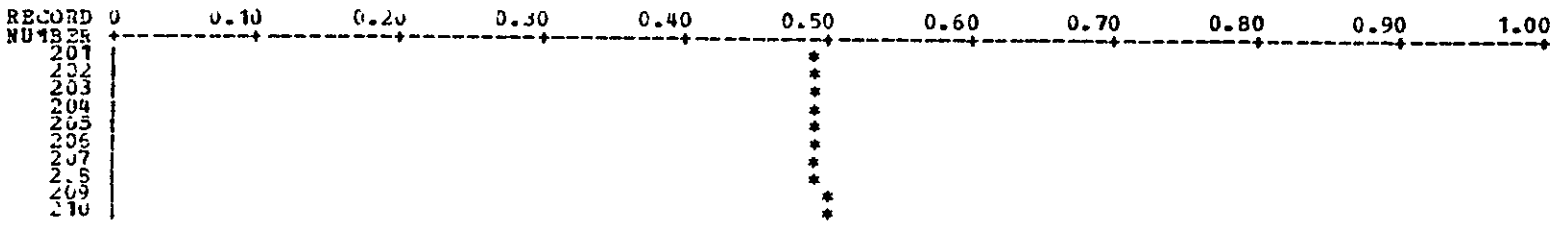

BIAS
1.79152
1.79152
1.77346
1.77346
1.45461
1.45461
1.77346
1.77346
1.95949
1.95949

Figure 4.2-12 (Sheet 5 of 5)

4.3 INTERDETECTOR CORRELATION PLOTS

Interdetector correlation plots of the means and root-mean-squared variation for 50 calibration wedge values were generated in order to display the relative radiometric characteristics of the six detectors and to evaluate the adequacy of the present linear MSS calibration procedure, as well as that of the various linear striping removal procedures. These plots use sample position within the calibration wedge to identify corresponding detector response samples. To the extent that the calibration radiances presented to each detector at corresponding sample positions are the same, the plots present the relationship which exists between the responses of the detector pairs. These plots are presented as Figures 4.3-1 through 4.3-5. A list of the sample positions in the calibration wedge data used to provide data for the plots is given in Table 4.3-1. Position 1 is the first sample of the calibration wedge data.

These plots are essentially two-dimensional histograms where the abscissa scale consists of radiometric values for the reference detector (detector 1), and the ordinate scale consists of radiometric values for detector n (n = 2,3,4,5,6). In constructing this plot, the mean value of calibration wedge sample k of detector 1, $\overline{i}_{1k}$, and the mean value of calibration sample k of detector n, $\overline{i}_{nk}$, plus and minus the corresponding standard deviations about these means, s_{1k} and s_{nk}, are used to specify a region of the plot array, and the counts in the array elements within this region are incremented by 1. The numbers in the interdetector correlation plots are counts thus accumulated. This sort of plot provides a graphic representation of the functional relationship between the radiometric response characteristics of the separate MSS detectors (e.g., for two detectors viewing a set of equal radiances, if the relationship between the radiometric responses of the two detectors is linear, the plot will be a straight line; if the responses of the two detectors are the same, the line will have unity slope and zero intercept).

Table 4.3-1. Positions in Calibration Wedge Data of Samples Represented in Interdetector Correlation Plots

160	380	530	680
180	390	540	690
200	400	550	700
220	410	560	710
240	420	570	720
260	430	580	730
280	440	590	750
300	450	600	770
310	460	610	790
320	470	620	810
330	480	630	830
340	490	640	850
350	500	650	870
360	510	660	890
370	520	670	910

All five of these plots show a relationship between detector responses which is essentially linear over the range from Ø to 80 along the reference detector axis, with a minor departure from this linearity from 80 to 110 for all detectors. Detectors 4 and 5 exhibit the most severe departures from a linear relationship, this amounting to 3 counts displacement from a linear trend at a reference detector value of 110.

In order to provide a quantitative comparison of the functional relationship among the six detectors the slopes, $p_n = \Delta i_n / \Delta i$, and intercepts, q_n, for each of the correlation plots over the linear region, from 0 to 80 with respect to detector 1, were calculated for straight lines manually laid on the plots. These slopes are presented in Table 4.3-2. Also presented in this table are corresponding slope and intercept values calculated from the typical gain and bias values (B and G) given in Table 4.2-2, which were obtained from the gain plots of the standard MSS calibration coefficients. To calculate these latter slope and intercept values, the linear calibration functions for detector 1 and detector n

$$\sigma_1 = g_1 \, i_1 + b_1$$

and

$$\sigma_n = g_n \, i_n + b_n$$

where σ_i is a calibrated sample value
i_i is an uncalibrated sample value
g_i is the gain coefficient G for detector i
b_i is the bias coefficient B for detector i

are used. Note that the calibration processing for a detector is performed so that, for a given incident detector excitation, r, the calibrated

Table 4.3-2. Functional Interdetector Relationship for MSS Calibration Wedge Data

Detectors	Functional Interdetector Relationship $i_n = p_n i_n + q_n$		Interdetector Relationship from MSS Calibration $i_n = p'_n i_n + q'_n$	
	p_n	q_n	p'_n	q'_n
1 vs 2	0.9866	0.0	1.1033	1.7513
1 vs 3	1.1059	1.1	1.0957	0.4120
1 vs 4	1.1586	0.9	1.1892	0.9545
1 vs 5	0.9794	1.0	1.0223	1.8724
1 vs 6	1.1055	1.5	1.1148	0.8156

sample value is independent of the detector. Therefore, it should be the case that:

$$\sigma_1 = g_1 i_1 (r) + b_1 = \sigma$$

and $$\sigma_n = g_n i_n (r) + b_n = \sigma$$

Thus independent of the incident detector excitation and calibrated sample value

$$g_n i_n + b_n = g_1 i_1 + b_1$$

or $$i_n = \frac{g_1}{g_n} i_n + \frac{b_1 - b_n}{g_n} = p'_n i_n + q'_n$$

Using the typical values established for the calibration function gain and bias for as g_i and b_i, the slope and intercept of the interdetector relationship can be calculated.

Figures 4.3-6 through 4.3-10 are plots of the lines whose slopes and intercepts are given in Table 4.2-2, comparing the interdetector relationship obtained from the calibration data with that obtained from the MSS calibration procedure. In these plots, the solid line presents the interdetector relationship established on the basis of the correlation plots, of calibration data, while the dashed line presents the interdetector relationship which MSS calibration processing anticipates. As can be seen from these plots, there is substantial agreement between the two different interdetector relationships for detectors 3, 4, and 6, while for detectors 2 and 5 the MSS calibration relationship anticipates a different relationship from that expected on the basis of the calibration data.

It is tempting to identify the discrepancy observed for detectors 2 and 5 as the cause of the observed striping. However, visual inspection of

the data in the smaller, low frequency region employed in the power spectrum analysis reveals that the striping evident in the data set produced by using the MSS calibration procedure on the calibration data for a full scene of uncalibrated data (type b2 radiometric processing) consists of an apparent discrepancy in the radiometric data values of detectors 1 and 3 (approximately level 19) with respect to detectors 2, 4, 5, and 6 (approximately level 21). This observation is inconsistent with the hypothesis that a faulty calibration procedure is the cause of striping in data from detectors 2 and 5.

The foregoing analysis indicates that while the MSS calibration procedure does not produce a completely accurate characterization of the relationships among the MSS detectors, as represented by the calibration data reported for the detectors, the phenomenon of striping cannot be attributed to such inaccuracies. It must also be noted that the validity of this analysis depends critically on the assumption that the calibration wedge data used to establish the interdetector relationships represents the response of the detector pairs to the same set of radiances. If the calibration lamps are not uniform, or the neutral density filter used to generate the wedge is not uniform across the detectors, then the interdetector plots would need to be compensated for any such nonuniformity before valid conclusions could be drawn.

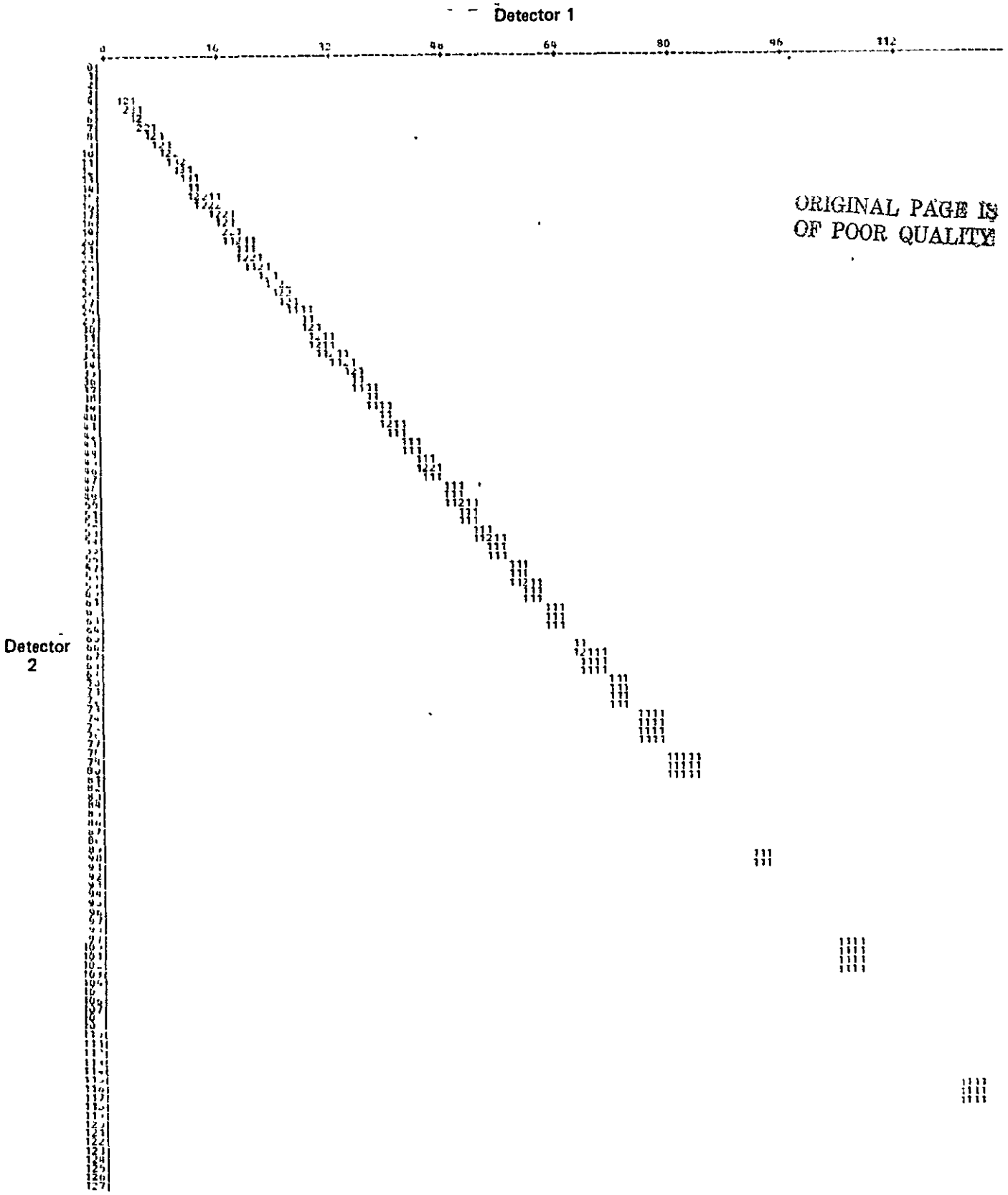

Figure 4.3-1. Interdetector Correlation Plot for Corresponding Decompressed Calibration Wedge Samples and their Standard Deviations, Detector 2 versus Detector 1, Band 1

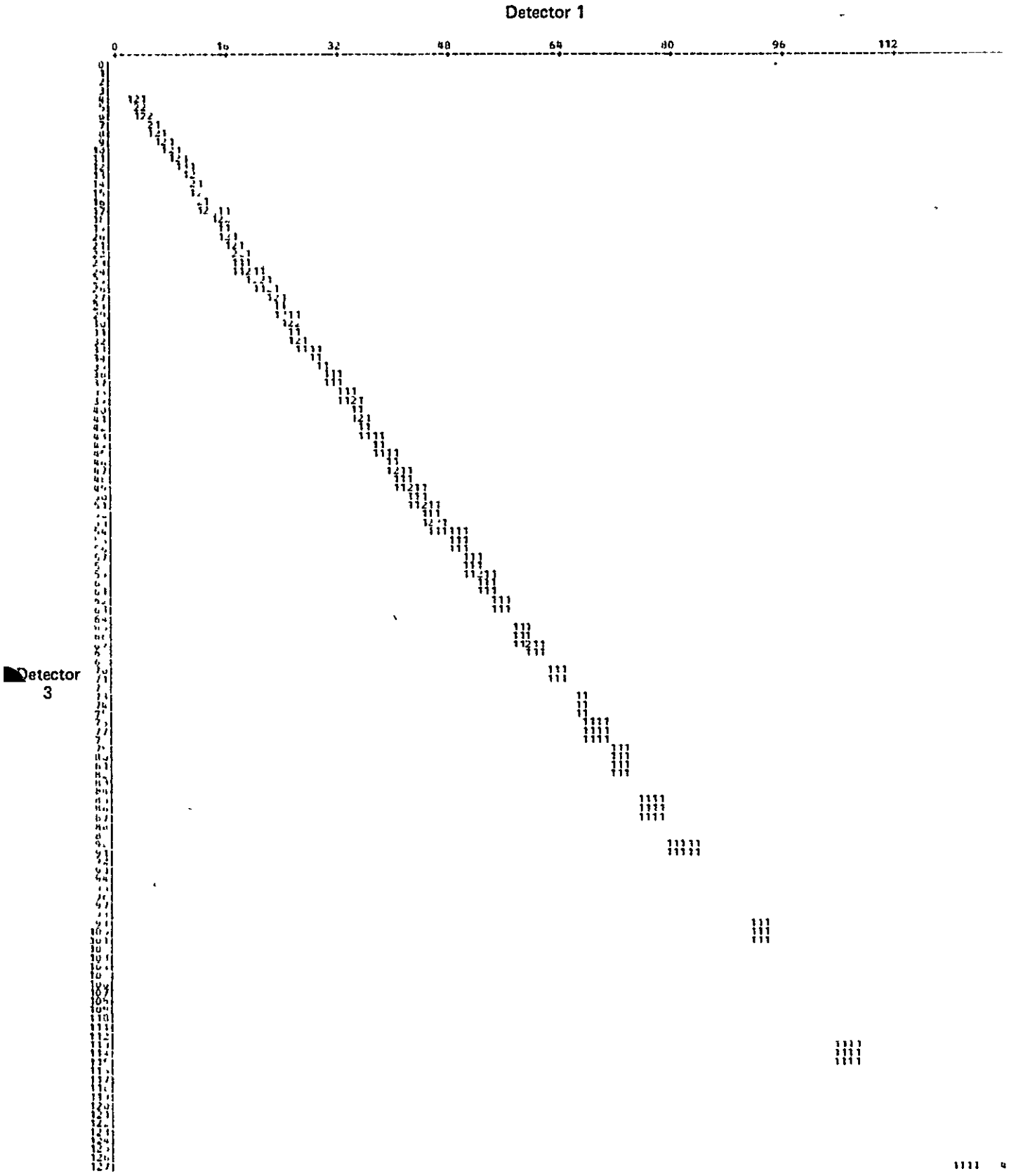

Figure 4.3-2. Interdetector Correlation Plot for Corresponding Decompressed Calibration Wedge Samples and their Standard Deviations, Detector 3 versus Detector 1, Band 1

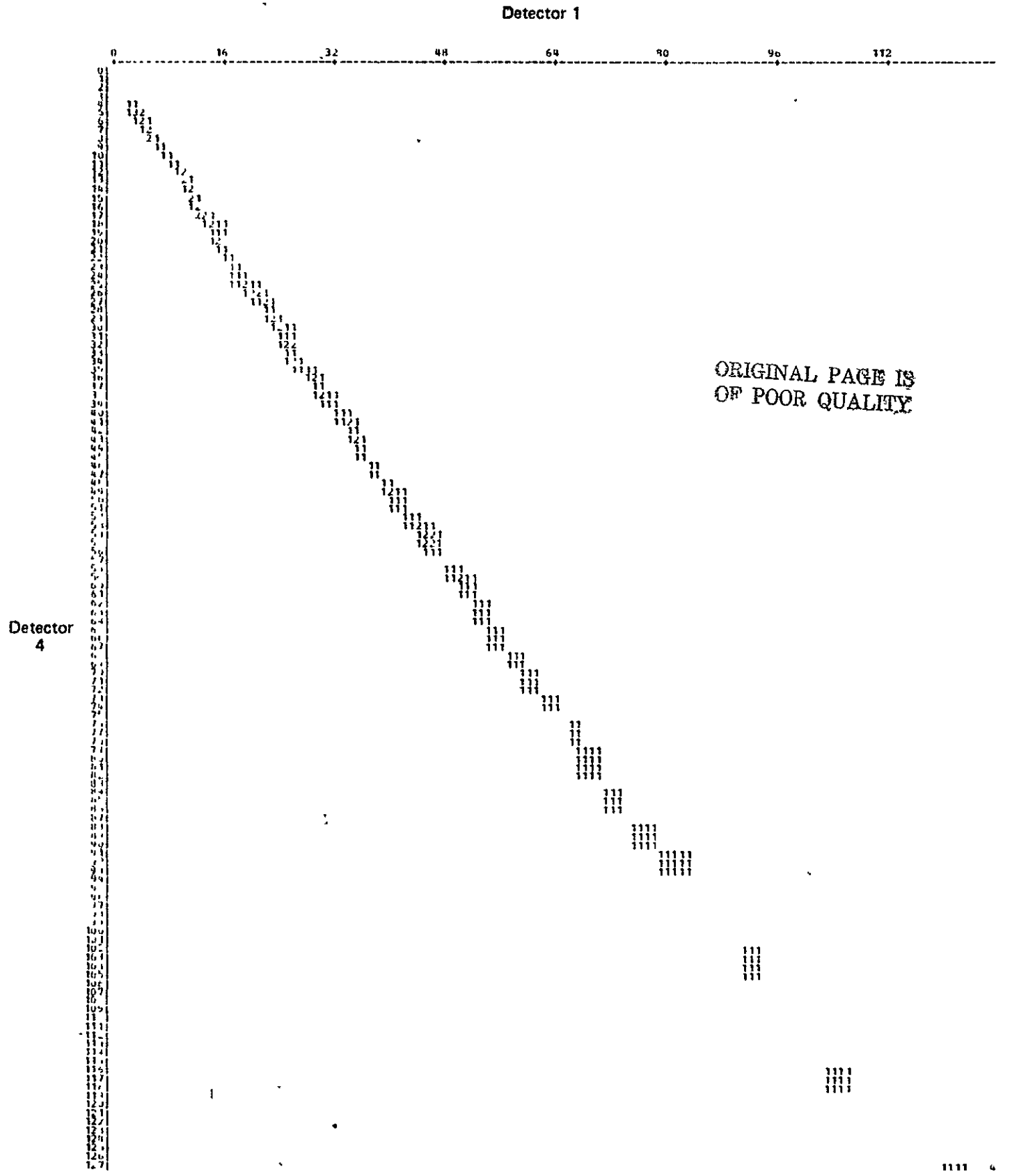

Figure 4.3-3. Interdetector Correlation Plot for Corresponding Decompressed Calibration Wedge Samples and their Standard Deviations, Detector 4 versus Detector 1, Band 1

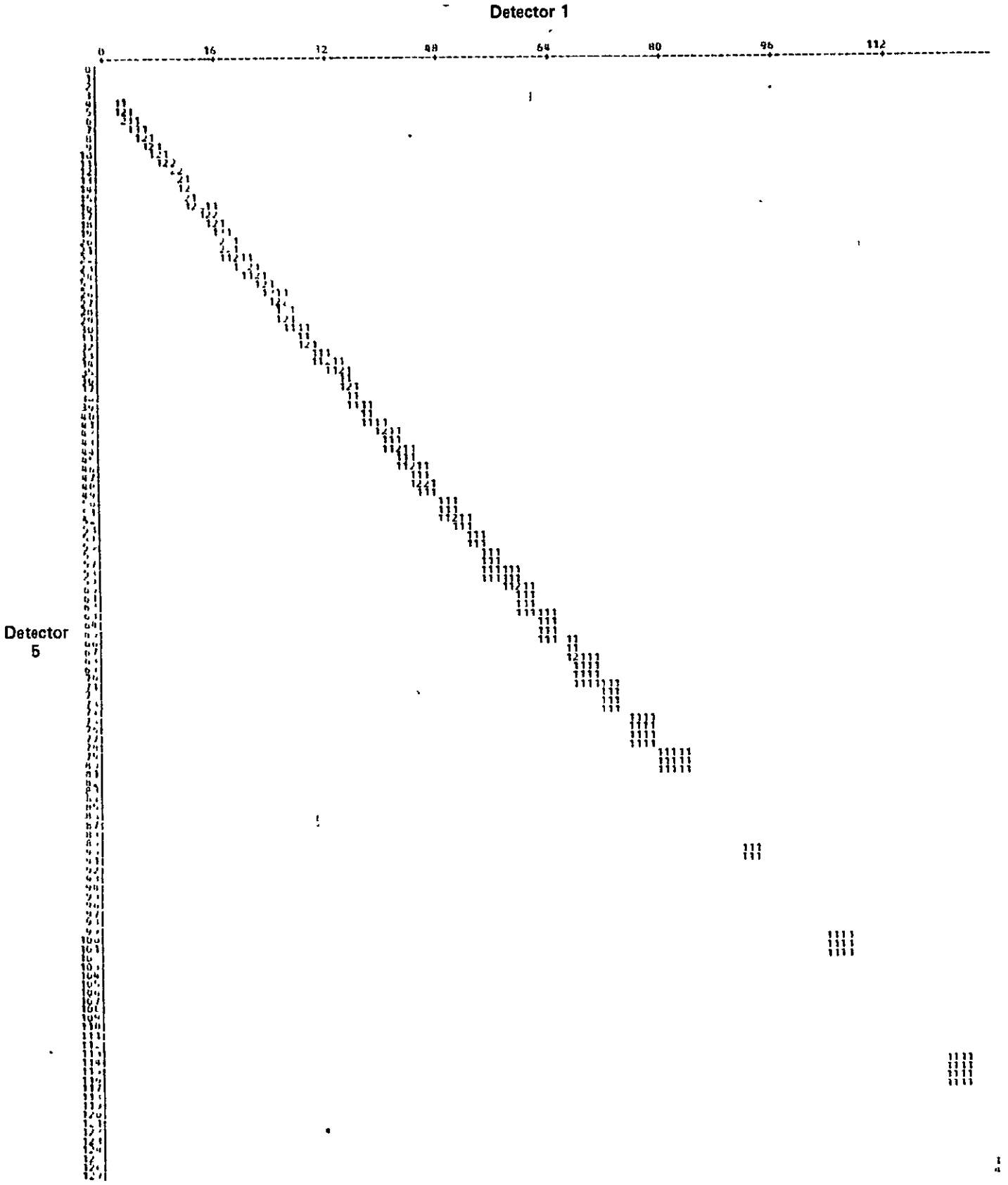

Figure 4.3-4. Interdetector Correlation Plot for Corresponding Decompressed Calibration Wedge Samples and their Standard Deviations, Detector 5 versus Detector 1, Band 1

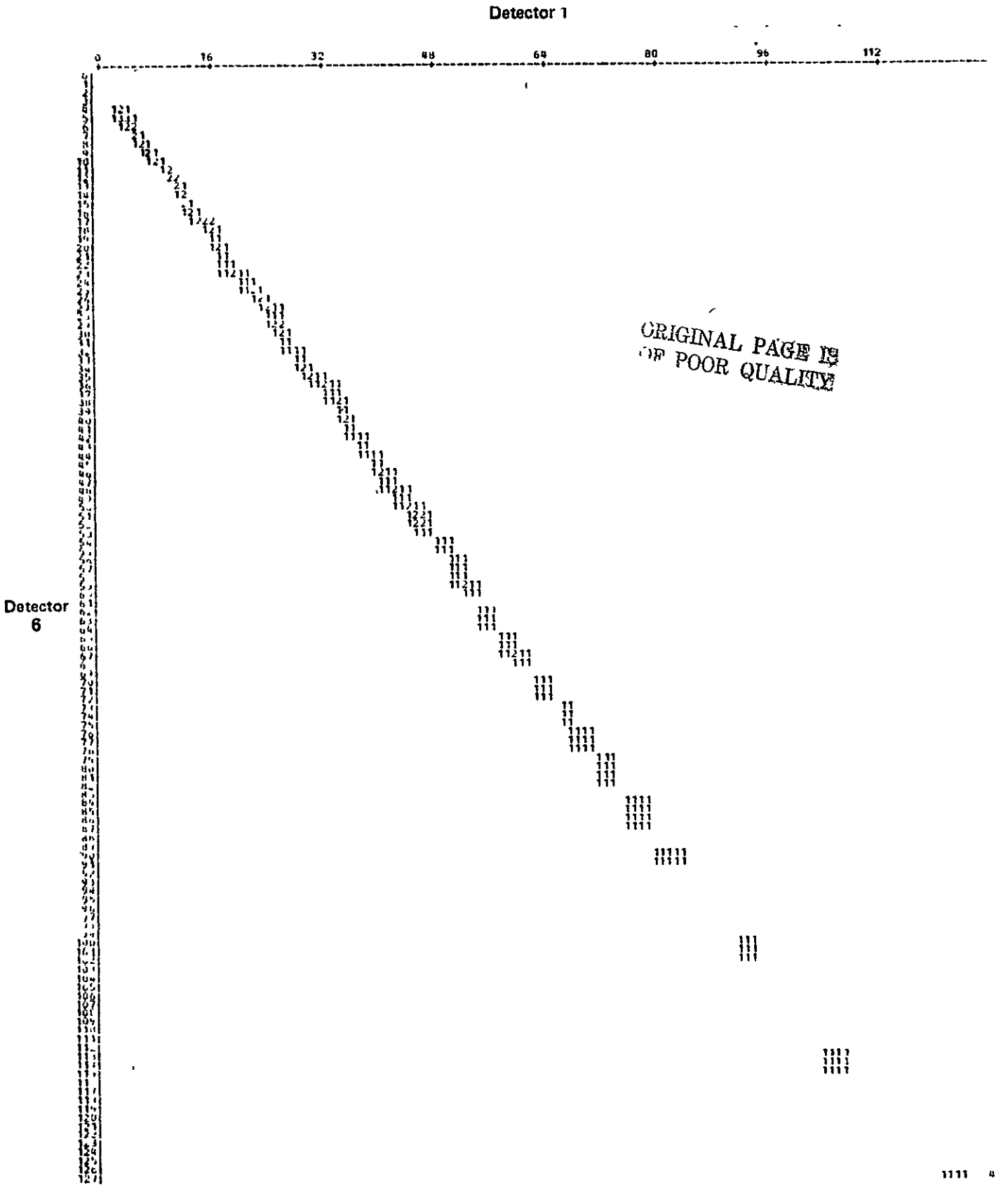

Figure 4.3-5. Interdetector Correlation Plot for Corresponding Decompressed Calibration Wedge Samples and their Standard Deviations, Detector 6 versus Detector 1, Band 1

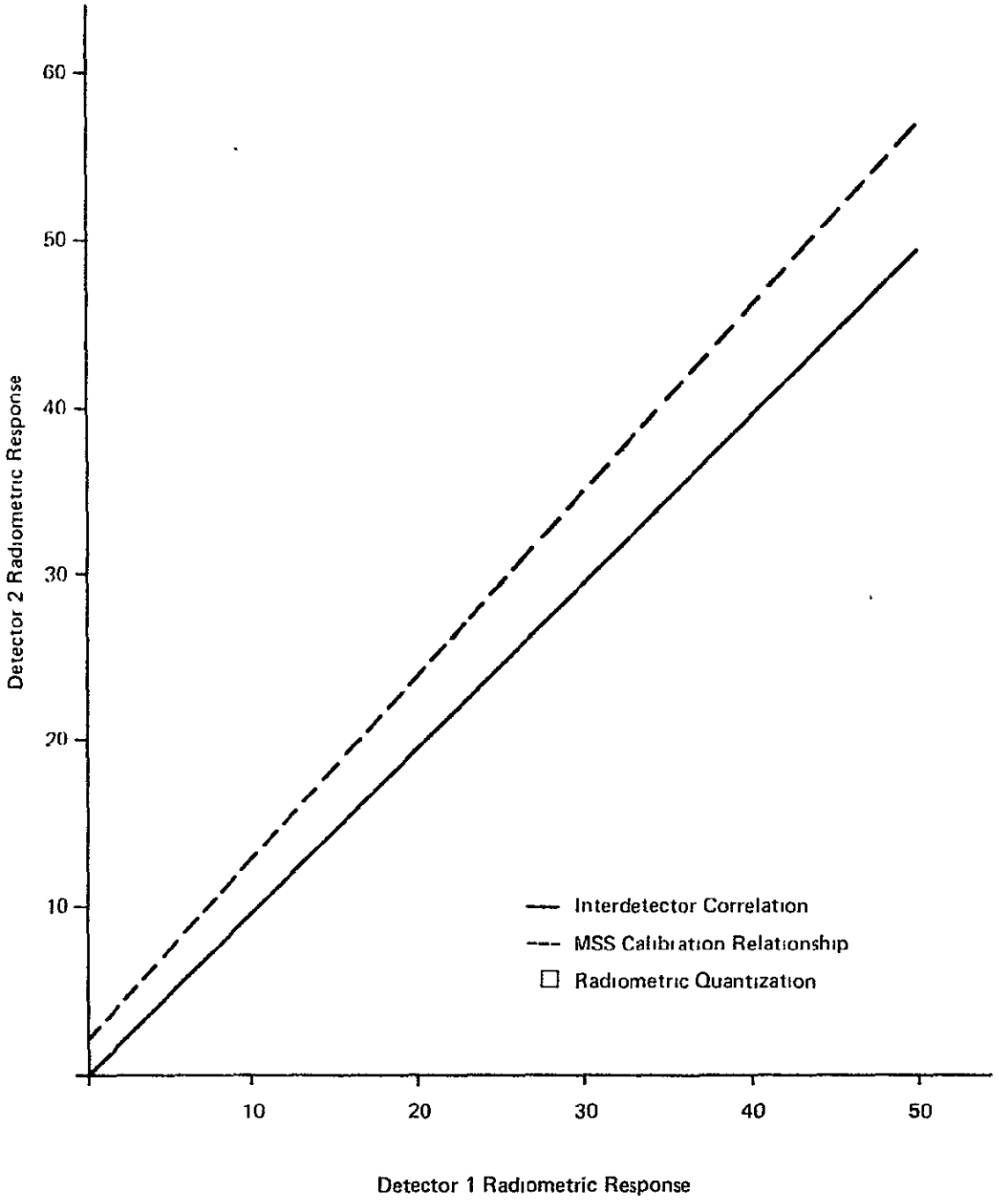

Figure 4.3-6. Interdetector Functional Relationships for Detector 1 and Detector 2, Band 1

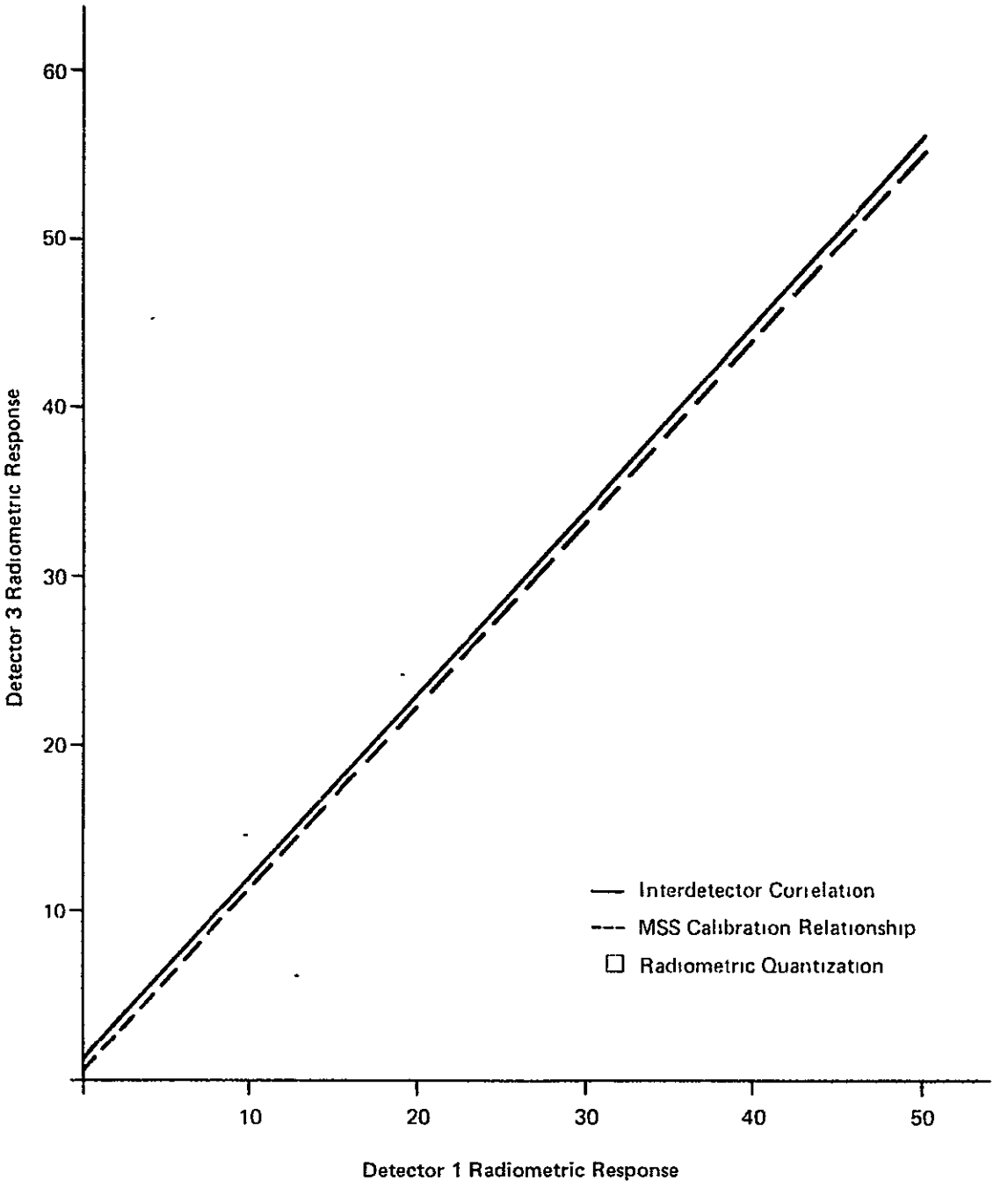

Figure 4.3-7. Interdetector Functional Relationships for Detector 1 and Detector 3, Band 1

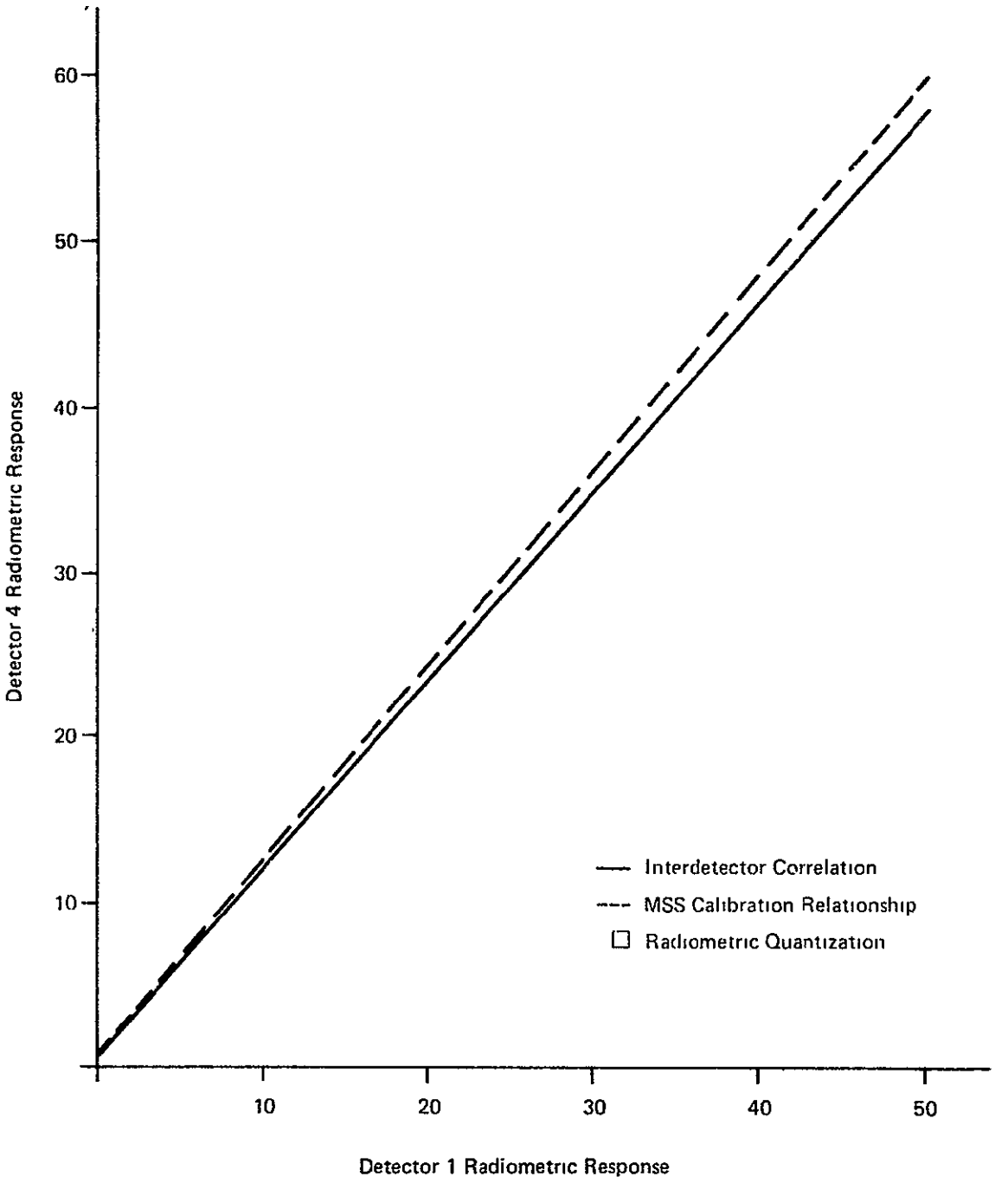

Figure 4.3-8. Interdetector Functional Relationships for Detector 1 and Detector 4, Band 1

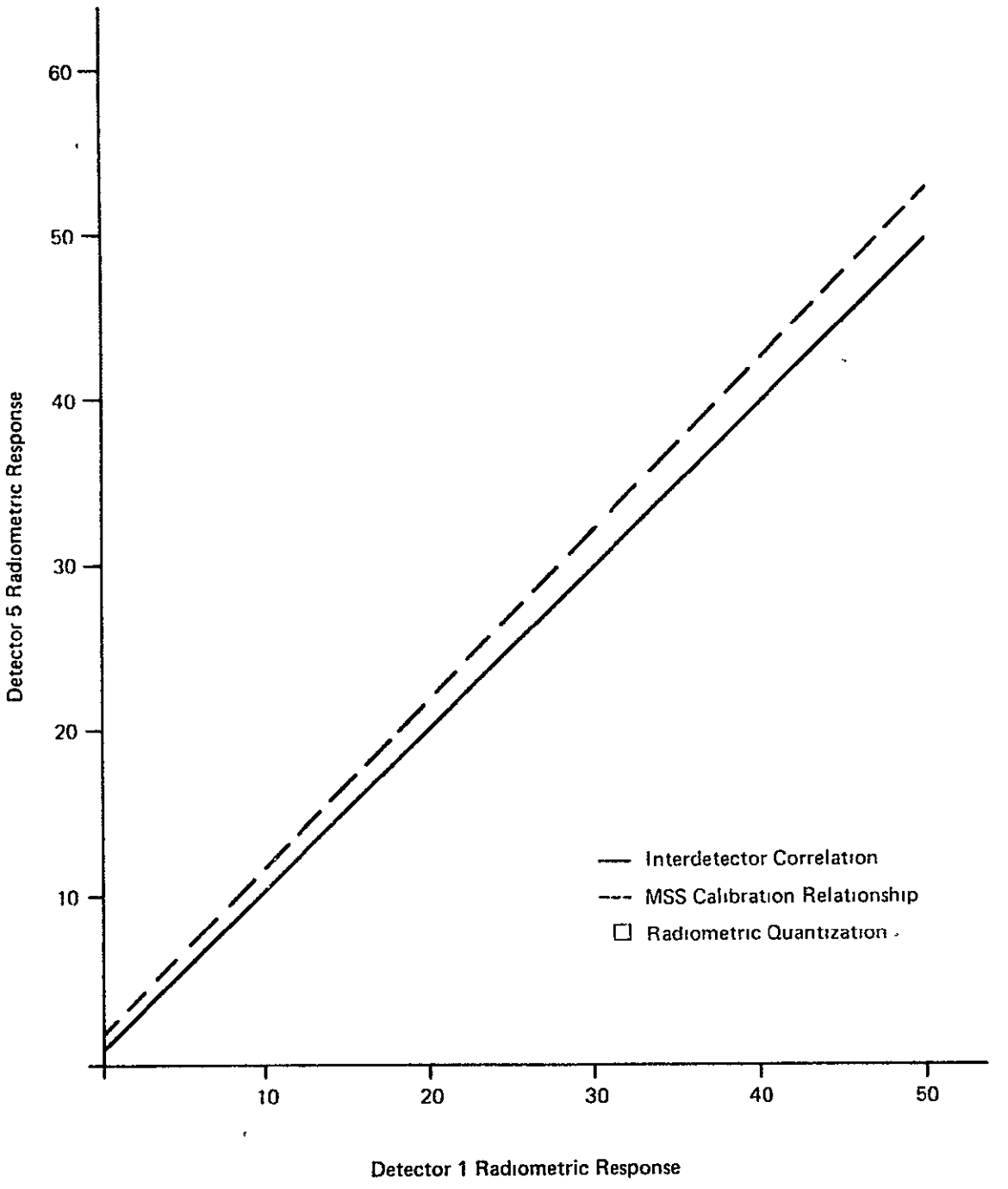

Figure 4.3-9. Interdetector Functional Relationships for Detector 1 and Detector 5, Band 1

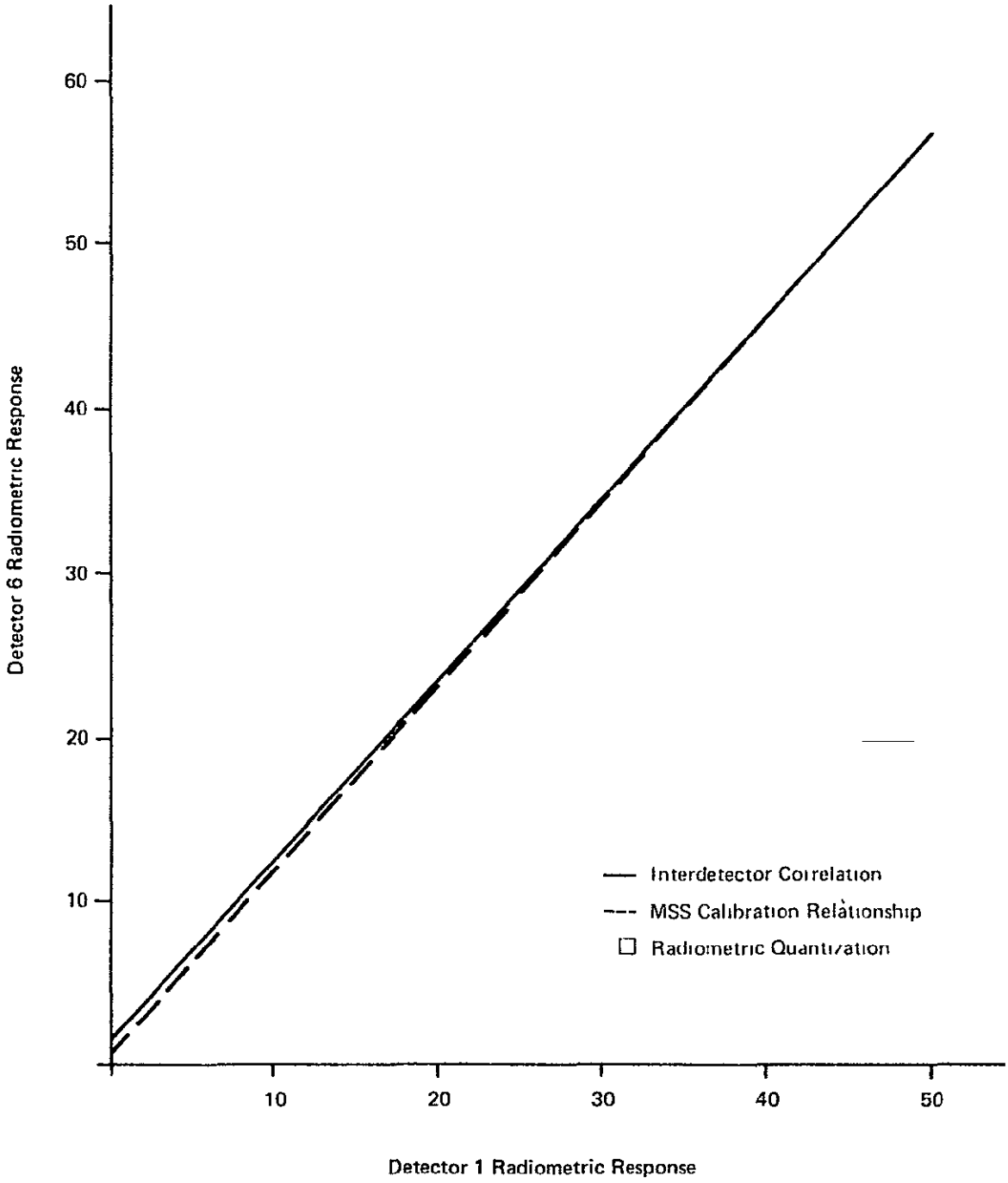

Figure 4.3-10. Interdetector Functional Relationships for Detector 1 and Detector 6, Band 1

4.4 SUMMARY OF CALIBRATION DATA EVALUATION

The analyses of the MSS calibration wedge data support the following
4.4 SUMMARY OF CALIBRATION DATA EVALUATION

The analyses of the MSS calibration wedge data support the following conclusions:

a. Calibration wedge sample values are stable to within $\pm$ 1 count (rms) for a given sample position in the reported data.

b. Variation in the bias adjustment in radiometric calibration of MSS detectors is at most $\pm$ 1 count for unsmoothed calibration constants.

c. Variation in the gain adjustment in radiometric calibration of MSS data is approximately $\pm$ 1 part in 20 for unsmoothed calibration constants.

d. There is no evidence of any correlation in the fluctuation of the calibration constants which would indicate this as the cause of striping.

e. The relationship between the response characteristics of any pair of MSS detectors, as a function of calibration wedge sample position, is linear over a wide dynamic range. This implies that linear radiometric transformations should be adequate to remove striping by equalizing the effective radiometric responses of the individual detectors in a given spectral band, unless, improbably, this linearity results from the cancellation of detector non-linearities by calibration wedge non-linearities.

f. Correlation plots of MSS calibration data reveal some inconsistencies between the linear interdetector relationship derived from the calibration data and that derived from the MSS calibration procedure. However, these inconsistencies cannot be identified as the cause of striping.

The analyses of calibration wedge data have failed to establish any causal link between MSS calibration procedures and the phenomenon of striping. One additional item worthy of investigation which could not be pursued in this study is the effect of applying the radiometric calibration developed from the MSS calibration procedure to the calibration wedge data itself. This study has already established that linear relationships exist among the radiometric responses of the MSS detectors as represented by the calibration data. If the MSS calibration procedure is adequate within the limits of the calibration data, and if the assumption is valid that, for all detectors, the same correspondence exists between calibration wedge sample number and radiance incident on the detector, then striping should be absent from the calibrated calibration data, and it would thus be firmly established that the cause of striping is not faulty calibration processing.

By concentrating on use of the calibration wedge data, one has a set of detector excitations whose properties uniquely suit them to analysis of interdector variations. Histogram shapes can reasonably be expected to be consistent without making assumptions regarding the statistical nature of image data. Along-track power spectra for different sample positions in the calibration wedge would differ primarily in the zero-frequency term, thus facilitating the identification of detector related, periodic, variations in response. With calibration wedge data, the along-track extent of the data sample used to produce a power spectrum is not limited by the size of imaged features, so that a finer frequency

resolution can be obtained. Finally, visual evaluation of the effectiveness of a radiometric processing techniques is performed for a standard pattern, so that this form of evaluation is not complicated by evaluator biases in selecting a particular section of the image on which to base a decision.

Section 5
INTERDETECTOR RESPONSE EQUALIZATION IN THE MDP

Analysis of the throughput reduction and microcode changes required to implement the selected destriping procedure in the MDP was performed. The results of this analysis are presented here.

The results presented in Section 3 of this report identified the type a2 radiometric processing of uncalibrated scene data as the best procedure for providing interdetector response equalization for MSS scene data. In this procedure, detector-specific histograms of the image data from the first 60 mirror sweeps of the input image data for a scene are generated and then characterized by their means and standard deviations. These 6 means and 6 standard deviations are then averaged to produce a target mean and standard deviation. For each detector, a linear gain and bias radiometric transformation is then determined which, when applied to the scene data from that detector, will transform it so the mean and standard deviation of the histogram of the transformed data are equal to the target mean and standard deviation. This section discusses the effect of incorporating this radiometric processing procedure in the Master Data Processor (MDP)

The radiometric calibration of MSS data which is now performed by the MDP is conceptually a two-step process:

1. Generation of the calibration function parameters, in which for each detector, six samples of the calibration wedge data, which is supplied every second MSS mirror sweep, are used to calculate the gain and bias parameters of a linear transformation of radiometric values for use on the scene data for that detector in each of the two mirror sweeps.

2. Application of this calibration function to the scene data.

Extraction of the calibration wedge samples is performed during Input Processing of the data stream from the HDT, and the samples are stored in a disk file. Generation of the calibration function parameters from the samples in this file is performed on blocks of these sample corresponding to an input data segment (i.e., the calibration samples corresponding to the data acquired between two successive nadir points in the World Reference System). These parameters are stored in a gain and bias file for that segment. Calibration of scene data is subsequently performed as an integral part of the resampling process, using parameters from these segment files which are identified by the Resampling Application Controller.

The type a2 radiometric processing does not employ any of the calibration wedge data which is available from the MSS. It, instead requires the computation of the mean and standard deviation of detector-specific histograms, as outlined above and detailed in Appendix A. Using a modification of the notation of Appendix A, the type a2 processing requires computation of the values:

$$m_i = \frac{1}{K} \sum_{k=1}^{K} \left[\frac{1}{J} \sum_{j=1}^{J} u_{ijk} \right]$$

$$s_i^2 = \frac{1}{K} \sum_{k=1}^{K} \left[\frac{1}{J} \sum_{j=1}^{J} (u_{ijk})^2 \right] - m_i^2$$

$$M = \frac{1}{I} \sum_{i=1}^{I} m_i$$

$$S = \frac{1}{I} \sum_{i=1}^{I} s_i$$

where u_{ijk} is the scene data value of sample j from detector i for MSS mirror sweep k

J is the number of samples in the line

I is the number of detectors used to collect scene data in one MSS band (6, if the thermal band is excluded)

K is the number of MSS mirror sweeps contained in the subimage employed for equalization (60 in the case of type a2 processing).

The quantities

$$\sum_{j=1}^{J} u_{ijk}$$

and

$$\sum_{j=1}^{J} (u_{ijk})^2$$

are already available to MDP, since they are contained in the 23 quality data pixels at the beginning of each major frame on the HDT (HDT-FM), and thus are available for each detector on a line basis. The MDP-MSS system could be modified to strip off these sums instead of the six calibration sample pixel values.

In the present MDP-MSS system, generation of the calibration function parameters is an autonomous task which is performed on an input segment basis, and which has no information available relating the specific input segment to an output frame. Because the type a2 radiometric processing requires interdetector equalization over the first 60 mirror sweeps of a frame, replacement of the present calibration parameter generation code with code to provide this radiometric equalization is not possible without considerable redesign of the MDP-MSS system.

However, if the equalization processing is performed on the scene data from the last 60 mirror sweeps in an input segment, rather than on the first 60 sweeps of the input data for an output frame, such code replacement is possible. This modification of the type a2 radiometric processing implies the reasonable assumption that any 60 sweep sample of the scene data for a frame is statistically equivalent to the first 60 sweeps. The radiometric equalization transformations obtained from this processing (one gain and bias set for each detector for each input data segment) would then be used for the output data frame containing the nadir reached at the end of the input data segment. It should be noted that this procedure, which requires only one gain and bias set per detector per output frame, may decrease the size of the gain and bias file, which at present is required to contain a gain and bias set for each detector for each sweep in a swath of MSS data.

In addition to the modifications discussed above, the present MDP-MSS system would have to be modified so that the Resampling Application Controller would cause the same gain and bias set per detector to be applied over an entire output data frame.

Since the changes required to perform this form of radiometric processing for destriping on the MDP-MSS system can be accomplished as described above, a procedure which does not require any major revisions to the system data flow, the system throughput can be expected to be unchanged.

Appendix A
IBM DESTRIPING PROCEDURES

A.1 SWEEP HISTOGRAM EQUALIZATION

An algorithm of the following type satisfies the requirement for adjusting detector gains and offsets between detectors to minimize striping.

a. Compute a histogram for each detector.

b. Adjust the gain and offset of each detector so that the mean and standard deviation of the histogram of its corrected output matches the average of the means and standard deviations of histograms produced for each detector.

Let the average mean and standard deviation for the detector histograms M, S: let the mean and standard deviation for the ith detector be m_i, s_i, and let the output of the ith detector for sample j be u_{ij}. The following equation then transforms u_{ij} into a variable w_{ij} having the mean and standard deviation of the ensemble:

$$w_{ij} = M + \frac{S}{s_i} \quad (u_{ij} - m_i)$$

The corrected output for the ith detector is w_{ij}. The gain and offset for the ith detector then are:

$$G_i = \frac{S}{s_i}$$

$$B_i = M - m_i G_i$$

The quantities m_i, s_i, M, and S should be evaluated over a span of data such that the ground area scanned by each detector is statistically equivalent. During a single sweep, the set of inputs to each detector is assumed to meet this criterion.

Let u_{ij} be the jth sample from the ith detector. Compute for i=1,2,3,4,5,6:

$$m_i = \frac{1}{n} \sum_{j=1}^{n} u_{ij} \qquad (n = \text{number of samples in the line})$$

$$s_i^2 = \left[\frac{1}{n} \sum_{j=1}^{n} (u_{ij})^2\right] - m_i^2$$

$$s_i = \left[s_i^2\right]^{1/2}$$

Then

$$M = \frac{1}{6} \sum_{i=1}^{6} m_i$$

$$S = \frac{1}{6} \sum_{i=1}^{6} s_i$$

These computations can be implemented as follows. While a scan line is being processed, the sum and the sum of squares are accumulated and used to calculate B_i and G_i values to be used on a following sweep. In the same pass the corrected values w_{ij} are calculated using the following equation:

$$w_{ij} = B_i + G_i \, u_{ij}$$

The values of B_i and G_i used are from the data of the sweep previous to the sweep being corrected. This technique avoids having to make two passes of each scan line: one to compute the B_i and G_i values and another to use those B_i and G_i values to modify the line.

A.2 SUBIMAGE HISTOGRAM EQUALIZATION

In the procedure for sweep histogram equalization described above, the assumption is made that the data provided by any detector for one mirror sweep is statistically equivalent to that provided by the other detectors in the same sweep. An alternative procedure, which has the advantage of increasing the data on which this statistical equivalence is imposed, is to base the interdetector equalization on the image data from some significant fraction of the entire image. This image fraction can be anywhere from one sweep to the entire image.

In this alternative equalization procedure, the gain and bias radiometric constants for each detector are calculated and outlined above, but based on histograms derived from all the image data contained in a specified subimage. The radiometric constants are then applied to the entire image data set.

Appendix B
MSS CALIBRATION PROCEDURE

The radiometric calibration formula employed for the four MSS bands available on Landsat 1 and 2 is:

$$V_c = \frac{KV_{max}}{\Delta R}\left[\frac{V - pa_s}{q\, b_s} - R_{min}\right] - r$$

where V_c = calibrated pixel value;

V = input (decompressed) pixel value;

V_{Max} = maximum pixel value (127 for three bands and 63 for the fourth band);

$\Delta R = R_{max} - R_{min}$, depending on each band;

K, p, q, and r are constants (expected to vary infrequently);

a_s = smoothed offset (computed per scan line);

b_s = smoothed gain or slope (computed per scan line).

This calibration formula assumes that the data either was taken in the linear mode or has been decompressed.

The offset and gain coefficients are determined once per scan line as follows:

$$a = \sum_i C_i V_i , \quad b = \sum_i D_i V_i$$

where i runs from 1 to 6.

The V_i are the linear or linerized detector calibration samples associated with the scan line; C_i, D_i are regression coefficients, which may differ for each detector and band, but remain constant during normal sensor performance.

Smoothed offset and gain coefficients, a_s and b_s, for each detector are calculated for every mirror sweep, n, as follows:

$$b_s(n) = b_s(n-1) + W(n)\left[b(n) - b_s(n-1)\right]$$

$$a_s(n) = a_s(n-1) + W(n)\left[a(n) - a_s(n-1)\right]$$

where

n = sequential number of mirror sweep;

b(n), a(n) = latest value of b and a determined;

$b_s(n)$, $a_s(n)$ = new smoothed value of b and a;

W(n) = 1/n+1 for n=1 to 15,

W(n) = 1/16 for $n \geq 16$.

The C_i and D_i are predetermined on the basis of prelaunch radiance test data.

Appendix C
PLATES

Plate 1 - MSS Scence 2183-16433, MSS Band 1, Uncalibrated Data

Plate 2 - MSS Scence 2183-16433, MSS Band 1, Uncalibrated Data after Type a1 Radiometric Processing

Plate 3 - MSS Scene 2183-16433, MSS Band 1, Uncalibrated Data after Type a2 Radiometric Processing

Plate 4 - MSS Scene 2183-16433, MSS Band 1, Uncalibrated Data after Type a3 Radiometer Processing

Plate 5 - MSS Scene 2183-16433, MSS Band 1, Uncalibrated Data after Type b1 Radiometric Processing

Plate 6 - MSS Scene 2183-16433, MSS Band 1, Uncalibrated Data after Type b2 Radiometric Processing

Plate 7 - Scene Overlay Showing Specific Regions Employed in Evaluations

(These plates are contained in the envelope at the end of this report)

Plate 1 - MSS Scene 2183-16433, MSS Band 1,
Uncalibrated Data

Plate 2 - MSS Scene 2183-16433, MSS Band 1, Uncalibrated Data after Type al Radiometric Processing

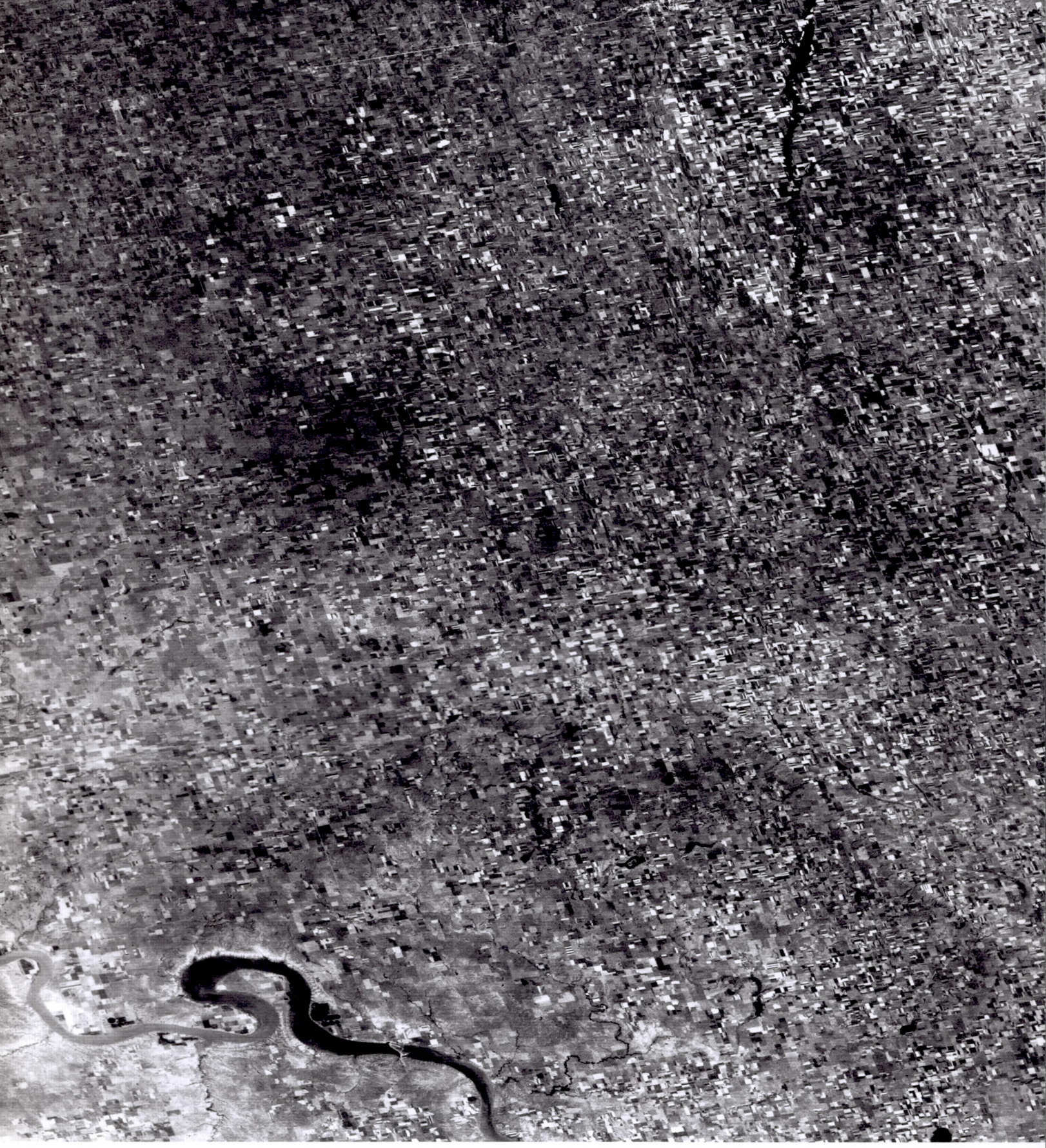

Plate 3 - MSS Scene 2183-16433, MSS Band 1, Uncalibrated Data after Type a2 Radiometric Processing

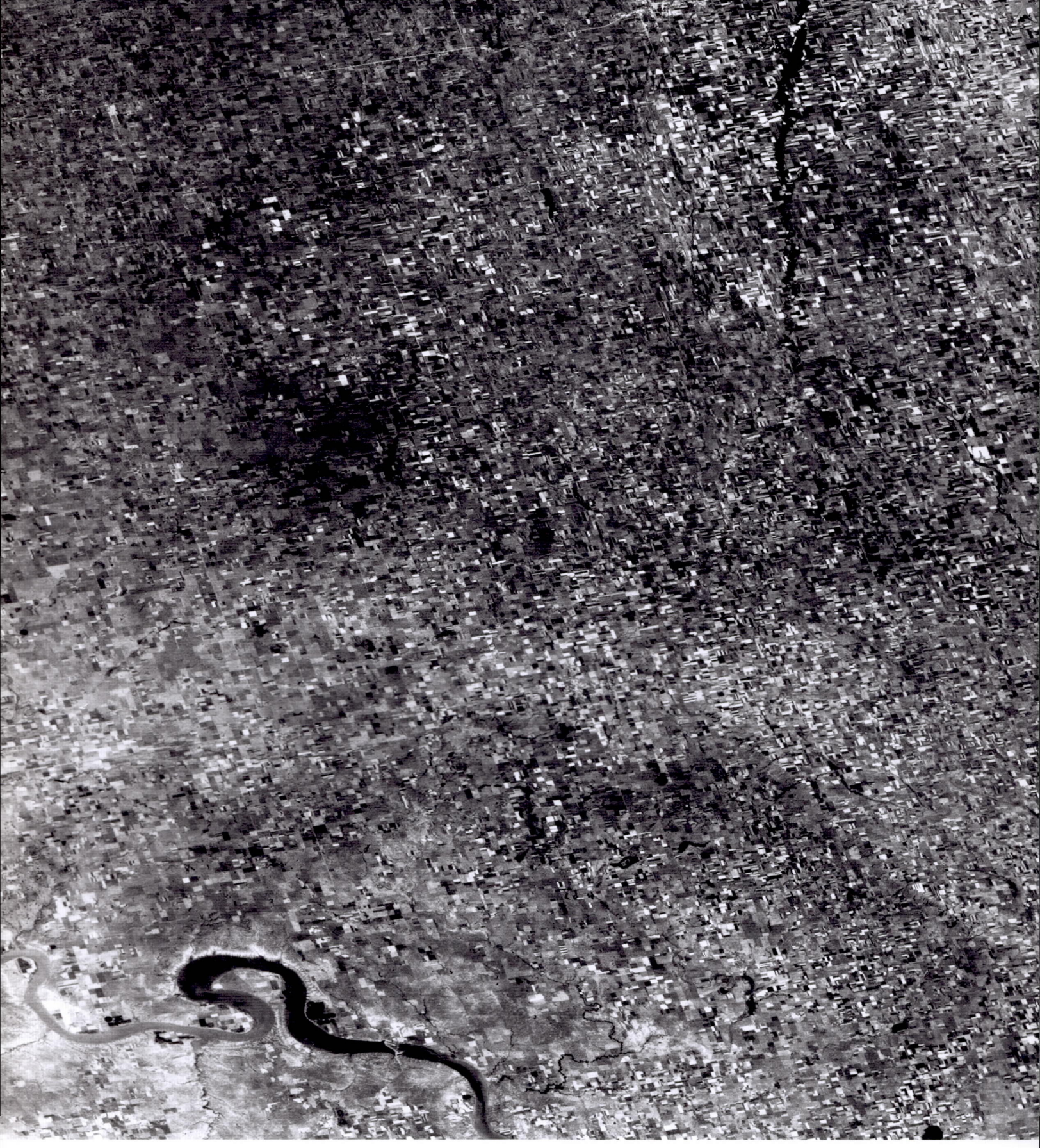

Plate 4 - MSS Scene 2183-16433, MSS Band 1, Uncalibrated Data after Type a3 Radiometric Processing

Plate 5 - MSS Scene 2183-16433, MSS Band 1, Uncalibrated Data after Type b1 Radiometric Processing

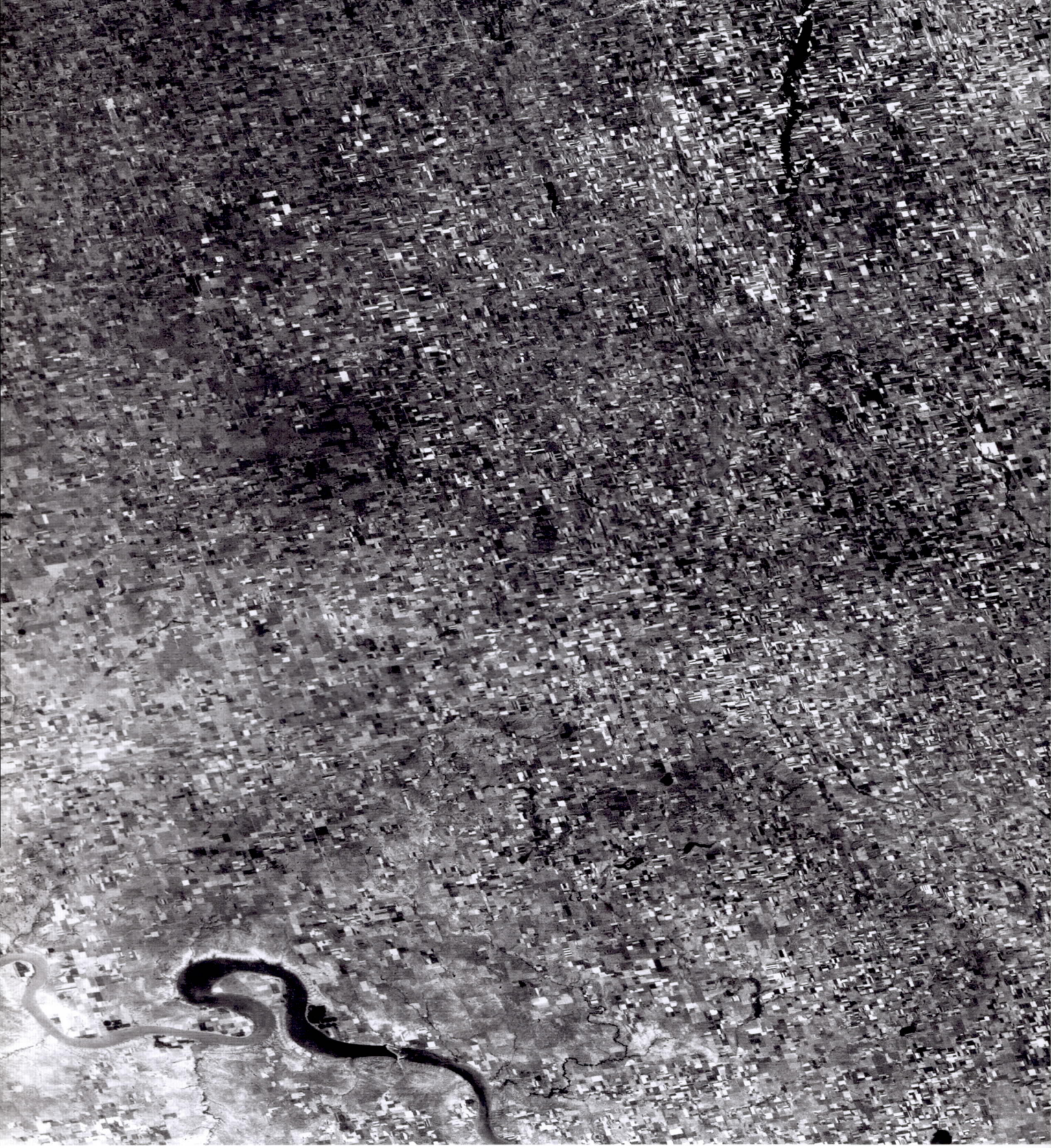

Plate 6 - MSS Scene 2183-16433, MSS Band 1, Uncalibrated Data after Type b2 Radiometric Processing

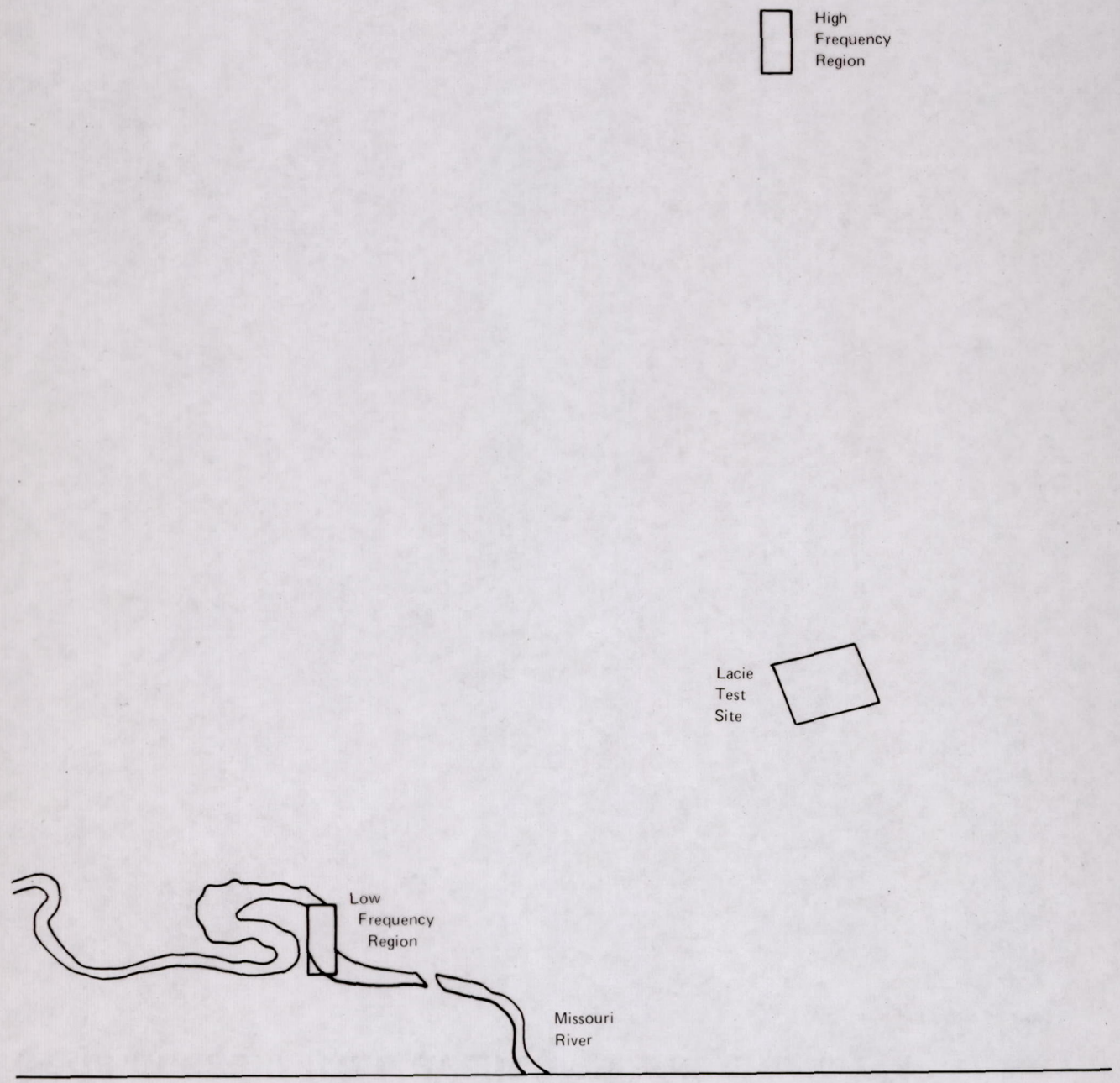

Plate 7 - Scene Overlay Showing Specific Regions Employed in Evaluations